Enhancement of Simple Adaptive Control for Industrial Feed Drive Systems

(産業機械送り駆動系のための単純適応制御の高性能化)

July, 2024

Doctor of Philosophy (Engineering)

Haryson Johanes Nyobuya

ハリソン ヨハネス ニョブヤ

Toyohashi University of Technology

別紙４－１（課程博士（英文））

Date of Submission（month day, year）: 07/08/2024

Department of Mechanical Engineering		Student ID Number	D219101	Supervisors	Naoki Uchiyama Junji Takahashi
Applicant's name	Haryson Johanes Nyobuya				

Abstract（Doctor）

Title of Thesis	Enhancement of Simple Adaptive Control for Industrial Feed Drive Systems

Approx. 800 words

In precision manufacturing, the ability to track a trajectory with high-precision while simultaneously reducing energy consumption is highly desirable. A wide range of industrial machines such as computer numerical control, industrial robots, and assembly equipment uses a ball-screw driven mechanism for micron-scale positioning applications. Ball-screw mechanisms are widely used because of their simple dynamic nature and low cost. The tasks performed by the ball-screw mechanisms are repetitive in nature, leading to high energy consumption. In addition, tracking error is induced by ball-screw assembly. Given the current worldwide situation of high energy costs, environmental effects, and the depletion of energy sources, energy-saving is needed. In addition, precise motion is vital for machines to manufacture high-quality products. Therefore, the industrial sector is driven by a high need for machines with accurate motion and energy-saving capabilities.

Adaptive control is one of the most effective methods, which can consider the parametric uncertainties and disturbances with online adaptive rules. Simple adaptive control (SAC) is a simplified approach to direct model referencing adaptive control. The SAC control technique has attracted much attention from researchers in recent decades because of its simplicity and the ease of implementing its algorithm. In addition, this control technique has the advantage of not requiring full state access or estimators in the control loop. Moreover, the SAC technique does not require full knowledge of the system's dynamics to implement. To successfully apply the SAC to a real system the "almost strictly positive real (ASPR)" property is required to be satisfied. ASPR ensures the stability of the system even when the gains are high. Most systems fail to meet the ASPR requirement and therefore, other methods are needed to meet the ASPR requirement. In the literature, many studies have focused

on the typically used parallel feedforward compensation (PFC) method. However, the PFC approach deviates the output signal from the desired which increases the tracking error. There have been numerous proposals for improving the situation by researchers to counteract this problem though parallel type structure design still holds.

To enhance machine performance in terms of tracking and contouring accuracy with less energy consumption in industrial machines, the proposed control approaches are described as follows in this thesis: Introductory remarks are presented in Chapter 1 followed by a literature review in Chapter 2 describing the related studies in adaptive control, simple adaptive control, integral terminal sliding mode control and industrial feed drive systems dynamics. Chapter 3 presents the use of jerk-based augmented output signal for the ASPR property. The proposed approach allows SAC to track the desired signal more precisely at high frequencies. This is achieved by placing the zeros of the system at effective locations. To verify the feasibility of the proposed approach, simulation and experiment are conducted. The results are compared with those of the commonly used PFC approach. Experimental results revealed that the proposed approach reduced the tracking error by about 80% compared to PFC without any additional control input. Moreover, the proposed approach has been proved to be energy-efficient by about 21% than PFC under similar tracking conditions. Simple adaptive contouring control (SACC) using jerk-based augmented output signal for the ASPR property is presented in Chapter 4. SACC is designed by following the tangent contour control scheme while using the SAC technique to enhance the contouring accuracy. Jerk-based augmented output signal ensures that the ASPR property is met and allows the SACC to track accurately the desired contour at high frequency. The proposed contouring approach achieves lower contour error and energy consumption by about 45% and 3% respectively, as compared to the most common parallel feedforward compensation approach.

Chapter 5 describes the approach focusing on application of integral terminal sliding mode control (ITSMC) to the feed drive system because of its robustness against disturbances and finite-time convergence of the tracking error. However, its design requires a good understanding of plant dynamics and estimated parameters. To alleviate this concern, a solution of modifying the original ITSMC law to an adaptive ITSMC law based on SAC technique. To implement SAC-like adaptive law to a real plant, ASPR property is required to be satisfied. ASPR property is satisfied using velocity-based augmented output signal that ensures the stability even when gains are high. Based on the experimental results, this formulation allows the adaptive controller to follow the reference trajectory more precisely than conventional methods. Lastly, Chapter 6 presents the concluding remarks of this thesis and prospective future works.

Declaration of Authorship

I, Haryson Johanes Nyobuya, declare that this thesis titled, " Enhancement of Simple Adaptive Control for Industrial Feed Drive Systems " and the work presented in it are my own. I confirm that:

- This work was done wholly or mainly while in candidature for a research degree at this University.
- Where any part of this thesis has previously been submitted for a degree or any other qualification at this University or any other institution, this has been clearly stated.
- Where I have consulted the published work of others, this is always clearly attributed.
- Where I have quoted from the work of others, the source is always given. With the exception of such quotations, this thesis is entirely my own work.
- I have acknowledged all main sources of help.
- Where the thesis is based on work done by myself jointly with others, I have made clear exactly what was done by others and what I have contributed myself.

Signed: ______________________________

Date: July, 2024

Abstract

In precision manufacturing, the ability to track a trajectory with high-precision while simultaneously reducing energy consumption is highly desirable. A wide range of industrial machines such as computer numerical control, industrial robots, and assembly equipment uses a ball-screw driven mechanism for micron-scale positioning applications. Ball-screw mechanisms are widely used because of their simple dynamic nature and low cost. The tasks performed by the ball-screw mechanisms are repetitive in nature, leading to high energy consumption. In addition, tracking error is induced by ball-screw assembly. Given the current worldwide situation of high energy costs, environmental effects, and the depletion of energy sources, energy-saving is needed. In addition, precise motion is vital for machines to manufacture high-quality products. Therefore, the industrial sector is driven by a high need for machines with accurate motion and energy-saving capabilities. Adaptive control is one of the most effective methods, which can consider the parametric uncertainties and disturbances with online adaptive rules. Simple adaptive control (SAC) is a simplified approach to direct model referencing adaptive control. The SAC control technique has attracted much attention from researchers in recent decades because of its simplicity and the ease of implementing its algorithm. In addition, this control technique has the advantage of not requiring full state access or estimators in the control loop. Moreover, the SAC technique does not require full knowledge of the system's dynamics to implement. To successfully apply the SAC to a real system the "almost strictly positive real (ASPR)" property is required to be satisfied. ASPR ensures the stability of the system even when the gains are high. Most systems fail to meet the ASPR requirement and therefore, other methods are needed to meet the ASPR requirement. In the literature, many studies have focused on the typically used parallel feedforward compensation (PFC) method. However, the PFC approach deviates the output signal from the desired which increases the tracking error. There have been numerous proposals for improving the situation by researchers to counteract this problem though

parallel type structure design still holds. To enhance machine performance in terms of tracking and contouring accuracy with less energy consumption in industrial machines, the proposed control approaches are described as follows in this thesis: Introductory remarks are presented in Chapter 1 followed by a literature review in Chapter 2 describing the related studies in adaptive control, simple adaptive control, integral terminal sliding mode control and industrial feed drive systems dynamics. Chapter 3 presents the use of jerk-based augmented output signal for the ASPR property. The proposed approach allows the SAC to track the desired signal more precisely at high frequencies. This is achieved by placing the zeros of the system at effective locations. To verify the feasibility of the proposed approach, simulation and experiment are conducted. The results are compared with those of the commonly used PFC approach. Experimental results revealed that the proposed approach reduced the tracking error by about 80% compared to PFC without any additional control input. Moreover, the proposed approach has been proved to be energy-efficient by about 21% than PFC under similar tracking conditions. Simple adaptive contouring control (SACC) using jerk-based augmented output signal for the ASPR property is presented in Chapter 4. SACC is designed by following the tangent contour control scheme while using the SAC technique to enhance the contouring accuracy. Jerk-based augmented output signal ensures that the ASPR property is met and allows the SACC to track accurately the desired contour at high frequency. The proposed contouring approach achieves lower contour error and energy consumption by about 45% and 3% respectively, as compared to the most common parallel feedforward compensation approach. Chapter 5 describes the approach focusing on application of integral terminal sliding mode control (ITSMC) to the feed drive system because of its robustness against disturbances and convergence of the tracking error in finite-time. However, its design requires a good understanding of plant dynamics and estimated parameters. To alleviate this concern, a solution of modifying the original ITSMC law to an adaptive ITSMC law based on SAC technique. To implement SAC-like adaptive law to a real plant, ASPR property is required to be satisfied. ASPR property is satisfied using velocity-based augmented output signal that ensures the stability. Based on the experiments' results, this formulation allows the adaptive controller to follow the reference trajectory more precisely than conventional methods. Lastly, Chapter 6 presents the concluding remarks of this thesis and prospective future works.

Acknowledgments

I am profoundly grateful to the Almighty God for bestowing upon me the health, strength, knowledge, and opportunity to successfully complete my studies.

My deepest appreciation goes to my mentor, Prof. Naoki Uchiyama, whose invaluable support and guidance have significantly contributed to my academic growth and societal impact.

I am indebted to the committee members, Prof. Kaiji Sato and Prof. Junji Takahashi, for their time, effort, and expertise in reviewing my research. I also extend my gratitude to all members of the System Engineering Laboratory for their unwavering support and camaraderie.

My heartfelt thanks to Toyohashi University of Technology for their assistance, and to Monbukagakusho for the scholarship that supported my studies.

To my beloved wife Madeline, your unconditional love, care, and patience have been my pillar of strength.

Finally, my sincere gratitude goes to my parents Johanes and Theresa, and my older siblings for their unwavering support, patience, and prayers.

Contents

List of Figures

List of Tables

Abbreviations

AC	Alternate current
AOS	Augmented output signal
AOS-v-a	Acceleration-based augmented output signal
AOS-v-a-j	Jerk-based augmented output signal
ASMC	Adaptive sliding mode control using simple adaptive control
ASPR	Almost strict positive real
AITSMC	Adaptive integral terminal sliding mode control using simple adaptive control
CCC	Cross-coupled controller
CGT	Command generator tracker
CNC	Computer numerical control
CNTSMC	Continuous non-singular fast terminal sliding mode controller
ITSM	Integral terminal sliding mode
ITSMC	Integral terminal sliding mode control

MPC	Model predictive control
P	Proportional
PFC	Parallel feedforward compensator
PI	Proportional-Integral
SAC	Simple adaptive control
SACC	Simple adaptive contouring control
SPR	Strictly positive real
TSM	Integral terminal sliding mode
TCC	Tangent-contouring control

Chapter 1

Introduction

1.1 Background

Ball-screw feed drive systems are transmission components used to convert the rotational motion of a motor into the translational motion. They are commonly used in manufacturing machinery, including Computer numerical control (CNC) machines, robotic manipulators, and milling equipment as shown in Fig. 1.1. In addition, they are are also useful in beyond manufacturing industry such as in aerospace, automotive and construction industries [1–3]. These systems have several distinctive advantages including higher precision, reliability, and efficiency, in almost every application as compared to sliding lead screw systems [4]. Due to the multiple transmission stages, the structure of the ball-screw system exhibits elasticity, resulting in slight discrepancies between the actual movement and the input command. Therefore, achieving high accuracy is crucial in motion control technology. Performance of these systems are based on their accuracy during operations and accuracy can be evaluated based on the measurements attained by the ability of table position to follow the desired positions. Accuracy can be divided into tracking and contouring accuracies which are evaluated by the tracking and contouring errors, respectively [5, 6]. Tracking error refers to the difference between desired and actual position along each feed drive axis and contour error is the minimum distance between desired and actual contour at the current time. Fig. 1.2 provides a detailed depiction of tracking

(a) Ball-screw driven nesting CNC: https://www.cncrouter-shop.com/pro/1325-ball-screw-driven-nesting-atc-cnc-router-with-two-tool-magazines/

(b) Welding manipulator: https://www.koike.com/cricket-ii-medium-duty-welding-manipulator-ideal-for-subarc-gtaw-gmaw-applications/

Figure 1.1: Ball-screw driven manufacturing machines

and contour errors. Here, tracking errors are represented by e_x and e_y, and the actual contour error is given as e_c, for estimation purposes e_n is typically used as an estimate due to complexities of its determination. To emphasis on energy consumption, the employed electric motor driven systems consume the largest amount of electricity of any end use are more than 40% of global electricity consumption [7]. Feed drives are also motor driven systems and their tasks performed are of repetitive nature. For instance, in a CNC milling machine, the ball-screw feed drive system is responsible for moving the cutting tool back and forth across a work piece, repeating this motion several times to achieve the desired shape and surface finish. This repetitive motion, while necessary for the operation of the machine, does lead to high energy consumption with taking into fact the massive number of on-clock machines running all over the world. Therefore, while the ball-screw feed drive systems are essential for many industrial applications, their energy consumption is a significant factor that must be taken into account in the overall system design and operation. Strategies such as improving system efficiency, optimizing operational parameters, or even exploring alternative drive mechanisms could be potential ways to address this issue. In conclusion, understanding the workings and dynamics

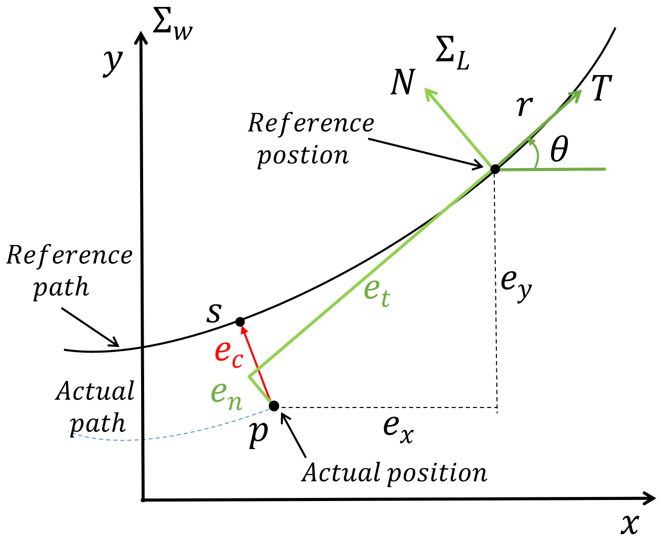

Figure 1.2: Contour error estimation

of ball-screw feed drive systems is crucial in the fields of mechanical and industrial engineering. It allows for the development of more efficient and sustainable machinery, contributing to the broader goals of energy conservation and environmental protection.

1.2 Tracking control

The main goal for the feed drive type of applications is to achieve high tracking accuracy. This is done by reducing the tracking error which is the difference between the desired and actual position of the table. For high tracking feedback controllers are immensely preferred.

Cascade P–PI controller is widely used in machine tool servo systems applications. This controller consists of a Proportional (P) component for the position feedback and a Proportional-Integral (PI) component for the velocity feedback [8]. In particularly when implementation, the servo gains for each component in the cascade controller are tuned by trial and error manner while checking the actual behavior for best performance. Although its performance is limited.

Many scholars have researched on improving the limitations of the P-PI cascade controller by inclusion of feedforward control to establish a robust feedback loop that will mitigate the influence changes in the dynamics and non-linearities dependent on its position [9]. Nonlinear model-based control approaches including model predictive control [10], sliding mode control [11], model-reference adaptive control [12], and robust control [13] have been applied in the feed drives to achieve high-performance in different situations. The effectiveness of these control approaches is significantly dependent on the accuracy of their model parameters. Incorrect or imprecise parameters can lead to sub-optimal performance. Therefore, ensuring parameter accuracy is crucial for achieving high-performance control.

As a nonlinear control approach, Model predictive control (MPC) employs a feedback mechanism to account for uncertainties in the model, state, and actuator constraints, according to Schwenzer *et al.* [14]. Stephens *et al.* [15] proposed the integration of trajectory horizons with control and prediction horizons in MPC to boost tracking accuracy. Modified reference trajectory for MPC was proposed by Yang *et al.* [16] for predicting errors offline in feed drive systems. However, MPC requires a considerable amount of computational power, even to the most straightforward applications.

In contrast to model-based methods, data-driven methods utilize measured data directly and do not need precise parametric models. Li *et al.* [17] proposed a neural network based on long short-term memory for the purpose of estimating errors and modifying reference trajectories. A neural network controller using a back-stepping method for state and error approximation was proposed by Xi *et al.* [18]. Data-driven methods are undoubtedly growing, but their fit for real-time applications is still up for consideration, given the concerns of online computation workload, network design, training methodologies, and issues related to control system stability.

In this thesis, SAC is opted for the requirement of meeting the high tracking performance. SAC is a simplified approach to the direct model referencing adaptive control as proposed by Sobel *et al.* [19]. Researchers have been increasingly drawn to this technique over the past few decades, largely due to its uncomplicated nature and the ease of its algorithm implementation [20]. Furthermore, this control technique has the advantage of not requiring the full knowledge of the systems dynamics to implement SAC [21].

1.3 Contouring control

In precision manufacturing, it is recommended to apply contouring control for multi-axis applications as it relates directly to the shape of the desired workpiece [22]. On the tracking approaches [11, 23–25], the axial controllers are used to reduce the tracking error and thereby indirectly reduce the resultant contour error. However, these approaches are limited to axial tracking. The most significant factor for the contouring performance of the motion systems is the contour error which needs to be addressed directly.

High contouring accuracy is achieved by reducing or eliminating the contour error [26], which is the shortest distance between the actual and desired contour as shown in Fig. 1.2. For the contour error to be zero, each axis must perfectly track its respective reference trajectory. In addition, the contour error is considered as one of the most significant performance indicators for a machine tool [27].

There is a substantial variety of approaches proposed by researchers to reduce or eliminate the contour error. Koren [28] proposed Cross-coupled controller (CCC) to improve the contouring accuracy of the biaxial systems. This is achieved by adding the correction control variables from the computed contour error to each control loop. The application of CCC has been used in variety of works including model predictive control [29], H_∞ control [30], iterative learning control [31], and terminal sliding mode control [32]. However, for the CCC to work effectively, it requires the accurate estimation of the contour error. This can be difficult to determine for complex shapes.

A real-time novel contouring control for polar coordinate motion systems was proposed by Wang *et al.* [33]. This method uses an iterative compensation to adjust the velocity and orientation of the motion system based on the contour error and curvature information of the desired trajectory. However, the method requires a high-performance real-time controller to implement the iterative compensation algorithm with updating velocity and orientation simultaneously at each sampling time.

Chiu and Tomizuka [34] proposed a task coordinate frame that moves along and rotates with the desired contour so that control law can be decoupled into tangential and normal directions of motion. Tangential velocity tracking approach was proposed by Ke *et al.* [35], this approach uses task coordinate frame, which focuses on adjusting the actual velocity to the desired contour. Tangential velocity tracking approach assumes that the tangential velocity equals the contour velocity. However, there is a possibility of exceeding the maximum speed of the machine, which is detrimental to the machine.

1.4 Objective of this study

On the basis of the description of the problem, the aim of this study is to develop and implement simple adaptive control algorithms that improve the tracking and contouring performances of industrial feed drive systems without the requirement of full knowledge to the plant parameters. As mentioned on the previous section, high tracking and contouring accuracy of the feed drive systems is highly in demand for high precision operations. Furthermore, the approach that uses less energy is equivalent desirable for contributions to environmental, natural resources and energy problems using model-free adaptive control strategy.

1.5 Thesis contributions and outline

1.5.1 Contributions

The main contributions of thesis are as follows:

- The jerk-based Augmented output signal (AOS) is proposed for the feed drive system. Specifically, SAC requires the plant to be ASPR for it to be applied. The ASPR property is difficult to be satisfied in physical systems. The proposed method guarantees ASPR property for the feed drive systems without altering the poles of the system. The jerk signal is introduced for the AOS to further increase the responsiveness of the system.
- Using the jerk-based augmented output signal, in terms of tracking accuracy, it is more superior to the Parallel feedforward compensator (PFC) approach, which is the typical method used. The proposed method modifies the feedback signal of the system by including the velocity, acceleration, and jerk signals to the plant's output, and relative gains are

assigned to each signal. The high tracking accuracy is achieved by selecting the maximum allowable values for the relative gains. This is verified by simulations and experiments with comparisons to the typical method of PFC.

- Based on the energy-saving capability, the proposed method has smoother control input than the PFC approach; this is due to the faster response achieved. by adding zeros to the transfer function, while the PFC method adds poles and relocates zeros to the system making the system response slow. In addition, the proposed method has little or no effect on plant performance at high frequencies, in contrast to the PFC approach, where significant tracking deviations to the plant were observed.

- Simple adaptive contouring control (SACC) for the bi-axial feed drive systems is proposed. The SACC technique is designed by using SAC and following tangent-contour control with the modified reference adjustment for estimating the contour and tangent errors. Reference adjustment is a coordinate transform-based methodology used to decouple tracking errors to tangent and normal components. The jerk-based augmented output signal is used for the ASPR property. The addition of the jerk signal to the AOS improves the response of the system resulting to a low steady-state error.

- A modified integral terminal sliding mode control is proposed for industrial feed drive systems. This is accomplished by using SAC to construct the equivalent control for fractional conventional integral terminal sliding mode control which will remove the problem of unknown plant parameters and dynamics. In addition augmented output signal with terminal sliding surface is used to derive the adaptive control law with switching corrective control input gain to counteract the disturbances. Simulation and experiments were conducted using the proposed approach compared to conventional approaches. The proposed approach has shown to achieve higher tracking accuracy compared to the conventional approaches under the same tracking conditions.

1.5.2 Design specifications

The main aim is to achieve zero steady-state error and fast transient response. This is accomplished by selecting the highest possible adaptation scaling factors for each controller to achieve the relative goal. The characteristics for transient response are summarized including the rise time, which is the time for the system to respond from 10% to 90% of its final value, and overshoot, percentage by which the response exceeds the desired value. In addition, settling time is the time required for the response to stay within a certain percentage (commonly 2% or 5%) of the final value, along with peak time, defined as the time taken to reach the maximum response and stability margin for unit step functions.

1.5.3 Outline

The remainder of this thesis is organized as follows: Chapter 2 presents fundamentals of simple adaptive control for ASPR plants are described to set precedent for the following chapters. Furthermore, the recent new concept of terminal at tractor inclusion to sliding mode and its shortcoming is also discussed and dynamics of a ball-screw feed drive systems used for simulation studies. Chapter 3 describes the use of jerk in augmented output signal feedback for ASPR property for SAC implementation in the feed drive systems. The ASPR property guarantees the stability of the ASPR property for the feed drive systems even when gains are high. The jerk signal is introduced for the AOS to further increase the responsiveness of the system. Chapter 4 extends the study in Chapter 3 by considering contouring control which is highly recommended for the feed drive applications and thus, Simple adaptive contouring control (SACC) is proposed. Chapter 5 proposes a modified SAC algorithm made of integral terminal sliding mode control procedures for industrial feed drive systems. In this chapter a more effective scheme is developed using augmented output signal. Chapter 6 presents conclusion and future works.

Chapter 2

Literature review and preliminaries

2.1 Simple adaptive control

In this section, a basic concept of the SAC is viewed for the sake of brevity of discussions in the following chapters. First, the command generator tracker Command generator tracker (CGT) theory which is a basic theory on the SAC scheme is discussed. A sufficient condition, under which the signals generated by the CGT are bounded. Almost strictly positive real (ASPR) conditions for single-input/single-output (SISO) plants are also described. The SAC is a direct model reference adaptive control based on the CGT theory. SAC adaptively adjusts parameters in the CGT to have the ideal control input for unknown plants. The SAC also is a control strategy based on the almost strictly positive realness (ASPR-ness) of the controlled plant. Under the ASPR condition, the stability of the closed-loop system with output feedback. In the SAC system, the feedback gain is required to ensure the stability of the control system is also adaptively adjusted.

2.1.1 Command generator tracker

The idea was proposed by Broussard and O'Brien [36] for which the ideal control input achieves perfect model output tracking with regard to a feedforward control problem. To understand this concept, consider the following continuous linear time-invariant plant:

$$\dot{\mathbf{x}}(t) = \mathbf{A}\mathbf{x}(t) + \mathbf{B}\mathbf{u}(t), \tag{2.1}$$

$$\mathbf{y}(t) = \mathbf{C}\mathbf{x}(t) + \mathbf{D}\mathbf{u}(t), \tag{2.2}$$

where $\mathbf{x}(t)$, $\mathbf{u}(t)$, and $\mathbf{y}(t)$ are vectors and $\mathbf{A}$, $\mathbf{B}$, $\mathbf{C}$, and $\mathbf{D}$ are matrices appropriate size. It is assumed that the pair $(\mathbf{A}, \mathbf{B})$ is controllable and the pair $(\mathbf{A}, \mathbf{C})$ is observable. Reference model is used to specify a desired response of an adaptive control system to a command input. It is essentially a command shaping filter to achieve a desired command following. Adaptive control is formulated as a command following or tracking control, the adaptation is operated on the tracking error between the reference model and the system output. A reference model must be designed properly for an adaptive control system to be able to follow. Typically, a reference model is formulated as a linear time invariant model. The reference model order is designed to match the nominal system combined with a compensator that meets system specifications. Consequently, the reference model order should be at least equal to the plant's order. The initial conditions for the reference model must be set so that the initial output vectors of both the plant and the reference model are identical [37]. The model to be followed is represented as

$$\dot{\mathbf{x}}_m(t) = \mathbf{A}_m\mathbf{x}_m(t) + \mathbf{B}_m\mathbf{u}_m(t), \tag{2.3}$$

$$\mathbf{y}_m(t) = \mathbf{C}_m\mathbf{x}_m(t) + \mathbf{D}_m\mathbf{u}_m(t), \tag{2.4}$$

where $\mathbf{x}_m(t)$, $\mathbf{u}_m(t)$, and $\mathbf{y}_m(t)$ are vectors, respectively. The constant matrices $\mathbf{A}_m$, $\mathbf{B}_m$, $\mathbf{C}_m$, and $\mathbf{D}_m$ are of appropriate size. The problem of determining the perfect tracking solution is formulated as follows: develop a control $\mathbf{u}(t)$ that forces the command error $\mathbf{e}_y(t)$ where

$$\mathbf{e}_y(t) = \begin{bmatrix} \mathbf{C} & \mathbf{D} \end{bmatrix} \begin{bmatrix} \mathbf{x}(t) \\ \mathbf{u}(t) \end{bmatrix} - \begin{bmatrix} \mathbf{C}_m & \mathbf{D}_m \end{bmatrix} \begin{bmatrix} \mathbf{x}_m(t) \\ \mathbf{u}_m(t) \end{bmatrix} = \mathbf{y}(t) - \mathbf{y}_m(t), \tag{2.5}$$

to be zero for all $t > 0$, if $\mathbf{e}_y(t) = 0$. When the command error is zero for $t > 0$, and perfect tracking occurs, the resulting plant state and control trajectories are denoted as $\mathbf{x}^*(t)$ and $\mathbf{u}^*(t)$. By definition, $\mathbf{x}^*(t)$ and $\mathbf{u}^*(t)$ satisfy

$$\mathbf{y}^*(t) = \begin{bmatrix} \mathbf{C} & \mathbf{D} \end{bmatrix} \begin{bmatrix} \mathbf{x}^*(t) \\ \mathbf{u}^*(t) \end{bmatrix} = \begin{bmatrix} \mathbf{C}_m & \mathbf{D}_m \end{bmatrix} \begin{bmatrix} \mathbf{x}_m(t) \\ \mathbf{u}_m(t) \end{bmatrix} = \mathbf{y}_m(t), \tag{2.6}$$

which attempts to move the plant toward those "ideal trajectories" that would guarantee perfect tracking and the various "ideal trajectories" are defined for reference as those trajectories that allow perfect tracking in ideal conditions, without disturbances. The exists, the ideal trajectories have the form

$$\dot{\mathbf{x}}^*(t) = \mathbf{A}\mathbf{x}^*(t) + \mathbf{B}\mathbf{u}^*(t), \tag{2.7}$$

and the ideal control signal is

$$\mathbf{u}^*(t) = \mathbf{K}_x^*\mathbf{x}_m(t) + \mathbf{K}_u^*\mathbf{u}_m(t), \tag{2.8}$$

for perfect following, the various gains in (2.7-2.8) must satisfy the assumption there exists $\mathbf{\Omega}_{ij}$ are solutions of the following expressions:

$$\begin{bmatrix} \mathbf{x}^*(t) \\ \mathbf{u}^*(t) \end{bmatrix} = \begin{bmatrix} \mathbf{S}_{11} & \mathbf{S}_{12} \\ \mathbf{K}_x^* & \mathbf{K}_u^* \end{bmatrix} \begin{bmatrix} \mathbf{x}_m(t) \\ \mathbf{u}_m(t) \end{bmatrix}, \tag{2.9}$$

$$\begin{bmatrix} \mathbf{A} & \mathbf{B} \\ \mathbf{C} & \mathbf{D} \end{bmatrix}^{-1} = \begin{bmatrix} \mathbf{\Omega}_{11} & \mathbf{\Omega}_{12} \\ \mathbf{\Omega}_{21} & \mathbf{\Omega}_{22} \end{bmatrix}, \tag{2.10}$$

provided the plant $\{\mathbf{A}, \mathbf{B}, \mathbf{C}, \mathbf{D}\}$ is non-singular. Its worth mentioning that no eigenvalue of $\mathbf{\Omega}_{11}$ is equal to the inverse of an eigenvalue of $\mathbf{A}_m$ and the condition

$$\begin{bmatrix} \mathbf{S}_{11} & \mathbf{S}_{12} \\ \mathbf{K}_x^* & \mathbf{K}_u^* \end{bmatrix} = \begin{bmatrix} \mathbf{\Omega}_{11} & \mathbf{\Omega}_{12} \\ \mathbf{\Omega}_{21} & \mathbf{\Omega}_{22} \end{bmatrix} \begin{bmatrix} \mathbf{S}_{11}\mathbf{A}_m & \mathbf{S}_{11}\mathbf{B}_m \\ \mathbf{C}_m & \mathbf{D}_m \end{bmatrix}, \tag{2.11}$$

holds, $\mathbf{K}_x^*$ and $\mathbf{K}_u^*$ are the constant feedforward gain matrices and their solutions including $\mathbf{S}_{11}$ and $\mathbf{S}_{12}$ exists under the ASPR conditions [38, 39]. The ASPR conditions are given in detailed in the next section.

2.1.2 Almost strict positive realness

The property of Almost Strict Positive Realness (ASPR-ness) for a plant is defined by the presence of an output feedback that makes the closed-loop transfer function a Strictly positive real (SPR). For the SAC adaptive algorithm, it requires for the plant to be SPR when constructing the Lyapunov function, which guarantees the stability of the entire adaptive system. The Almost strict positive real (ASPR) characteristic of the plant is a more lenient requirement than SPR. Its worth noting that ASPR transfer functions remain stable under any high-gain positive definite feedback, whether its either fixed, nonlinear, or non-stationary.

ASPR condition for single-input-single-output plants [37]:

1. The relative degree of the plant transfer function is not exceeding unity,
2. The plant transfer function is stable and minimum-phase,
3. The leading coefficient of the plant transfer function is positive.

2.1.3 Control adaptive algorithm

If an 'ideal' solution for the fixed gains that perform perfect tracking exists, adaptive algorithms can be implemented to reach ideal gains after adaptation. In the CGT methodology, one forms the following 'ideal control' input to the plant:

$$\mathbf{u}^*(t) = \mathbf{K}_e^*(\mathbf{y}_m(t) - \mathbf{y}(t)) + \mathbf{K}_x^*\mathbf{x}_m(t) + \mathbf{K}_u^*\mathbf{u}_m(t), \tag{2.12}$$

where $\mathbf{K}_e^*$ is any stabilizing gain, while $\mathbf{K}_x^*$ and $\mathbf{K}_u^*$ are the ideal feedforward control gains to track the model perfectly when it moves along the ideal trajectories $\mathbf{x}_p^*(t)$. Otherwise, there is a state error $\mathbf{e}_x(t)$ between the desired trajectory and the actual plant trajectory given as $\mathbf{e}_x^*(t) = \mathbf{x}^*(t) - \mathbf{x}(t)$ and from state error, the tracking error can be defined as

$$\mathbf{e}_y(t) = \mathbf{y}_m(t) - \mathbf{y}(t) = \mathbf{C}\mathbf{x}^*(t) + \mathbf{D}\mathbf{u}^*(t) - \mathbf{C}\mathbf{x}(t) - \mathbf{D}\mathbf{u}(t), \tag{2.13}$$

$$\mathbf{e}_y(t) = \mathbf{C}\mathbf{e}_x(t) + \mathbf{D}(\mathbf{u}^*(t) - \mathbf{u}(t)), \tag{2.14}$$

As it is difficult to realize full knowledge about the plant parameters, an adaptive algorithm can be used to implement the control gains. The constructed SAC system is shown in Fig. 2.1. The constant ideal gains in (2.12) are replaced with time-varying adaptive gains that are calculated

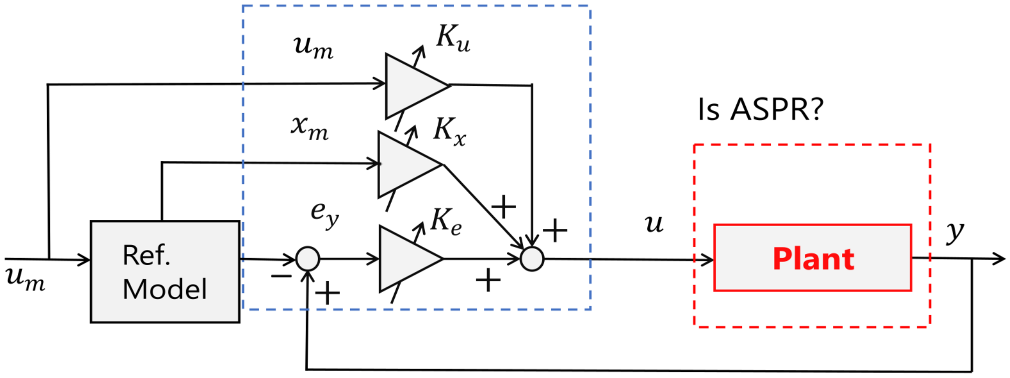

Figure 2.1: Overall block-diagram of SAC architecture

by an adaptive algorithm as follows:

$$\mathbf{u}(t) = \mathbf{K}_e(t)\mathbf{e}_y(t) + \mathbf{K}_x(t)\mathbf{x}_m(t) + \mathbf{K}_u(t)\mathbf{u}_m(t), \tag{2.15}$$

$$\mathbf{u}(t) = \mathbf{K}(t)\mathbf{r}(t), \tag{2.16}$$

with

$$\mathbf{K}(t) = \begin{bmatrix} \mathbf{K}_e(t) & \mathbf{K}_x(t) & \mathbf{K}_u(t) \end{bmatrix}, \tag{2.17}$$

$$\mathbf{r}(t) = \begin{bmatrix} \mathbf{e}_y^{\mathrm{T}}(t) & \mathbf{x}_m^{\mathrm{T}}(t) & \mathbf{u}_m^{\mathrm{T}}(t) \end{bmatrix}^{\mathrm{T}}, \tag{2.18}$$

using the measurable tracking error $\mathbf{e}_y(t)$ and available signals, the adaptive gain is adjusted as proportional and integral terms as follows:

$$\mathbf{K}(t) = \mathbf{K}_I(t) + \mathbf{K}_p(t), \tag{2.19}$$

with integral term adjusted as

$$\dot{\mathbf{K}}_I(t) = \mathbf{e}_y(t)\mathbf{r}^{\mathrm{T}}(t)\mathbf{\Gamma}_I, \tag{2.20}$$

$$\mathbf{K}_I(0) = \mathbf{K}_{I0}, \tag{2.21}$$

$$\mathbf{\Gamma}_I = \begin{bmatrix} \mathbf{\Gamma}_{eI} & \mathbf{0} & \mathbf{0} \\ \mathbf{0} & \mathbf{\Gamma}_{xI} & \mathbf{0} \\ \mathbf{0} & \mathbf{0} & \mathbf{\Gamma}_{uI} \end{bmatrix}, \tag{2.22}$$

where $\mathbf{K}_{I0}$ is the initial integral gain and the proportional adaptive gain is given as

$$\mathbf{K}_p(t) = \mathbf{e}_y(t)\mathbf{r}^{\mathrm{T}}(t)\mathbf{\Gamma}_p, \tag{2.23}$$

$$\mathbf{\Gamma}_p = \begin{bmatrix} \mathbf{\Gamma}_{eP} & \mathbf{0} & \mathbf{0} \\ \mathbf{0} & \mathbf{\Gamma}_{xP} & \mathbf{0} \\ \mathbf{0} & \mathbf{0} & \mathbf{\Gamma}_{uP} \end{bmatrix}, \tag{2.24}$$

the matrices $\mathbf{\Gamma}_I$ and $\mathbf{\Gamma}_p$ are time-invariant weighting matrices that control the rate of adaptation to the tracking error convergence. In addition, the proportional gain has the effect of increasing the rate of convergence of the system towards perfect tracking. The partitioned matrices are given as

$$\mathbf{K}_e(t) = \mathbf{K}_{I_e}(t) + \mathbf{K}_{p_e}(t), \tag{2.25}$$

$$\mathbf{K}_x(t) = \mathbf{K}_{I_x}(t) + \mathbf{K}_{p_x}(t), \tag{2.26}$$

$$\mathbf{K}_u(t) = \mathbf{K}_{I_u}(t) + \mathbf{K}_{p_u}(t), \tag{2.27}$$

where

$$\dot{\mathbf{K}}_{Ie}(t) = \mathbf{e}_y(t)\mathbf{e}_y^{\mathrm{T}}(t)\mathbf{\Gamma}_{eI}, \mathbf{\Gamma}_{eI} > 0, \tag{2.28}$$

$$\mathbf{K}_{p_e}(t) = \mathbf{e}_y(t)\mathbf{e}_y^{\mathrm{T}}(t)\mathbf{\Gamma}_{eP}, \mathbf{\Gamma}_{eP} \geq 0, \tag{2.29}$$

$$\dot{\mathbf{K}}_{Ix}(t) = \mathbf{e}_y(t)\mathbf{x}_m^{\mathrm{T}}(t)\mathbf{\Gamma}_{xI}, \mathbf{\Gamma}_{xI} > 0, \tag{2.30}$$

$$\mathbf{K}_{p_x}(t) = \mathbf{e}_y(t)\mathbf{x}_m^{\mathrm{T}}(t)\mathbf{\Gamma}_{xP}, \mathbf{\Gamma}_{xP} \geq 0, \tag{2.31}$$

$$\dot{\mathbf{K}}_{Iu}(t) = \mathbf{e}_y(t)\mathbf{u}_m^{\mathrm{T}}(t)\mathbf{\Gamma}_{uI}, \mathbf{\Gamma}_{uI} > 0, \tag{2.32}$$

$$\mathbf{K}_{p_u}(t) = \mathbf{e}_y(t)\mathbf{u}_m^{\mathrm{T}}(t)\mathbf{\Gamma}_{uP}, \mathbf{\Gamma}_{uP} \geq 0, \tag{2.33}$$

The first term, $\mathbf{K}_e(t)\mathbf{e}_y(t)$ in (2.15) is required for the stability of the adaptive control system. The other two terms are introduced because of their contribution to the performance of the adaptive system, expressed by the negative terms in the derivative of the Lyapunov function. The proportional term is known to add an immediate penalty to the large errors driving them to small errors very fast [40]. The integral gain given in (2.20) is used to guarantee convergence. The stability proofs of SAC formulation and theorems in great detail are shown in [37]. Barkana [39] proved that the adaptive gains are made up of constant terms and of converging, diverging, or steady sinusoidal waves bounded. SPR systems are designed to maintain stability in adaptive systems, even with large gains. This allows for very high adaptation to be used as scaling factors, ensuring that the negative terms are weighted more heavily, which significantly reduces tracking errors. However, the gains can also become excessively or undesirably large.

2.1.4 Parallel feedforward compensator

The boundedness of all signals in the SAC system are guaranteed under the ASPR condition. However, most actual plants do not satisfy the ASPR condition. Hence this condition imposes a severe restriction on the plant with respect to the practical applicability of SAC. With this in mind Bar-Kana [41] first suggested that the non-ASPR plant can be made ASPR by implementing a PFC $F(s)$ on the plant. That is, if the plant is stabilized by a suitable dynamic output compensator $F(s)^{-1}$ and the gain of $F(s)$ can be selected small enough, then the augmented plant with PFC becomes ASPR and SAC is applied for the thus obtained augmented plant is obtained. However, its shown that PFC at low frequencies is relative small that the condition between the augmented output and actual plant is small compared to the high frequencies [42]. The PFC configuration can be designed with only simple first-order pole with low gain [43]. Higher-order PFC system with relative degree of 1 tends to possess more complex dynamics due to additional poles and the presence of the zeros can influence the transient response, potentially adding an overshoot or altering the initial slope of the response. However, because the relative degree is 1, there is a similarity to the first-order system on how the system eventually responds to a step input, particularly in the long-term behavior.

2.2 Integral terminal sliding mode control

In recent years, Integral terminal sliding mode control (ITSMC) has demonstrated impressive control performance. The significant features of integral terminal sliding mode control are better robustness and fast response with finite-time convergence. Finite-time convergence of the tracking errors and integral errors is obtained by integral terminal sliding mode control without the singular problem in comparison with conventional terminal sliding mode control [44]. The concept of terminal sliding mode was introduced by a notion of the use the terminal attractors which is a first-order dynamics with fractional-power. Consider the following dynamical model given as

$$\dot{\mathbf{x}}(t) = \mathbf{A}\mathbf{x}(t) + \mathbf{b}u(t) + \mathbf{b}d(t), \tag{2.34}$$

where $\mathbf{x}(t)$ is an n_p th-order plant state vector, $u(t)$ is the control input, $\mathbf{A}$ and $\mathbf{b}$ are matrix and vector of appropriate dimensions, respectively. $d(t)$ denotes the disturbances, which satisfy $|d(t)| \leq \bar{d}$, where $\bar{d} > 0$ has a constant. The state error $\mathbf{e}(t) = \mathbf{x}_d(t) - \mathbf{x}(t) = \begin{bmatrix} e_y(t) & \dot{e}_y(t) & ,\ldots, & e_y^{n_p-1}(t) \end{bmatrix}^{\mathrm{T}}$, ($\mathbf{x}_d(t)$, the desired state vector), then the sliding mode surface is designed as follows:

$$e_z(t) = \mathbf{c}^{\mathrm{T}}\mathbf{e}(t), \tag{2.35}$$

where $\mathbf{c} = \begin{bmatrix} c_1 & c_2 & ,\ldots, & c_{n_p} \end{bmatrix}^{\mathrm{T}}$ is the slope of the sliding surface. It is chosen that $c_{n_p} = 1$ and the coefficients $c_1, \ldots, c_{n_p-1}$ describe the sliding surface at $e_z(t) = 0$. The integral terminal sliding function s as follows:

$$s(t) = e_z(t) + \beta e_{Iz}(t), \tag{2.36}$$

where $e_z(t)$ is with (2.35), and $e_{Iz}(t)$ can be designed as

$$\dot{e}_{Iz}(t) = \mathrm{sign}(e_z(t))|e_z(t)|^{\chi}, \tag{2.37}$$

$$\dot{e}_{Iz} = \mathrm{sign}(e_z)|e_z|^{\chi}, \tag{2.38}$$

where $\beta > 0$, $0 < \chi < 1$, for any initial condition $e_z(0)$, $e_z(t)$ will converge to zero in the finite time given by

$$t_s = \beta^{-1}(1-\chi)^{-1}|e_z(0)|^{1-\chi}, \tag{2.39}$$

the reaching time t_s is adjustable using the parameters χ and β. Sliding functions (2.35 - 2.36) compose a recursive form ITSM. Given a proper control input to maintain $s(t) = 0$, the system will move along the sliding surface $s(t) = 0$ and then $e_z(t) = 0$ to the origin in finite time, respectively. The process of sliding mode control is divided into two phases, the approaching phase with $s(t) = 0$ and the sliding phase with $s(t) = 0$. A sufficient condition to guarantee that the trajectory of the error vector $\mathbf{e}(t)$ will translate from the approaching phase to the sliding phase is to select the control strategy such that

$$s(t)\dot{s}(t) \geq -\eta|s(t)|, \tag{2.40}$$

where η is a constant specifying the converging rate of $s(t)$, condition (2.40) is called the reaching condition [45]. Corresponding to the two phases, two types of control law can be derived separately. In the sliding phase, $s(t) = 0$ and $\dot{s}(t) = 0$, then the equivalent control $u_{eq}(t)$, which will force the system dynamics to stay on the sliding surface at $d(t) = 0$, is chosen as

$$\begin{aligned}
\dot{s}(t) &= \dot{e}_z(t) + \beta\dot{e}_{Iz}(t),\\
&= \mathbf{c}^{\mathrm{T}}\big[\ \dot{\mathbf{x}}_d(t) - \mathbf{A}\mathbf{x}(t) - \mathbf{b}u_{eq}(t)\big] + \beta\mathrm{sign}(e_z(t))|e_z(t)|^{\chi},\\
&= \mathbf{c}^{\mathrm{T}}\dot{\mathbf{x}}_d(t) - \mathbf{c}^{\mathrm{T}}\mathbf{A}\mathbf{x}(t) - \mathbf{c}^{\mathrm{T}}\mathbf{b}u_{eq}(t) + \beta\mathrm{sign}(e_z(t))|e_z(t)|^{\chi},\\
&= 0.
\end{aligned} \tag{2.41}$$

the equivalent control law $u_{eq}(t)$ is given by

$$u_{eq}(t) = (\mathbf{c}^{\mathrm{T}}\mathbf{b})^{-1}\big[\ \mathbf{c}^{\mathrm{T}}\dot{\mathbf{x}}_d(t) - \mathbf{c}^{\mathrm{T}}\mathbf{A}\mathbf{x}(t) + \beta\mathrm{sign}(e_z(t))|e_z(t)|^{\chi}\big], \tag{2.42}$$

$$u_{eq} = (\mathbf{c}^{\mathrm{T}}\mathbf{b})^{-1}\big[\ \mathbf{c}^{\mathrm{T}}\dot{\mathbf{x}}_d - \mathbf{c}^{\mathrm{T}}\mathbf{A}\mathbf{x} + \beta\mathrm{sign}(e_z)|e_z|^{\chi}\big], \tag{2.43}$$

in the approaching phase, where $s(t) \neq 0$, in order to satisfy the reaching condition (2.40), a corrective control term (or the so-called switching function) $(u_n(t))$ is added. The corrective control can be chosen as

$$u_n(t) = K_s\mathrm{sign}(s(t)), K_s = (\mathbf{c}^{\mathrm{T}}\mathbf{b})^{-1}k_s, k_s \geq \bar{d} + \eta, \tag{2.44}$$

where K_s is the switching gain. The control input will be designed in the following form:

$$u(t) = u_{eq}(t) + u_n(t). \tag{2.45}$$

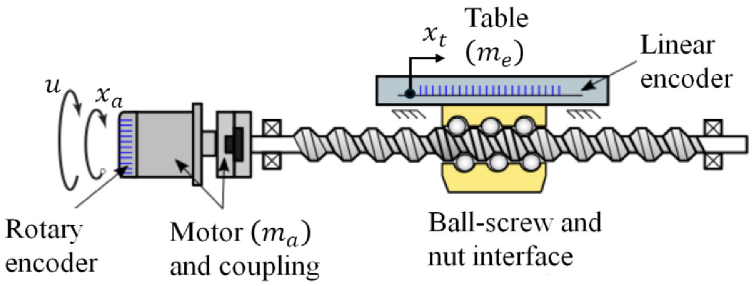

(a) Schematic of ball-screw mechanism

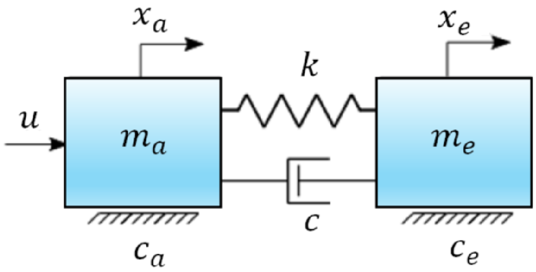

(b) Two-mass lumped model

Figure 2.2: Feed drive system structure

The main disadvantage of this approach is the difficulty in calculating equivalent control law $u_{eq}(t)$ in (2.43) of ITSMC as it requires thorough knowledge of the controlled plant parameters and dynamics. In this thesis, the ITSMC law is modified by using SAC for equivalent control law and neglecting the need for plant parameters and dynamics. For the sake of clarity, the time index t will be removed from this point on and used only when necessary.

2.3 Industrial feed drive systems

Most industrial feed drive systems are driven by ball-screw transmission mechanisms. A schematic diagram of the mechanical structure of a ball-screw feed drive system is shown in Fig. 2.2 (a), and its physical two mass lumped-mass model is illustrated in Fig. 2.2 (b). A rotary motor drives a ball-screw to realize linear motion of the table. Because of their simple structure transmission components, most ball-screw feed drives are flexible, and their attainable positioning accuracy is limited by structural vibrations [46]. The drive system generates the motor torque u and transmits it to the moving table via the ball-screw, to achieve a high-precision position control of the table. The equation of motion for the concentrated mass model is written as:

$$m_a \ddot{x}_a = u - c_a \dot{x}_a - c(\dot{x}_a - \dot{x}_e) - k(x_a - x_e), \tag{2.46}$$

$$m_e \ddot{x}_e = -c_e \dot{x}_e - c(\dot{x}_e - \dot{x}_a) - k(x_e - x_a) \tag{2.47}$$

where m_a and m_e denote motor and table inertia, whereas k and c are spring and viscous damping coefficients. c_a and c_e depict viscous friction originating from guide ways and bearing systems. Furthermore, where x_a and x_e are the motor and table displacements. u is the control signal. Equations (2.46) and (2.47) are converted to state-space form by selecting of four states. In typical ball-screw setups, motor and table positions and velocities are measured from rotary and scale systems [9]. Select the state vector as $\mathbf{x} = \begin{bmatrix} x_e & \dot{x}_e & x_a & \dot{x}_a \end{bmatrix}^{\mathrm{T}}$ yields the following state-space system:

$$\dot{\mathbf{x}} = \begin{bmatrix} 0 & 1 & 0 & 0 \\ \frac{-k}{m_e} & \frac{-c-c_e}{m_e} & \frac{k}{m_e} & \frac{c}{m_e} \\ 0 & 0 & 0 & 1 \\ \frac{k}{m_a} & \frac{c}{m_a} & \frac{-k}{m_a} & \frac{-c-c_a}{m_a} \end{bmatrix} \mathbf{x} + \begin{bmatrix} 0 \\ 0 \\ 0 \\ \frac{1}{m_a} \end{bmatrix} u. \tag{2.48}$$

Equation (2.48) is assumed to be both controllable and observable. Industrial feed drive systems typically use collocated control schemes for higher stability margins [47]. This strategy ensures that the motor follows the reference position command precisely, and it is assumed that the table follows the motor accurately. This representation is used in the coming chapters for simulation purposes. Experimental verification is completed by an industrial feed drive system represented by schematic diagram shown in Fig. 2.3 with AC servo motor specifications described in Table. 2.1.

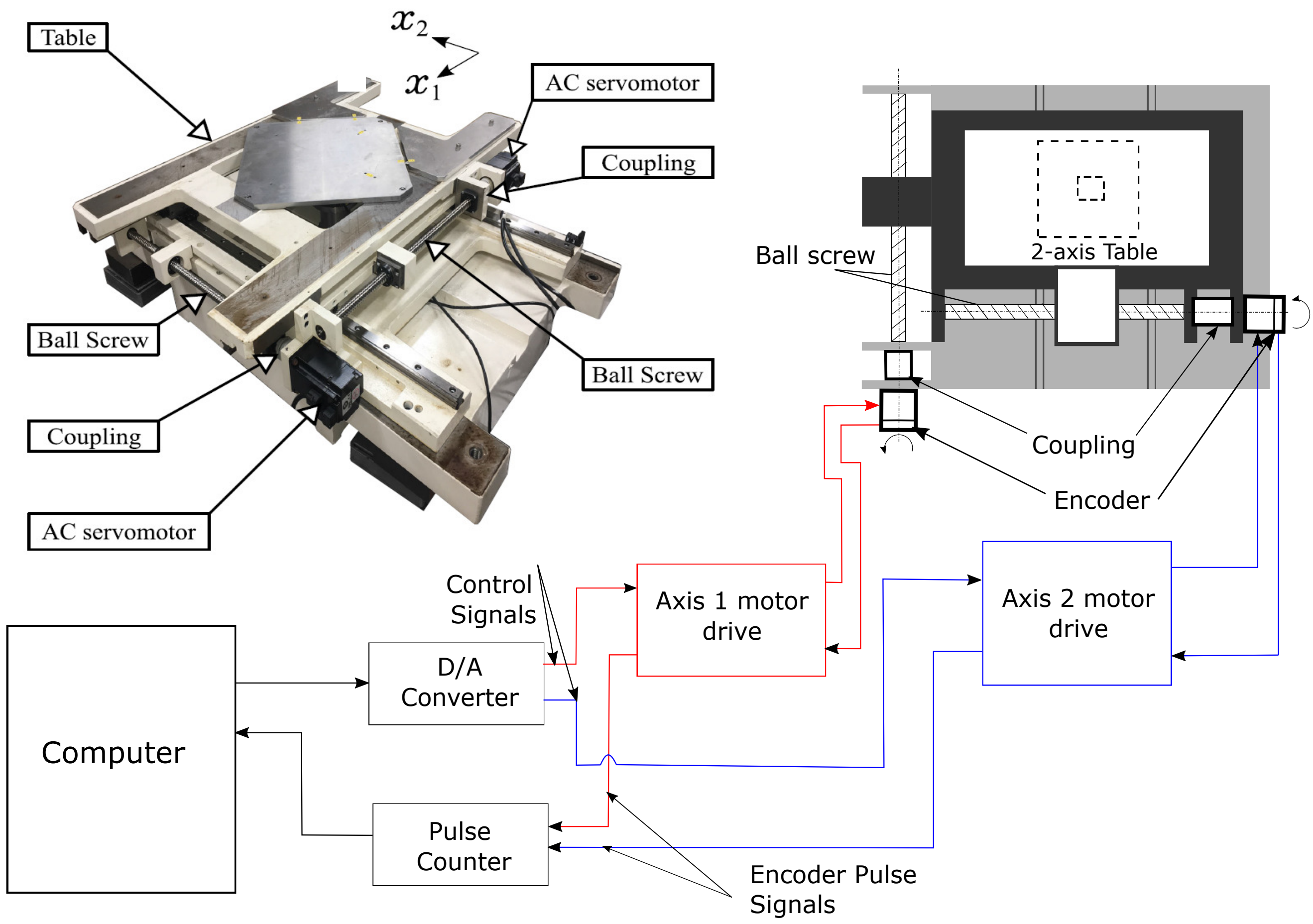

Figure 2.3: Schematic diagram for the industrial feed drive system

Table 2.1: AC Servo motor overview

Specification	1st axis	2nd axis
Power capacity	200 W	400 W
Rated torque	0.637 Nm	1.27 Nm
Rated rotation speed	3000 rpm	6000 rpm
Encoder	17bit incremental	17bit incremental
Linear resolution	76.29 nm	76.29 nm

Chapter 3

Simple adaptive control using a jerk-based augmented output signal

This chapter proposes the use of jerk-based augmented output signal for the ASPR property in SAC implementation for industrial feed drive systems. The application of the SAC requires that the "almost strictly positive real (ASPR)" property is satisfied and there is a command general tracking solution for the plant and the reference model. The ASPR property is difficult to be satisfied in physical systems. The proposed approach allows the SAC to track the desired signal at high frequencies more precise and is achieved by placing the zeros of the system at effective locations. To verify the feasibility of the proposed approach, simulation and experiment are conducted. The results are compared with those of the commonly used parallel feedforward compensation (PFC) approach. Experimental results revealed that the proposed approach reduced the tracking error by about 80% compared to PFC without any additional control input. Moreover, the proposed approach has been proved to be energy-efficient by about 21% than PFC under similar tracking conditions.

In this chapter, the jerk signal is introduced for the augmented output signal to improve the responsiveness of the system, and apart from the ASPR property, other merits of the proposed method are higher tracking accuracy, the proposed method is superior to the PFC approach. The proposed method modifies the feedback signal of the system by including the velocity, acceleration, and jerk signals to the plant's output and constant relative gains are assigned to each signal, respectively. The high tracking accuracy is achieved by selecting the maximum allowable values for the relative gains. Furthermore, the proposed method has little or no effect on plant performance at high frequencies, in contrast to the PFC approach, where significant tracking deviations to the plant were observed. In addition, the proposed method has smoother control input than the PFC approach, this is due to the faster response achieved by adding zeros to the transfer function while the PFC method adds poles and relocate zeros to the system making the system response slow.

This chapter is organized as follows: Section 3.1 presents the related works. A dynamic model of system is presented in section 3.2. Design of SAC is described in section 3.3, followed by simulation and experiment in section 3.4. Section 3.5 discusses results, followed by concluding remarks in section 3.6.

3.1 Related works

To successfully apply the SAC to a real system, a compound general tracking (CGT) solution and the "almost strictly positive real (ASPR)" property are required to be satisfied [42]. The typical dynamic models used in ball-screw control applications are second and fourth-order models that are not ASPR. Therefore, other methods are needed to meet the ASPR requirement. The parallel feedforward compensation (PFC) method was introduced by Bar-Kana [41] to make the system ASPR. Many applications of the SAC have employed the PFC [20, 48, 49]. However, the PFC approach deviates the output signal from the desired which increases the tracking error. There have been numerous proposals for improving the situation by researchers. Sato *et al.* [50] proposed a null space steady-state tracking error making the PFC output zero, leaving the augmented system output in a steady state. However, the approach is associated to have with a spike in the control variable and stability is not fully analyzed. Adaptive PFC with a filter and the radial basis function is proposed in [51] for the ASPR property on unstable systems. Despite the robustness of the work in [51] there is still a lag on tracking error performance. Guan *et al.* [52] proposed a data driven principal component analysis with the PFC approach to increase performance of the output feedback for the strictly passive systems. However, the tracking error has not been significantly reduced. Harada and Uchiyama [53] proposed robust simple adaptive control with friction compensation using the augmented output signal with position and velocity information for the ASPR property. Sato and Uchiyama [54] proposed an approach of the SAC using augmented output signal with position, velocity, and acceleration information for the ASPR property using accelerometer for acceleration and encoder for position measurement. The results of these studies have shown a considerable improvement in tracking accuracy of the feed drive system.

3.2 Dynamic model

A two-mass lumped model as shown in Fig. 3.1 is used to represent a dynamic model for industrial feed drive systems, and its state-space model is described as follows:

$$\dot{\mathbf{x}}_p = \mathbf{A}_p \mathbf{x}_p + \mathbf{b}_p u_p, \tag{3.1}$$

$$y_p = \mathbf{c}_p^{\mathrm{T}} \mathbf{x}_p + d_p u_p, \tag{3.2}$$

with

$$\mathbf{A}_p = \begin{bmatrix} 0 & 1 & 0 & 0 \\ \frac{-g}{m_e} & \frac{-c-c_e}{m_e} & \frac{g}{m_e} & \frac{c}{m_e} \\ 0 & 0 & 0 & 1 \\ \frac{g}{m_a} & \frac{c}{m_a} & \frac{-g}{m_a} & \frac{-c-c_a}{m_a} \end{bmatrix}, \tag{3.3}$$

$$\mathbf{b}_p = \begin{bmatrix} 0 & 0 & 0 & 1/m_a \end{bmatrix}^{\mathrm{T}}, \tag{3.4}$$

$$\mathbf{x}_p = \begin{bmatrix} x_e & \dot{x}_e & x_a & \dot{x}_a \end{bmatrix}^{\mathrm{T}}, \tag{3.5}$$

$$\mathbf{c}_p = \begin{bmatrix} 1 & 0 & 0 & 0 \end{bmatrix}^{\mathrm{T}}, \tag{3.6}$$

$$d_p = 0, \tag{3.7}$$

where m_a and m_e are the actuator and table masses, respectively. The masses are connected by a damper (viscous friction coefficient c) and a spring (spring constant g). The masses m_a and m_e are subjected to viscous friction coefficients c_a and c_e, respectively. The output of the feed drive system is the position of the table mass m_e. State variables x_e and $\dot{x}_e$ are the position and velocity of the table, respectively. x_a and $\dot{x}_a$ are the state variables of the position and velocity of the actuator, respectively. f_a is the control input of the model.

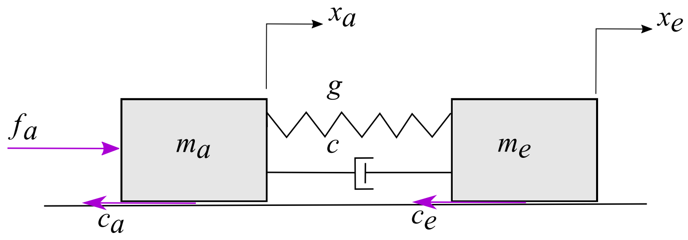

Figure 3.1: Two-mass lumped model

3.3 Design of simple adaptive control

3.3.1 Preliminaries

This section considers the SAC for an unknown single-input and single-output plant. The SAC implementation requires a compound general tracking (CGT) solution and ASPR property in a plant [55]. A reference model is defined as

$$\dot{\mathbf{x}}_m = \mathbf{A}_m \mathbf{x}_m + \mathbf{b}_m u_m, \tag{3.8}$$

$$y_m = \mathbf{c}_m^{\mathrm{T}} \mathbf{x}_m + d_m u_m, \tag{3.9}$$

where $\mathbf{x}_m \in R^{n_m}$, $y_m \in R$, and $u_m \in R$ are the states, output, and input, respectively. $\mathbf{A}_m$, $\mathbf{b}_m$, $\mathbf{c}_m$, and d_m correspond to systems matrix, input vector, output vector, and feed through coefficient, respectively.

The reference model defines the desired system behavior. It is necessary for the order of a reference model to be equal or larger than that of a plant to ensure perfect tracking. When the plant is considered as the mass lumped model, the reference model is considered to be set with the dimension of $n_p + 1$, where n_p is the order of the plant model. Input u_m is assumed to be bounded and piece-wise continuous.

The perfect output tracking occurs when $y_p = y_m$ for $t \geq 0$, there exists an ideal plant with corresponding ideal states $\mathbf{x}_p^*$, input u_p^*, and output y_p^* for which state space representation is given as

$$\dot{\mathbf{x}}_p^* = \mathbf{A}_p^* \mathbf{x}_p^* + \mathbf{b}_p^* u_p^*, \tag{3.10}$$

$$y_p^* = \mathbf{c}_p^{*\mathrm{T}} \mathbf{x}_p^* + d_p^* u_p^*. \tag{3.11}$$

$\mathbf{A}_p^*$, $\mathbf{b}_p^*$, $\mathbf{c}_p^*$, and d_p^* are the ASPR plant matrix, vector with appropriate dimensions and scalar, respectively. Since $\mathbf{x}_m$ and u_m are of arbitrary in nature, by selecting the stable and correct coefficients of the characteristic equation, the CGT condition can be satisfied [37]. The ideal output is identical to output of the reference model given as

$$y_p^* = y_m, \tag{3.12}$$

$$\begin{bmatrix} \mathbf{c}_p^{*\mathrm{T}} & d_p^* \end{bmatrix} \begin{bmatrix} \mathbf{x}_p^* \\ u_p^* \end{bmatrix} = \begin{bmatrix} \mathbf{c}_m^{\mathrm{T}} & d_m \end{bmatrix} \begin{bmatrix} \mathbf{x}_m \\ u_m \end{bmatrix}, \tag{3.13}$$

with tracking error defined as $e_y = y_m - y_p$, then the following control input was proposed [37]:

$$u_p = k_e e_y + \mathbf{k}_x^{\mathrm{T}} \mathbf{x}_m + k_u u_m. \tag{3.14}$$

The regressor vector $\mathbf{r}$ and adaptive gains $\mathbf{k}$ are defined as

$$\mathbf{r} = \begin{bmatrix} e_y & \mathbf{x}_m^{\mathrm{T}} & u_m \end{bmatrix}^{\mathrm{T}}, \tag{3.15}$$

$$\mathbf{k} = \begin{bmatrix} k_e & \mathbf{k}_x^{\mathrm{T}} & k_u \end{bmatrix}^{\mathrm{T}}. \tag{3.16}$$

The adaptive gains are combination of integral and proportional terms as

$$\mathbf{k} = \mathbf{k}_p + \mathbf{k}_I, \tag{3.17}$$

on which

$$\mathbf{k}_p = \mathbf{\Gamma}_p \mathbf{r} e_y, \tag{3.18}$$

$$\dot{\mathbf{k}}_I = \mathbf{\Gamma}_I \mathbf{r} e_y - \xi \mathbf{k}_I, \xi \geq 0. \tag{3.19}$$

$\mathbf{\Gamma}_p$ and $\mathbf{\Gamma}_I$ are the positive semi-definite and positive definite matrices, respectively. The adaptive control law (3.14) is given by

$$u_p = \mathbf{k}^{\mathrm{T}} \mathbf{r}, \tag{3.20}$$

A system $G(s)$ is said to be ASPR if there exists a gain k_e^* that makes a closed loop transfer function become $Z(s) = G(s)\{1 + k_e^* G(s)\}^{-1}$ "strictly positive real (SPR)". If $Z(s)$ is SPR then $Z^{-1}(s)$ is strictly stable. The sufficient conditions for a system to be ASPR are given as follows [37]:

1. The plant must have the relative degree of 0 or 1.
2. The plant must be minimum-phase.
3. The highest frequency gain of the plant must be positive.

The plant (3.1) in s-domain has a relative degree of 3 and condition 1 is not satisfied. A static feedback only cannot stabilize the plant, and hence approaches for the ASPR are presented as follows.

3.3.2 PFC approach for ASPR property

Figure 3.2 shows a stable PFC controller $F(s)$ placed parallel with plant $G_p(s)$ sharing the same control input u_p. This gives an extended system $G_a(s) = G_p(s) + F(s)$ and the closed loop system becomes $Z(s) = G_p(s)F^{-1}(s)\{1 + G_p(s)F^{-1}(s)\}^{-1}$. Adding the stabilizing controller $F(s)$ leads to output signal $y_a(s) = \{G_p(s) + F(s)\}u_p(s)$, $F(s)$ must have a relative degree of 1. This ensures the augmented plant $G_a(s)$ results to a relative degree of 1, hence the ASPR property is satisfied.

3.3.3 AOS approach for ASPR property

The augmented output signal (AOS) is another approach to ensure the ASPR property is achieved for mass lumped models. The AOS with position and velocity signals for industrial feed drive system is used to achieve the ASPR property [53]. In this approach, a single-mass lumped model with a relative degree of 2 was considered for the design and the AOS with position and velocity signals was applied, resulting in an augmented system with a relative degree of 1 that satisfies the ASPR property. In addition, the AOS with position, velocity, and acceleration signals using a two-mass lumped model for the industrial drive system is considered to meet the ASPR property [54]. This study extends the augmented output signal approach for

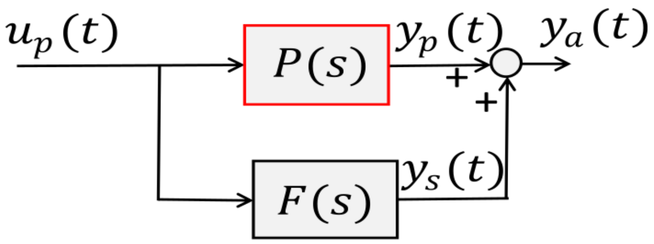

Figure 3.2: Parallel feedforward compensation approach

the ASPR property by including the position, velocity, acceleration, and jerk signals (Jerk-based AOS) from the plant as shown in Fig. 3.3. The jerk signal improves the system responsiveness and the plant becomes ASPR with a relative degree of 0. The transfer function with jerk-based AOS is given by

$$G_p = \frac{(cs+g)(1+\lambda_1 s+\lambda_2 s^2+\lambda_3 s^3)}{\sigma_1 s^4+\sigma_2 s^3+\sigma_3 s^2+\sigma_4 s+\sigma_5}, \tag{3.21}$$

with

$$\sigma_1 = m_a m_e, \tag{3.22}$$
$$\sigma_2 = c\,(m_a+m_e)+c_a m_e+c_e m_a, \tag{3.23}$$
$$\sigma_3 = g\,(m_a+m_e)+cc_a+cc_e+c_a c_e, \tag{3.24}$$
$$\sigma_4 = gc_a+gc_e, \tag{3.25}$$
$$\sigma_5 = 0. \tag{3.26}$$

Where s is the variable of Laplace transform. On this case it is assumed that $1+\lambda_1 s+\lambda_2 s^2+\lambda_3 s^3$ is Hurwitz stable polynomial. The jerk-based AOS for the plant is given as

$$y_{pa} = y_p+\lambda_1\dot{\hat{y}}_p+\lambda_2\ddot{\hat{y}}_p+\lambda_3\dddot{\hat{y}}_p, \tag{3.27}$$
$$y_{ma} = y_m+\lambda_1\dot{y}_m+\lambda_2\ddot{y}_m+\lambda_3\dddot{y}_m. \tag{3.28}$$

The signals $\dot{\hat{y}}_p, \ddot{\hat{y}}_p$, and $\dddot{\hat{y}}_p$ are estimated derivatives of y_p and the signals $\dot{y}_m, \ddot{y}_m$, and $\dddot{y}_m$ are calculated derivatives of y_m. Hence, the augmented error signal given as

$$e_a = e_y+\lambda_1\dot{e}_y+\lambda_2\ddot{e}_y+\lambda_3\dddot{e}_y. \tag{3.29}$$

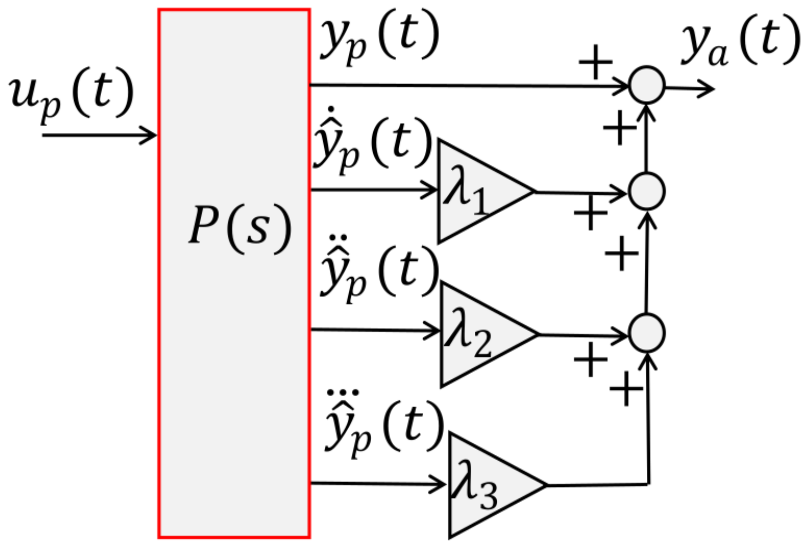

Figure 3.3: Jerk-based augmented output signal approach

The velocity, acceleration, and jerk signals are required in equations (3.20-3.29). These signals are obtained using the Kalman filter design [56].

3.3.4 State estimation

The proposed approach requires higher-order derivatives of the table position, namely velocity, acceleration and jerk states for the controller implementation. The discrete derivation method amplifies the existing noise in the measured position values to higher-order derivatives. Therefore, the kinematic model using Taylor series can be used in industrial feed drive systems for the higher-order derivatives estimation [57]. In addition, the kinematic model is not affected by system dynamics or modeling inaccuracies. The kinematic model is given in discrete-state space model as

$$\mathbf{x}_e(k+1) = \underbrace{\begin{bmatrix} 1 & T_s & T_s^2/2 & T_s^3/6 \\ 0 & 1 & T_s & T_s^2/2 \\ 0 & 0 & 1 & T_s \\ 0 & 0 & 0 & 1 \end{bmatrix}}_{\mathbf{\Phi}_k} \mathbf{x}_e(k), \tag{3.30}$$

$$y(k) = \mathbf{c}_k^{\mathrm{T}} \mathbf{x}_e(k), \tag{3.31}$$

$$\mathbf{c}_k = \begin{bmatrix} 1 & 0 & 0 & 0 \end{bmatrix}^{\mathrm{T}}, \tag{3.32}$$

where T_s is the sampling time of the control loop at the k^{th} sample. $\mathbf{\Phi}_k$ is the kinematic state transition matrix. $\mathbf{c}_k$ is the state measurement vector. $\mathbf{x}_e$ and y are the state vector and the measured value at the k^{th} sample, respectively. The state observer is designed to use table position measurement and state vector estimate $\hat{\mathbf{x}}_e$ by two iterative steps of the Kalman filter procedure as

$$\hat{\mathbf{x}}_e^-(k) = \mathbf{\Phi}_k \hat{\mathbf{x}}_e(k-1), \tag{3.33}$$

$$\mathbf{P}_k^-(k) = \mathbf{\Phi}_k \mathbf{P}_k(k-1) \mathbf{\Phi}_k^{\mathrm{T}} + \mathbf{Q}_k, \tag{3.34}$$

where $\mathbf{P}_k, \mathbf{P}_k^-$, and $\hat{\mathbf{x}}_e^-$ are the current predicted estimate uncertainty matrix, prior predicted estimate uncertainty matrix, and prior state vector estimate at the k^{th} sample, respectively. $\mathbf{Q}_k$ is the constant process noise covariance matrix which is obtained by

$$\mathbf{Q}_k = \mathbf{\Phi}_k \mathbf{J} \mathbf{\Phi}_k^{\mathrm{T}}, \mathbf{J} = \mathrm{diag}\{0, 0, 0, \sigma_j^2\}, \tag{3.35}$$

where σ_j^2 is the random variance in jerk. Equations (3.30 - 3.34) and (3.35) summaries the prediction step which is essential for the process, and then followed by correction step which is given as

$$\mathbf{k}_k(k) = \mathbf{P}_k^-(k) \mathbf{h}_k (\mathbf{h}_k^{\mathrm{T}} \mathbf{P}_k^-(k) \mathbf{h}_k + r_k)^{-1}, \tag{3.36}$$

$$\hat{\mathbf{x}}_e(k) = \hat{\mathbf{x}}_e^-(k) + \mathbf{k}_k(k)[y(k) - \mathbf{h}_k^{\mathrm{T}} \hat{\mathbf{x}}_e^-(k)], \tag{3.37}$$

$$\mathbf{P}_k(k) = \mathbf{P}_k^-(k) - \mathbf{k}_k(k) \mathbf{h}_k^{\mathrm{T}} \mathbf{P}_k^-(k), \tag{3.38}$$

where $\mathbf{k}_k$ is the Kalman gain vector at the k^{th} sample. $\mathbf{h}_k$ is the constant observation vector which is the same as $\mathbf{c}_k$. r_k is the measurement noise covariance coefficient. The values r_k and σ_j^2 are selected by trial and error manner to achieve best performance. Initial values are also assigned to $\mathbf{P}_k$.

3.3.5 Stability analysis

The stability analysis of the SAC with the PFC approach have been presented [49, 50, 58]. This subsection provides a stability proof of the SAC with the jerk-based AOS system. The proposed method alters the output of the system making $y_{pa} = (\mathbf{c}_p + \delta\mathbf{c}_p)^{\mathrm{T}}\mathbf{x}_p + d_p u_p = \mathbf{c}_p^{*\mathrm{T}}\mathbf{x}_p + d_p^* u_p$. $\delta\mathbf{c}_p$ is defined by

$$\delta\mathbf{c}_p = \begin{bmatrix} 0 & \lambda_1 & \lambda_2 & \lambda_3 \end{bmatrix}^{\mathrm{T}}. \tag{3.39}$$

Lyapunov function candidate is defined as

$$V = \mathbf{e}_x^{\mathrm{T}}\mathbf{P}\mathbf{e}_x + \mathrm{tr}\left\{\mathbf{S}^{\mathrm{T}}(\mathbf{k}_I - \tilde{\mathbf{k}})^{\mathrm{T}}\mathbf{\Gamma}_I^{-1}(\mathbf{k}_I - \tilde{\mathbf{k}})\mathbf{S}\right\}, \tag{3.40}$$

where $\mathbf{P}$ and $\mathbf{\Gamma}_I$ are the positive definite symmetric matrix and positive definite matrix, respectively. $\mathbf{S}$ is the non-singular matrix and $\tilde{\mathbf{k}}$ is unspecified vector. The time derivative of V is given as

$$\dot{V} = \dot{\mathbf{e}}_x^{\mathrm{T}}\mathbf{P}\mathbf{e}_x + \mathbf{e}_x^{\mathrm{T}}\mathbf{P}\dot{\mathbf{e}}_x + 2\mathrm{tr}\{\mathbf{S}^{\mathrm{T}}\dot{\mathbf{k}}_I^{\mathrm{T}}\mathbf{\Gamma}_I^{-1}[\mathbf{k}_I - \tilde{\mathbf{k}}]\mathbf{S}\} \tag{3.41}$$

The augmented output error is given as $e_a = \mathbf{c}_{pc}^{\mathrm{T}}\mathbf{e}_x - d_p[\mathbf{k} - \tilde{\mathbf{k}}]^{\mathrm{T}}\mathbf{r}$. The state error is given by $\mathbf{e}_x = \mathbf{x}_p^* - \mathbf{x}_p$ and its derivative is given by $\dot{e}_x = \mathbf{A}_{pc}\mathbf{e}_x - \mathbf{b}_{pc}[\mathbf{k} - \tilde{\mathbf{k}}]^{\mathrm{T}}\mathbf{r} + \mathbf{m}$. As d_p^* exist for this design, passivity relation for "strict positive realness" conditions [37] are given as

$$\mathbf{P}\mathbf{A}_{pc} + \mathbf{A}_{pc}^{\mathrm{T}}\mathbf{P} = -\mathbf{Q} - \mathbf{L}^{\mathrm{T}}\mathbf{L} < 0, \tag{3.42}$$

$$\mathbf{P}\mathbf{B}_{pc} = \mathbf{c}_{pc}^{\mathrm{T}} - \mathbf{L}^{\mathrm{T}}\mathbf{W}, \tag{3.43}$$

$$d_{pc} + d_{pc}^{\mathrm{T}} = \mathbf{W}^{\mathrm{T}}\mathbf{W}, \tag{3.44}$$

where $\mathbf{L}$, $\mathbf{W}$, and $\mathbf{Q}$ are positive definite. Perfect tracking of the plant to reference model is possible when disturbances are not considered. The perfect tracking requires $y_p^* = y_m$ condition is met. The ideal state and input correspond to the state and input of the reference model as

$$\mathbf{x}_p^* = \mathbf{X}\mathbf{x}_m + \mathbf{u}u_m, \tag{3.45}$$

$$u_p^* = \tilde{\mathbf{k}}_x^{\mathrm{T}}\mathbf{x}_m + \tilde{k}_u u_m, \tag{3.46}$$

where $\mathbf{X}$ and $\mathbf{u}$ are the time-varying coefficient matrix and vector with appropriate dimensions. $\tilde{\mathbf{k}}_x$ and $\tilde{k}_u$ are the constant vector and parameter, respectively. Introducing the terms $\mathbf{A}_p^*\mathbf{x}_p^* + \mathbf{b}_p^*u_p^* - \mathbf{A}_p^*\mathbf{x}_p^* - \mathbf{b}_p^*u_p^*$ into derivative of $\mathbf{x}_p^*$, and substituting the term $\dot{\mathbf{x}}_m$ from (3.8) into $\dot{\mathbf{x}}_p^*$ leads to

$$\begin{aligned}\dot{\mathbf{x}}_p^* = \mathbf{A}_p^*\mathbf{x}_p^* + \mathbf{b}_p^*u_p^* + [\dot{\mathbf{X}} + \mathbf{X}\mathbf{A}_m - \mathbf{A}_p^*\mathbf{X} - \\ \mathbf{b}_p^*\tilde{\mathbf{k}}_x^{\mathrm{T}}]\mathbf{x}_m + [\mathbf{X}\mathbf{b}_m + \dot{\mathbf{u}} - \mathbf{A}_p^*\mathbf{u} - \mathbf{b}_p^*\tilde{\mathbf{k}}_u]u_m + \mathbf{u}\dot{u}_m.\end{aligned} \tag{3.47}$$

The state error is defined as $\mathbf{e}_x = \mathbf{x}_p^* - \mathbf{x}_p$ and its derivative $\dot{\mathbf{e}}_x = \dot{\mathbf{x}}_p^* - \dot{\mathbf{x}}_p$. The system dynamics (3.1) derives the states of position and velocity for the actuator and table. Thus, a different representation is required to provide accessibility to the higher-order derivatives of table position [59]. Substituting $\dot{\mathbf{x}}_p^*$ from (3.47) and $\dot{\mathbf{x}}_p$ from (3.1) into state error derivative, the equation becomes

$$\dot{\mathbf{e}}_x = \mathbf{A}_p^*\mathbf{e}_x + \mathbf{b}_p^*(u_p^* - u_p) + \mathbf{m}, \tag{3.48}$$

where $\mathbf{m}$ is assumed to be globally bounded and contains the rest of the terms, which is considered to vanish upon the following two conditions are satisfied [37]:

$$[\mathbf{X}\mathbf{c}_p^* + \tilde{\mathbf{k}}_x d_p^* - \mathbf{c}_m]^{\mathrm{T}}\mathbf{x}_m + [\mathbf{c}_p^{*\mathrm{T}}\mathbf{u} + d_p^*\tilde{k}_u]u_m = 0, \tag{3.49}$$

$$[\dot{\mathbf{X}} + \mathbf{X}\mathbf{A}_m - \mathbf{A}_p^*\mathbf{X} - \mathbf{b}_p^*\tilde{\mathbf{k}}_x^{\mathrm{T}}]\mathbf{x}_m + [\mathbf{X}\mathbf{b}_m + \dot{\mathbf{u}} - \mathbf{A}_p^*\mathbf{u} - \mathbf{b}_p^*\tilde{\mathbf{k}}_u]u_m + \mathbf{u}\dot{u}_m = 0, \tag{3.50}$$

for this case, the conditions (3.49) and (3.50) hold. Adding and subtracting $\mathbf{b}_p^*\tilde{k}_e e_a$ into (3.48) leads to

$$\dot{e}_x = \mathbf{A}_p^*\mathbf{e}_x - \mathbf{b}_p^*\tilde{k}_e e_a - \mathbf{b}_p^*[\mathbf{k} - \tilde{\mathbf{k}}]^{\mathrm{T}}\mathbf{r}. \tag{3.51}$$

The augmented error signal is defined as $e_a = y_{ma} - y_{pa}$ given as

$$e_a = \mathbf{c}_p^{*\mathrm{T}} \mathbf{x}_p^* + d_p^* u_p^* - \mathbf{c}_p^{*\mathrm{T}} \mathbf{x}_p - d_p^* u_p, \tag{3.52}$$

where $\mathbf{c}_p^*$ is from (3.39). Substituting u_p^* from (3.46) and u_p from (3.14) into (3.52) leads to

$$e_a = \mathbf{c}_{pc}^{\mathrm{T}} \mathbf{e}_x - d_{pc}[\mathbf{k} - \tilde{\mathbf{k}}]^{\mathrm{T}} \mathbf{r}, \tag{3.53}$$

where $\mathbf{c}_{pc} = \mathbf{c}_p^{*\mathrm{T}}(1 + d_p^* \tilde{k}_e)^{-1}$. Hence, substituting (3.53) into (3.48) lead to

$$\dot{\mathbf{e}}_x = \mathbf{A}_{pc} \mathbf{e}_x - \mathbf{b}_{pc}[\mathbf{k} - \tilde{\mathbf{k}}]^{\mathrm{T}} \mathbf{r}, \tag{3.54}$$

where $\mathbf{A}_{pc} = \mathbf{A}_p^* - \mathbf{b}_p^* \tilde{k}_e (1 + d_p^* \tilde{k}_e)^{-1} \mathbf{c}_p^{*\mathrm{T}}$ and $\mathbf{b}_{pc} = \mathbf{b}_p^* - \mathbf{b}_p^* \tilde{k}_e (1 + d_p^* \tilde{k}_e)^{-1} d_p^*$. Substituting $\dot{\mathbf{e}}_x$ from (3.54) and $\dot{\mathbf{k}}_I$ from (3.18) and replacing e_y with e_a into (3.40) gives

$$\begin{aligned}
\dot{V} = &\left[\mathbf{A}_{pc}\mathbf{e}_x - \mathbf{b}_{pc}[\mathbf{k} - \tilde{\mathbf{k}}]^{\mathrm{T}}\mathbf{r}\right]^{\mathrm{T}} \mathbf{P}\mathbf{e}_x + \mathbf{e}_x^{\mathrm{T}}\mathbf{P}\left[\mathbf{A}_{pc}\mathbf{e}_x - \mathbf{b}_{pc}[\mathbf{k} - \tilde{\mathbf{k}}]^{\mathrm{T}}\mathbf{r}\right] + \\
&2\mathrm{tr}\left\{\mathbf{S}^{\mathrm{T}}\left[\mathbf{k}_I - \tilde{\mathbf{k}}\right]\mathbf{\Gamma}_I^{-1}\left[e_a\mathbf{r}^{\mathrm{T}}\mathbf{\Gamma}_I - \xi\mathbf{k}_I^{\mathrm{T}}\right]\mathbf{S}\right\},
\end{aligned} \tag{3.55}$$

from equation (3.17) and replacing e_y with e_a; $\mathbf{k}_I = \mathbf{k} - \mathbf{k}_p = \mathbf{k} - \mathbf{\Gamma}_p \mathbf{r} e_a$, (3.55) leads to

$$\begin{aligned}
\dot{V} = &\mathbf{e}_x^{\mathrm{T}}\left(\mathbf{A}_{pc}^{\mathrm{T}}\mathbf{P} + \mathbf{P}\mathbf{A}_{pc}\right)\mathbf{e}_x - \mathbf{b}_{pc}^{\mathrm{T}}[\mathbf{k} - \tilde{\mathbf{k}}]\mathbf{r}^{\mathrm{T}}\mathbf{P}\mathbf{e}_x - \mathbf{e}_x^{\mathrm{T}}\mathbf{P}\mathbf{b}_{pc}[\mathbf{k} - \tilde{\mathbf{k}}]^{\mathrm{T}}\mathbf{r} \\
&+ e_a^{\mathrm{T}}[\mathbf{k} - \tilde{\mathbf{k}}]\mathbf{r}\mathbf{S}^{\mathrm{T}}\mathbf{S} + \mathbf{r}^{\mathrm{T}}[\mathbf{k} - \tilde{\mathbf{k}}]^{\mathrm{T}} e_a \mathbf{S}^{\mathrm{T}}\mathbf{S} - 2e_a^{\mathrm{T}} e_a \mathbf{r}^{\mathrm{T}}\mathbf{r}\Gamma_p\mathbf{S}^{\mathrm{T}}\mathbf{S} \\
&- 2\xi\mathrm{tr}\left\{[\mathbf{k}_I - \tilde{\mathbf{k}}]\mathbf{\Gamma}_I^{-1}\mathbf{k}_I^{\mathrm{T}}\mathbf{S}^{\mathrm{T}}\mathbf{S}\right\}.
\end{aligned} \tag{3.56}$$

The passivity relations (3.42 - 3.44) into (3.56) and constraint on the output matrix $\mathbf{c}_{pc} = (\mathbf{S}^{\mathrm{T}}\mathbf{S})^{-1}(\mathbf{b}_{pc}^{\mathrm{T}}\mathbf{P}) + \mathbf{L}^{\mathrm{T}}\mathbf{W}$, leads to

$$\begin{aligned}
\dot{V} = &-\mathbf{e}_x^{\mathrm{T}}\mathbf{Q}\mathbf{e}_x - \mathbf{e}_x^{\mathrm{T}}\mathbf{L}^{\mathrm{T}}\mathbf{L}\mathbf{e}_x \\
&- \mathbf{c}_{pc}^{\mathrm{T}}[\mathbf{k} - \tilde{\mathbf{k}}]\mathbf{r}^{\mathrm{T}}\mathbf{e}_x\mathbf{S}^{\mathrm{T}}\mathbf{S} + \mathbf{L}^{\mathrm{T}}\mathbf{W}[\mathbf{k} - \tilde{\mathbf{k}}]\mathbf{r}^{\mathrm{T}}\mathbf{e}_x \\
&- \mathbf{c}_{pc}^{\mathrm{T}}\mathbf{e}_x^{\mathrm{T}}[\mathbf{k} - \tilde{\mathbf{k}}]^{\mathrm{T}}\mathbf{r}\mathbf{S}^{\mathrm{T}}\mathbf{S} + \mathbf{L}^{\mathrm{T}}\mathbf{W}\mathbf{e}_x^{\mathrm{T}}[\mathbf{k} - \tilde{\mathbf{k}}]^{\mathrm{T}}\mathbf{r} \\
&+ \mathbf{c}_{pc}^{\mathrm{T}}\mathbf{e}_x^{\mathrm{T}}[\mathbf{k} - \tilde{\mathbf{k}}]\mathbf{r}\mathbf{S}^{\mathrm{T}}\mathbf{S} - d_{pc}^{\mathrm{T}}[\mathbf{k} - \tilde{\mathbf{k}}]^{\mathrm{T}}\mathbf{r}^{\mathrm{T}}[\mathbf{k} - \tilde{\mathbf{k}}]\mathbf{r} \\
&+ \mathbf{c}_{pc}\mathbf{e}_x\mathbf{r}^{\mathrm{T}}[\mathbf{k} - \tilde{\mathbf{k}}]^{\mathrm{T}}\mathbf{S}^{\mathrm{T}}\mathbf{S} - d_{pc}[\mathbf{k} - \tilde{\mathbf{k}}]\mathbf{r}^{\mathrm{T}}[\mathbf{k} - \tilde{\mathbf{k}}]^{\mathrm{T}}\mathbf{r} \\
&- 2e_a^{\mathrm{T}} e_a\mathbf{r}^{\mathrm{T}}\mathbf{r}\mathbf{\Gamma}_p\mathbf{S}^{\mathrm{T}}\mathbf{S} - 2\xi\mathrm{tr}\left\{[\mathbf{k}_I - \tilde{\mathbf{k}}]\mathbf{\Gamma}_I^{-1}\mathbf{k}_I^{\mathrm{T}}\mathbf{S}^{\mathrm{T}}\mathbf{S}\right\}.
\end{aligned} \tag{3.57}$$

The third and fifth terms cancel with the seventh and ninth terms, respectively and with the choice of $\mathbf{k} = \tilde{\mathbf{k}}$ which is required for implementation, rearranging the equation (3.57) becomes

$$\begin{aligned}\dot{V} &= -\mathbf{e}_x^{\mathrm{T}}\mathbf{Q}\mathbf{e}_x - \mathbf{e}_x^{\mathrm{T}}\mathbf{L}^{\mathrm{T}}\mathbf{L}\mathbf{e}_x - 2e_a^{\mathrm{T}}e_a\mathbf{r}^{\mathrm{T}}\mathbf{r}\mathbf{\Gamma}_p\mathbf{S}^{\mathrm{T}}\mathbf{S} \\ &-2\xi\mathrm{tr}\left\{\mathbf{S}^{\mathrm{T}}[\mathbf{k}_I - \tilde{\mathbf{k}}]\tilde{\mathbf{k}}^{\mathrm{T}}\mathbf{\Gamma}_I^{-1}\mathbf{S}\right\} - 2\xi\mathrm{tr}\left\{\mathbf{S}^{\mathrm{T}}[\mathbf{k}_I - \tilde{\mathbf{k}}]^{\mathrm{T}}[\mathbf{k}_I - \tilde{\mathbf{k}}]\mathbf{\Gamma}_I^{-1}\mathbf{S}\right\}. \end{aligned} \tag{3.58}$$

Introducing non-negative coefficients $\beta_1, \beta_2, \beta_3..., \beta_6$ leads to

$$\begin{aligned}\dot{V} &\leq -\beta_1\|\mathbf{e}_x\|^2 - \beta_2\|e_a\|^4 - \beta_3\|e_a\|^2\|\mathbf{x}_m\|^2 - \beta_4\|e_a\|^2\|u_m\|^2 - \beta_5\|\mathbf{k}_I - \tilde{\mathbf{k}}\| \\ &-\beta_6\|\mathbf{k}_I - \tilde{\mathbf{k}}\|^2, \end{aligned} \tag{3.59}$$

thus, $\dot{V} \leq 0$ is shown which guarantees all signals (namely, $\mathbf{e}_x$, $\mathbf{k}_I$ and e_a) are bounded. Since V in (3.40) is lower bounded and $\dot{V}$ is negative semi-definite, to apply the Barbalat's lemma requires $\dot{V}$ to be uniformly continuous. The derivative of $\dot{V}$ is

$$\begin{aligned}\ddot{V} &= -2\dot{\mathbf{e}}_x^{\mathrm{T}}\mathbf{Q}\mathbf{e}_x - 2\dot{\mathbf{e}}_x^{\mathrm{T}}\mathbf{L}^{\mathrm{T}}\mathbf{L}\mathbf{e}_x - \\ &-4\dot{e}_a^{\mathrm{T}}e_a\mathbf{r}^{\mathrm{T}}\mathbf{r}\mathbf{\Gamma}_p\mathbf{S}^{\mathrm{T}}\mathbf{S} - 4e_a^{\mathrm{T}}e_a\dot{\mathbf{r}}^{\mathrm{T}}\mathbf{r}\mathbf{\Gamma}_p\mathbf{S}^{\mathrm{T}}\mathbf{S} \\ &-2\xi\mathrm{tr}\left\{\mathbf{S}^{\mathrm{T}}\dot{\mathbf{k}}_I\tilde{\mathbf{k}}^{\mathrm{T}}\mathbf{\Gamma}_I^{-1}\mathbf{S}\right\} \\ &-2\xi\mathrm{tr}\left\{\mathbf{S}^{\mathrm{T}}[\mathbf{k}_I - \tilde{\mathbf{k}}]\mathbf{\Gamma}_I^{-1}\dot{\mathbf{k}}_I^{\mathrm{T}}\mathbf{S}\right\}. \end{aligned} \tag{3.60}$$

The derivative of $\mathbf{e}_x$ from (3.54); $\dot{\mathbf{e}}_x = \mathbf{A}_{pc}\mathbf{e}_x$ when $\mathbf{k} = \tilde{\mathbf{k}}$ is selected and as $\mathbf{e}_x$ is shown to be bounded from (3.59), then $\dot{\mathbf{e}}_x$ is also bounded. The augmented tracking error e_a is bounded from (3.59) and its derivative is given as $\dot{e}_a = \mathbf{c}_{pc}^{\mathrm{T}}\dot{\mathbf{e}}_x$ with $\mathbf{k} = \tilde{\mathbf{k}}$ selected for implementation, and since $\dot{\mathbf{e}}_x$ is shown to be bounded, then $\dot{e}_a$ is also bounded.

It is assumed that the reference signals u_m and $\dot{u}_m$ are bounded and piece wise continuous, thus the state $\mathbf{x}_m$ is bounded. This in turn implies from (3.8) that $\dot{\mathbf{x}}_m$ and y_m are also bounded. The regressor vector $\mathbf{r}$ on this design contains signals e_a, $\mathbf{x}_m$, and u_m which are all bounded and their derivatives $\dot{e}_a$, $\dot{\mathbf{x}}_m$, and $\dot{u}_m$ are also bounded, making the regressor derivative $\dot{\mathbf{r}}$ bounded.

The derivative of integral gain term from (3.19); $\dot{\mathbf{k}}_I = \mathbf{\Gamma}_I\mathbf{r}e_a - \xi\mathbf{k}_I$, the signals e_a and $\mathbf{k}_I$ are bounded from (3.59) and $\mathbf{r}$ is bounded and thus, the term $\dot{\mathbf{k}}_I$ is bounded. This shows that $\ddot{V}$ is bounded, hence $\dot{V}$ is uniformly continuous and the Barbalat's lemma can be applied. Lyapunov candidate derivative becomes negative semi-definite as the derivation shown (3.59). According to Barbalat's lemma,

$$\lim_{t\to\infty} \mathbf{e}_x = 0,$$

is guaranteed and all signals in the closed-loop system are bounded. In other words, perfect tracking is achieved.

3.4 Simulation and experiment

3.4.1 Conditions

To verify the effectiveness of the proposed controller, comparative simulation and experiment were conducted with the reference trajectory:

$$y_m = 10 \sin\left(\frac{\pi}{0.875} t\right) \text{ mm}, \tag{3.61}$$

and the reference model is given as

$$\dot{\mathbf{x}}_m = \begin{bmatrix} 0 & 1 & 0 & 0 & 0 \\ 0 & 0 & 1 & 0 & 0 \\ 0 & 0 & 0 & 1 & 0 \\ 0 & 0 & 0 & 0 & 1 \\ 2p & -8p^2 & 8p^3 & -2p^4 & p^5 \end{bmatrix} \mathbf{x}_m + \begin{bmatrix} 0 \\ 0 \\ 0 \\ 0 \\ 1 \end{bmatrix} u_m, \tag{3.62}$$

where p is a negative real pole. For the reference model, states vectors $\mathbf{x}_m$ and derivatives in (3.62) are known, and hence the control variable u_m is available. The plant parameters and controller values are given in Tables 3.1 and 3.2, respectively. The following ASPR imposing controllers are composed:

- Parallel feedforward compensation (PFC),
- Augmented output signal with velocity and acceleration information (AOS-v-a),
- Jerk-based augmented output signal (AOS-v-a-j).

Table 3.1: Plant parameters

Parameter	Values
L_l	0.01 m
M_I	1.16×10^{-5} kgm^2
B_I	5.57×10^{-5} kgm^2
C_I	7.92×10^{-5} kgm^2
m_e	88.08 Ns^2/m
c	535.20 Ns/m
g	36.58 N/m
c_e	172.81 Ns/m
c_a	384.38 Ns/m

The common PI control is also included for evaluation. In addition, the disturbance term $45.7\sin(\text{rand}(10))$ N is added to the control input, and Coulomb friction 44.5 N equivalent magnitude as in [60] is also added. Here, rand(10) refers to a random number from 1 to 10.

Industrial feed drive system is actuated by rotational motor that has inertia consists of rotor, ball-screw shaft, and coupling. The equivalent mass of an actuator is given as

$$m_a = \frac{4\pi^2(M_I + B_I + C_I)}{L_l^2}, \tag{3.63}$$

where L_l is the lead of the ball nut, M_I, B_I, and C_I are the motor inertia, ball-screw inertia, and coupling inertia, respectively [54]. PFC is designed as a first-order transfer function given as

$$F(s) = \frac{D}{s + {}^1\!/\!_\alpha}, D, \alpha > 0. \tag{3.64}$$

$F(s)$ brings a difference between the original and augmented plant and gain D is important to be set small to provide the ASPR property.

Table 3.2: Simulation control parameters

Parameter	Values
p	-1.5
ξ	10^{-4}
D	10^{-3}
α	0.4
$\mathbf{\Gamma}_P, \mathbf{\Gamma}_I$	PFC, AOS-v-a : $\mathrm{diag}\{10^{11}, 1, 1, 1, 10^{-1}, 10^{-1}, 10^{-1}\}$ AOS-v-a-j : $\mathrm{diag}\{10^{12}, 1, 1, 1, 10^{-1}, 10^{-1}, 10^{-1}\}$
λ_1,λ_2,λ_3	AOS-v-a: 10^{-4}s, 10^{-7}s^2, 0 AOS-v-a-j: 10^{-4}s, 10^{-7}s^2, 10^{-10}s^3

Table 3.3: Experimental control parameters

Parameter	Values
p	-1.5
ξ	10^{-4}
D	10^{-3}
α	0.4
$\mathbf{\Gamma}_P$	PFC : $3.3 \times \mathrm{diag}\{10^3, 1, 10^{-2}, 10^{-4}, 10^{-6}, 10^{-8}, 10^{-10}\}$ AOS-v-a : $4.5 \times \mathrm{diag}\{10^4, 10, 10^{-1}, 10^{-3}, 10^{-5}, 10^{-7}, 10^{-9}\}$ AOS-v-a-j : $6.0 \times \mathrm{diag}\{10^4, 10, 10^{-1}, 10^{-3}, 10^{-5}, 10^{-7}, 10^{-9}\}$
$\mathbf{\Gamma}_I$	PFC, AOS-v-a, AOS-v-a-j : $\mathrm{diag}\{10^3, 1, 10^{-2}, 10^{-4}, 10^{-6}, 10^{-8}, 10^{-10}\}$
λ_1,λ_2,λ_3	AOS-v-a: 10^{-3}s, 10^{-6}s^2, 0 AOS-v-a-j: 10^{-4}s, 10^{-6}s^2, 10^{-11}s^3

3.4.2 Experimental setup

To test the efficacy of the suggested controllers, an industrial feed drive system in Fig. 2.3 was employed. This system uses a ball-screw mechanism powered by an AC servo motor. A rotary encoder with a resolution of 76.29 nm was attached in the feed drive to measure the actual position of the table at a 0.35 ms sampling time. Energy consumption was measured using a power analyser (HIOKI 3390) connected to the motor driver with values obtained at a 50 ms

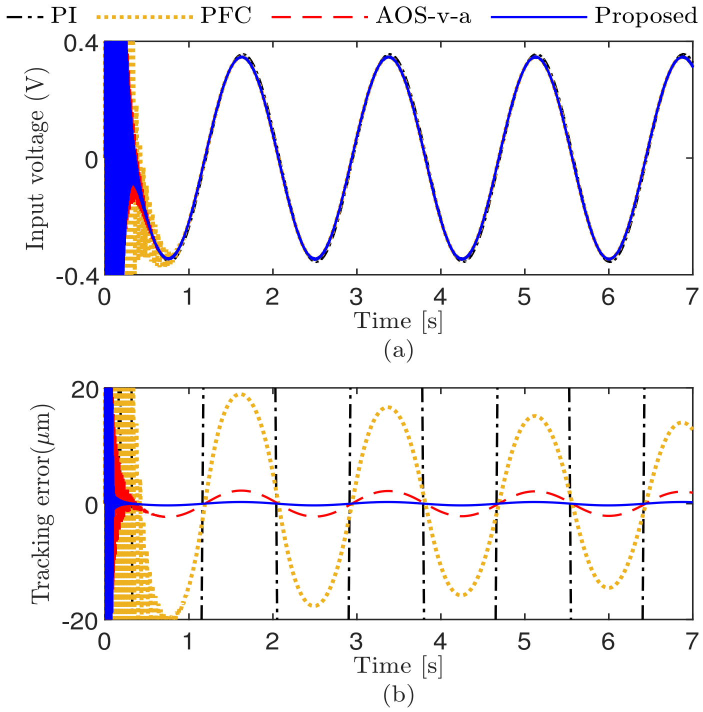

Figure 3.4: Simulation results; (a) Input voltage and (b) Tracking error

data interval update. The feed drive is connected to a personal computer (OS:Ubuntu 15.04 64 bit operating system in Xenomai 3.0 real time framework, CPU: 3.50 GHZ, RAM: 8 GB) for control purposes. Using C/C++ programming environment the control law in (3.20) with the ASPR imposed methods were implemented. The control parameters given in Table 3.3 are used, and adaptive gains $\mathbf{\Gamma}_p$ and $\mathbf{\Gamma}_I$ were selected by trial manner until best performance was obtained. For AOS-v-a and AOS-v-a-j, the Kalman filter in (3.30-3.38) was implemented with σ_j^2 and R_k selected as 10^{14} and 0.002 mm, respectively.

3.4.3 Simulation results

Figure 3.4 shows simulation results on tracking performance and control input voltage for all controllers. The PI controller was tuned using MATLAB Simulink® to achieve best assigned gains, P gain: 44152 N/mm and I gain: 112 Ns^{-1}/mm. However, the results were inferior compared to SAC and its imposing methods, maximum error is around 71.6 μm. The AOS

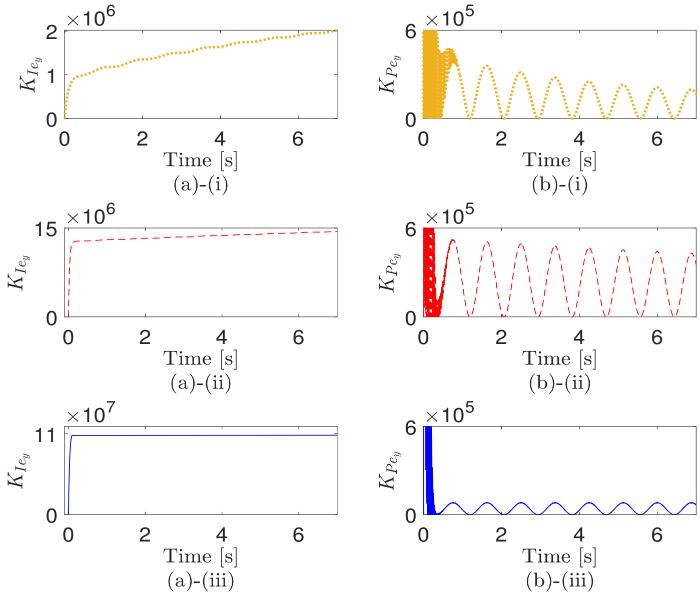

Figure 3.5: Simulation results; (a) Adaptive Gains (Integral) for tracking error (b) Adaptive Gains (Proportional); (i) SAC-PFC (ii) SAC-AOS-v-a (iii) Proposed

based controllers show better and stable performance in simulation compared to the PFC approach. To further analyze the effectiveness of the proposed method, AOS-v-a-j was compared with AOS-v-a3 . The proposed AOS-v-a-j demonstrated better tracking accuracy results that required less input than the AOS-v-a. Fig. 3.5 shows error proportional and integral adaptive gains for all controllers. The proposed AOS-v-a-j displayed faster adaptation with less control input to reach the ideal gains for perfect tracking as compared to the PFC and AOS-v-a, respectively. To further understand performances on the three systems, Fig. 3.6 shows the frequency property of the plant, plant with PFC and plant with the proposed method. The proposed AOS-v-a-j has less effect than the PFC at high frequencies.

3.4.4 Experimental results

An experiment was performed with the sinusoidal trajectory given in (3.61) to evaluate the tracking error and energy-saving capability of the proposed controller. Two objectives were sought to be fulfilled as follows: the first objective was to confirm the tracking effectiveness of

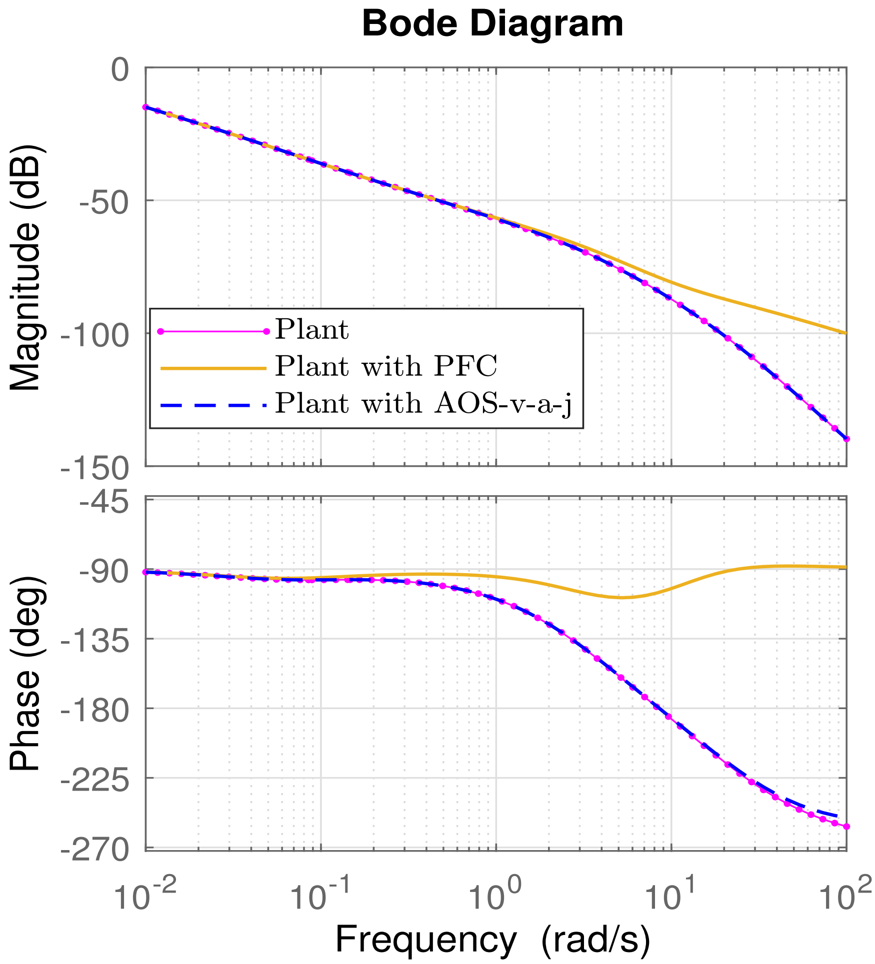

Figure 3.6: Bode plot of original plant, plant with PFC, and plant with AOS-v-a-j

the proposed method (AOS-v-a-j) by comparing it to the PFC and AOS-v-a, and the second objective was to confirm the energy-saving capability under similar tracking conditions.

3.4.4.1 Tracking error perspective

Adaptive gains were tuned to achieve the best output performance. The proposed AOS-v-a-j was more robust in incorporating high gains compared to the AOS-v-a and PFC. This led to faster response and higher tracking capabilities. The experimental data was analyzed on the steady state starting from 0.3 s by removing transient state. The results are plotted on Fig. 3.7 (a) and (b) showing tracking error and control input voltage, respectively. P and I gains are

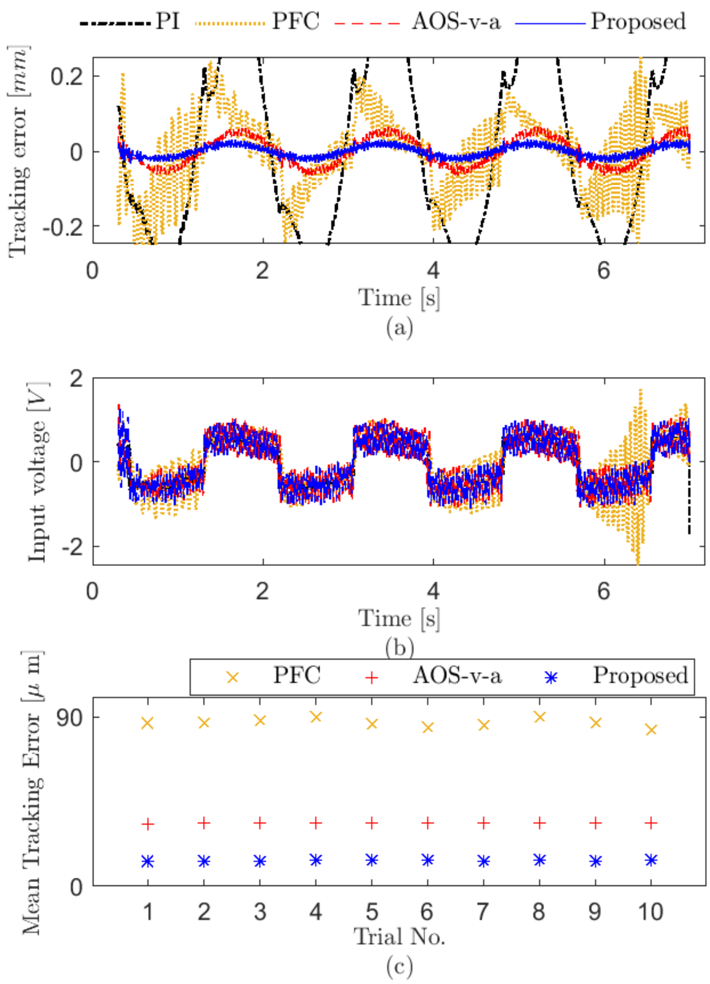

Figure 3.7: Experimental results; (a) Tracking error, (b) Control input variable, and (c) Absolute mean tracking error

4500 N/mm, and 100 Ns^{-1}/mm, respectively, adjusted from simulation which exhibits inferior performance clearly. The same experiment design was repeated 10 times for each control scheme in which energy consumption was measured and control input variance was calculated using

$$\sigma^2 = \frac{\sum_{j=1}^{N}(u_j - \mu)^2}{N}, \tag{3.65}$$

where u_j represents the control input value at the j^{th} sampling instant, N is the total number of samples ($j = 1, 2...N$) and μ is the average of all control values. The results for the mean tracking error of 10 trials are presented in Fig. 3.7 (c). Equivalent results of energy-saving and

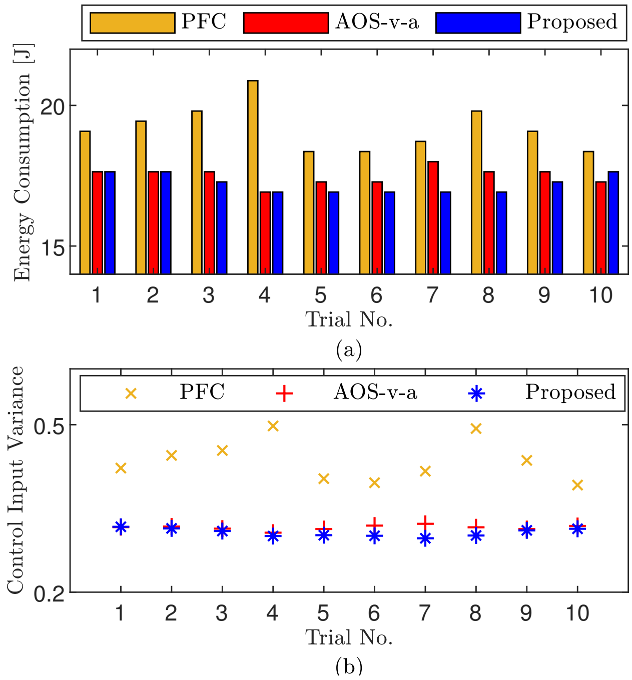

Figure 3.8: Experimental results; (a) Energy consumption, and (b) Control input variance

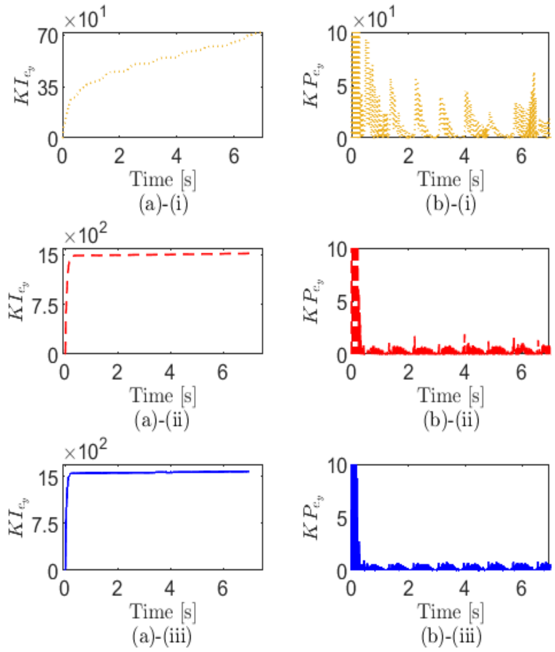

Figure 3.9: Experiment results; (a) Adaptive gains (Integral) for tracking error (b) Adaptive gains (Proportional); (i) SAC-PFC (ii) SAC-AOS-v-a (iii) Proposed

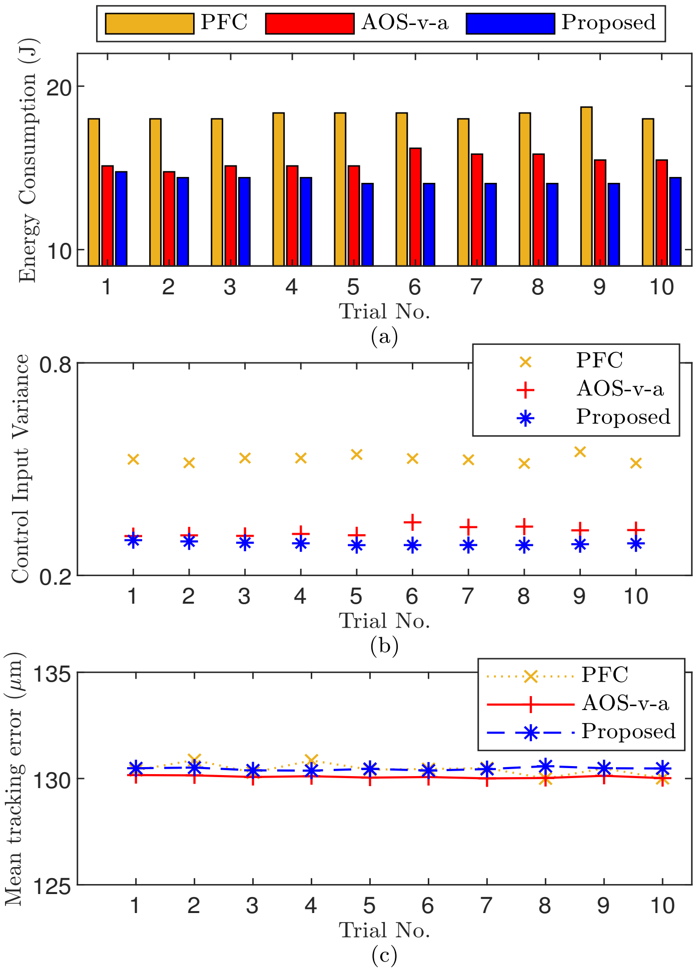

Figure 3.10: Experimental results; (a) Mean tracking error, (b) Energy consumption, and (c) Control input variance

control input variance for 10 trials are presented in Fig. 3.8 (a) and (b), respectively. Both results show the proposed AOS-v-a-j has the capability in achieving higher tracking accuracy with no extra energy required when compared to the PFC and AOS-v-a. Adaptive gains behavior for Fig. 3.7 (a) and (b) is presented in Fig. 3.9. These results show the proposed AOS-v-a-j performed much better when compared to the PFC and AOS-v-a without any additional electrical energy. The proposed AOS-v-a-j reduced mean tracking error by 80.17% when compared to the PFC and also reduced mean tracking error about 51.25% compared to AOS-v-a. Under the same results the proposed AOS-v-a-j provided better energy-saving capabilities by about 10.32% when compared to the PFC and 1.67% to AOS-v-a. In addition, the proposed AOS-v-a-j

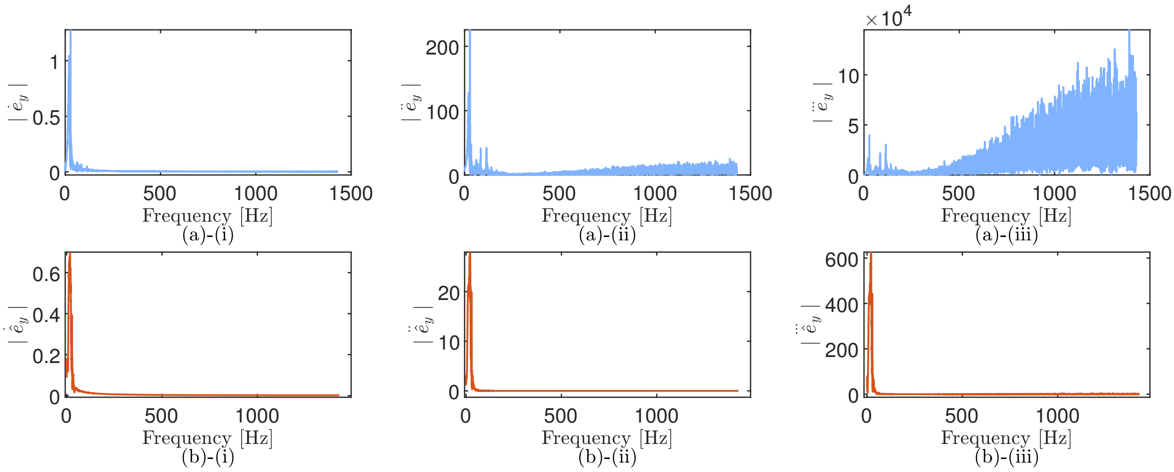

Figure 3.11: Single-sided amplitude spectrum for velocity error signals, acceleration error signals and jerk error signals ; (a) Tracking error using discrete derivation, (b) Tracking errors using kinematic model with Kalman filter

showed the lowest control input variance when compared to the PFC and AOS-v-a by around 11.32% and 4.90%, respectively. PI controller displayed an average of mean tracking error of 0.2453 mm after selection of effective gains by trial and error manner.

3.4.4.2 Energy-saving perspective

For the same reference trajectory, all controllers were tuned to achieve a similar tracking error. Tracking error was decided to be achieved around 130μm for a total of 10 trials as shown in Fig. 3.10 (c). Fig. 3.10 (a) and (b) show that the proposed AOS-v-a-j performed better by attaining the assigned tracking error with minimum energy consumption and control input variance. In terms of energy-saving, the proposed AOS-v-a-j saved by about 21.74% when compared to the PFC and 7.48% to AOS-v-a. Further comparison, the proposed AOS-v-a-j has around 45.19% lower control input variance compared to the PFC and 10.67% to AOS-v-a.

3.5 Discussion

In general, PFC is the most common method used to attain ASPR property [20, 48–50] and AOS-v-a is a recent approach proposed in our group [54] to attain it. AOS-based controllers perform better compared to the PFC in terms of tracking error and energy-saving capability. The proposed AOS-v-a-j gives additional zeros to the system in the accurate locations, which makes the system faster in the transient response and achieves a smaller steady-state error.

Fig. 3.11 shows the comparison of velocity error, acceleration and jerk error signals single-sided amplitude comparison of using discrete derivation and using kinematic model with Kalman filter design. This design significantly reduce the magnitude of the error signals across the frequency spectrum, especially at higher frequencies, indicating improved tracking performance. This is because, the kinematic model is not affected by system dynamics or modeling inaccuracies and the Kalman filter design provides optimal, noise-reduced, and model-based estimates that are continuously updated. These augmented error signals are used in AOS-v-a-j and AOS-v-a. Figs. 3.5 and 3.9 show the adaptive gains for simulation and experimental results, respectively, and they have similar behaviors. The PI controller was seen to retain large tracking error, and has a certain limitation of performance. Furthermore, the frequency response on Fig. 3.6 aims to show the deviation of the augmented plant of PFC, the augmented plant with AOS-v-a-j especially on higher frequencies. The efficiency of the adaptive control diminishes with higher deviation.

Fig. 3.12 shows the FFT of the open-loop system identification using , highlighting the amplitude of vibrations across different frequencies, with notable peaks indicating resonances. The bottom graph presents the FFT results for three closed-loop control algorithms: PFC, AOS-v-a, and the Proposed method. These results demonstrate the effectiveness of the control algorithms in reducing the error magnitude across the frequency spectrum, where the Proposed method achieves the lowest error, indicating superior vibration suppression and better control performance.

shows the frequency response of the error signal obtained using different control methods, analyzed through Fast Fourier Transform approach. The frequency range extends up to 2500 Hz, showing how the error amplitude varies across frequencies for each approach. PFC approach

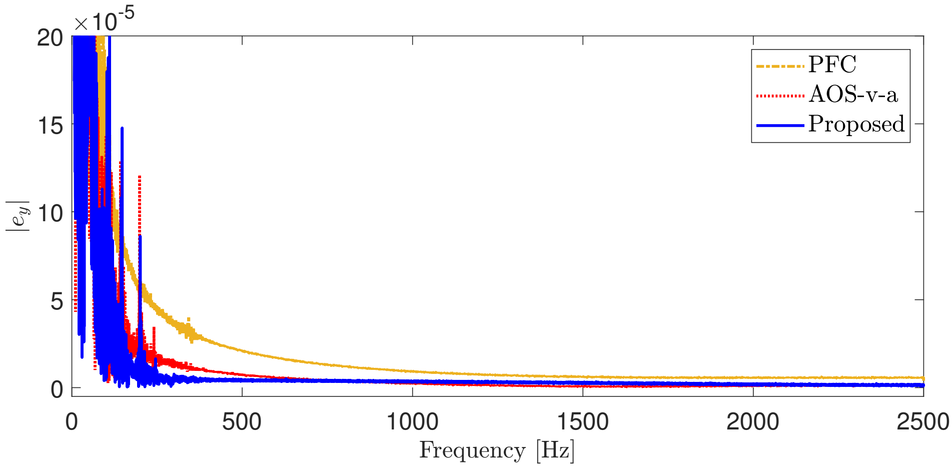

Figure 3.12: Single-sided amplitude spectrum for tracking error signals for all controllers

exhibits higher oscillations and a slower decay in the low-frequency range compared to the AOS-v-a and proposed approach. Proposed approach shows the lowest error amplitude across all frequencies, indicating superior performance in minimizing oscillations. This suggests that the proposed approach effectively suppresses high-frequency oscillations, leading to a more stable response.

3.6 Summary

Simple adaptive control with a jerk-based augmented output signal is proposed for the ASPR property, which achieves high tracking accuracy and low control input for the industrial feed drive system. The effectiveness of the proposed control scheme is verified by simulation and experiment. The proposed method shows better performance in simulation compared with the parallel feedforward compensation approach and acceleration-based augmented output signal. Two cases are considered for the experiment: the first case demonstrates the effectiveness of the proposed jerk-based augmented output signal in reducing the tracking error, and the second case demonstrates the proposed approach in terms of energy-saving capability. In the first case, the mean tracking error was reduced by about 80% compared to the conventional approach of parallel feedforward compensation and by 51% to the acceleration-based augmented output signal without additional electrical energy. For the second case, under similar tracking conditions, the energy consumption and control input variance were reduced by about 21% and 45% compared to the parallel feedforward compensation approach and by about 7% and 11% to the acceleration-based augmented output signal, respectively.

Chapter 4

Simple adaptive contouring control using a jerk-based augmented output signal

This chapter proposes simple adaptive contouring control (SACC) using jerk-based augmented output signal for the ASPR property. Implementation of the SAC technique requires that the “almost strict property real (ASPR)” property is satisfied which guarantees the stability of the controlled system even when adaptive gains are high. SACC is designed by following the tangent-contour control scheme while using the SAC technique to enhance the contouring accuracy. In addition, jerk-based augmented output signal ensures that the ASPR property is met and allows the SACC to track accurately the desired contour at high frequency. The simulation analysis and experimental validation are provided to illustrate the effectiveness of the proposed technique. The proposed contouring approach achieves lower contour error and energy consumption by about 45%, and 3% respectively, as compared to the most common parallel feedforward compensation approach.

This chapter is organized as follows: Section 4.1 describes the related works. Dynamic model of the plant is presented in section 4.2. Design of SACC is described in section 4.3, followed by simulation and experiment in section 4.4. Section 4.5 discusses results, followed by concluding remarks in section 4.6.

4.1 Related works

Reference adjustment approach was proposed by Uchiyama *et al.* [61] to estimate the contour error. The approach uses task coordinate frame to allow decoupling of the tangent and normal components to modify the reference trajectory in estimating the contour error. In addition, the approach allows for high contouring control performance with low control input variance. Mohammed *et al.* [62] proposed sliding mode contouring control using nonlinear sliding surface and used the modified reference adjustment approach in parametric trajectory to estimate the contour error. Despite the robustness and high accuracy of these works [61, 62], they depend on model parameters that requires occasional identification periodically to ensure their continued effectiveness.

Adaptive robust controllers are known to improve the contouring performance of motion systems when combined with coordinate transform-based methodologies [63–65]. Nonetheless, these controllers require a dense identification process for certain parameters. SAC is known for its simple structure, ease of implementation, and the ability to track systems with uncertain and time-varying parameters [37]. With SAC, only output data is required, whereas in adaptive controllers, full state estimates are required. In addition, while most adaptive controllers need dense system identification, a system of any degree can be used as the reference model for SAC. However, to apply SAC requires a plant to have the "almost strict positive real (ASPR)" property and a compound generated tracker solution should be realized. The ASPR property ensures that SAC is stable and can achieve asymptotic tracking even when adaptive gains are high [66]. Typically, the most common approach for achieving the ASPR property of a system is the addition of parallel feedforward compensation (PFC) to the plant. The addition of PFC ensures the system stability, but the control performance may deteriorate due to parallel structures [66]. There has been substantial works to increase the performance of using PFC design. Takagi and Mizumoto [67] proposed a PFC design using differential evolution in selecting the required parameters, though the method still hold the same parallel structure design.

Augmented output signal (AOS) approaches are proposed [53, 54, 68, 69], where the higher-order derivatives of the plant output are independently assigned relative gain and used as feedback for control purposes. This chapter proposes simple adaptive contouring control (SACC) for the biaxial feed drive systems. The SACC is designed by combining SAC and tangent-contour

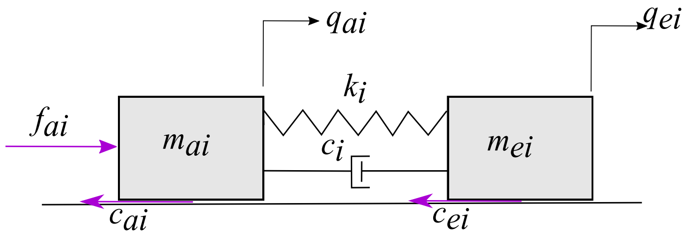

Figure 4.1: Two-mass lumped model

control using the modified reference adjustment which is a coordinate transform-based methodology. The jerk-based augmented output signal is used for the ASPR property. The addition of the jerk signal to the AOS improves the response of the system resulting to a low steady state error.

4.2 Dynamic model

Feed drive dynamics are generally represented by the fourth-order system [47, 70] as shown in Fig. 4.1 given in the following state space representation:

$$\dot{\mathbf{x}}_p = \mathbf{A}_p\mathbf{x}_p + \mathbf{B}_p\mathbf{u}_p, \tag{4.1}$$

$$\mathbf{y}_p = \mathbf{C}_p\mathbf{x}_p + \mathbf{D}_p\mathbf{u}_p, \tag{4.2}$$

with

$$\mathbf{A}_p = \begin{bmatrix} 0 & 0 & 1 & 0 & 0 & 0 & 0 & 0 \\ 0 & 0 & 0 & 1 & 0 & 0 & 0 & 0 \\ \frac{-k_1}{m_{e1}} & 0 & \frac{-c_1-c_{e1}}{m_{e1}} & 0 & \frac{k_1}{m_{e1}} & 0 & \frac{c_1}{m_{e1}} & 0 \\ 0 & \frac{-k_2}{m_{e2}} & 0 & \frac{-c_2-c_{e2}}{m_{e2}} & 0 & \frac{k_2}{m_{e2}} & 0 & \frac{c_2}{m_{e2}} \\ 0 & 0 & 0 & 0 & 0 & 0 & 1 & 0 \\ 0 & 0 & 0 & 0 & 0 & 0 & 0 & 1 \\ \frac{k_1}{m_{a1}} & 0 & \frac{c_1}{m_{a1}} & 0 & \frac{-k_1}{m_{a1}} & 0 & \frac{-c_1-c_{a1}}{m_{a1}} & 0 \\ 0 & \frac{k_2}{m_{a2}} & 0 & \frac{c_2}{m_{a2}} & 0 & \frac{-k_2}{m_{a2}} & 0 & \frac{-c_2-c_{a2}}{m_{a2}} \end{bmatrix}, \tag{4.3}$$

$$\mathbf{x}_p = \begin{bmatrix} q_{e1} & q_{e2} & \dot{q}_{e1} & \dot{q}_{e2} & q_{a1} & q_{a2} & \dot{q}_{a1} & \dot{q}_{a2} \end{bmatrix}^{\mathrm{T}}, \tag{4.4}$$

$$\mathbf{B}_p = \begin{bmatrix} 0 & 0 & 0 & 0 & 0 & 0 & \frac{1}{m_{a1}} & 0 \\ 0 & 0 & 0 & 0 & 0 & 0 & 0 & \frac{1}{m_{a2}} \end{bmatrix}^{\mathrm{T}}, \tag{4.5}$$

$$\mathbf{u}_p = \begin{bmatrix} f_{a1} & f_{a2} \end{bmatrix}^{\mathrm{T}}, \tag{4.6}$$

$$\mathbf{C}_p = \begin{bmatrix} 1 & 0 & 0 & 0 & 0 & 0 & 0 & 0 \\ 0 & 1 & 0 & 0 & 0 & 0 & 0 & 0 \end{bmatrix}, \tag{4.7}$$

$$\mathbf{D}_p = \begin{bmatrix} 0 & 0 \\ 0 & 0 \end{bmatrix}. \tag{4.8}$$

In s-domain the state space above follows open-loop transfer functions expressed as

$$\begin{bmatrix} q_{e1} \\ q_{e2} \end{bmatrix} = \begin{bmatrix} \frac{c_1 s + k_1}{Q_1(s)} & 0 \\ 0 & \frac{c_2 s + k_2}{Q_2(s)} \end{bmatrix} \begin{bmatrix} f_{a1} \\ f_{a2} \end{bmatrix}, \tag{4.9}$$

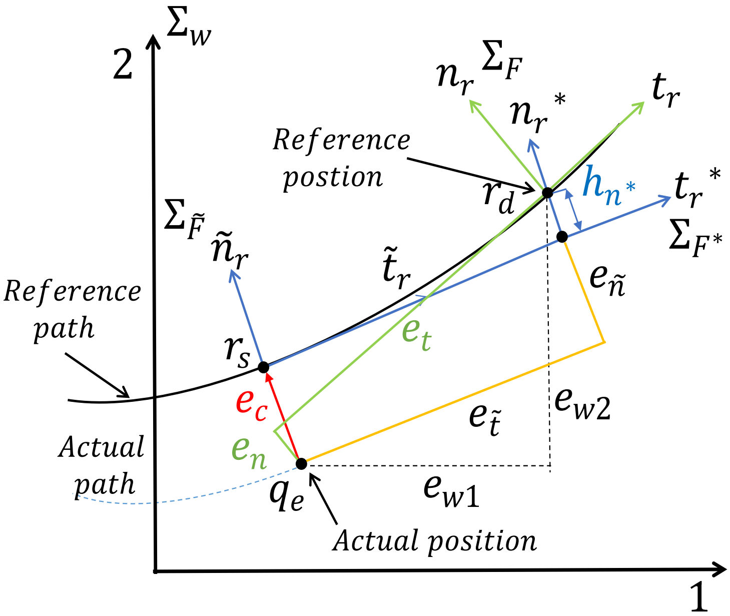

Figure 4.2: Contour error definition

with

$$Q_i(s) = \sigma_{0i}s^4 + \sigma_{1i}s^3 + \sigma_{2i}s^2 + \sigma_{3i}s + \sigma_{4i}, \tag{4.10}$$

$$\sigma_{0i} = m_{ai}m_{ei}, \tag{4.11}$$

$$\sigma_{1i} = c_i\left(m_{ai} + m_{ei}\right) + c_{ai}m_{ei} + c_{ei}m_{ai}, \tag{4.12}$$

$$\sigma_{2i} = k_i\left(m_{ai} + m_{ei}\right) + c_ic_{ai} + c_ic_{ei} + c_{ai}c_{ei}, \tag{4.13}$$

$$\sigma_{3i} = k_ic_{ai} + k_ic_{ei}, \tag{4.14}$$

$$\sigma_{4i} = 0,\ i(=1,2), \tag{4.15}$$

where s is the variable in the Laplace transform. m_{ai} and m_{ei} are the actuator and table masses of the i^{th} axis, respectively. The masses are connected by a damper (viscous friction coefficient c_i) and a spring (spring constant k_i) of the i^{th} axis. The masses m_{ai} and m_{ei} are subjected to viscous friction coefficients c_{ai} and c_{ei}, respectively.

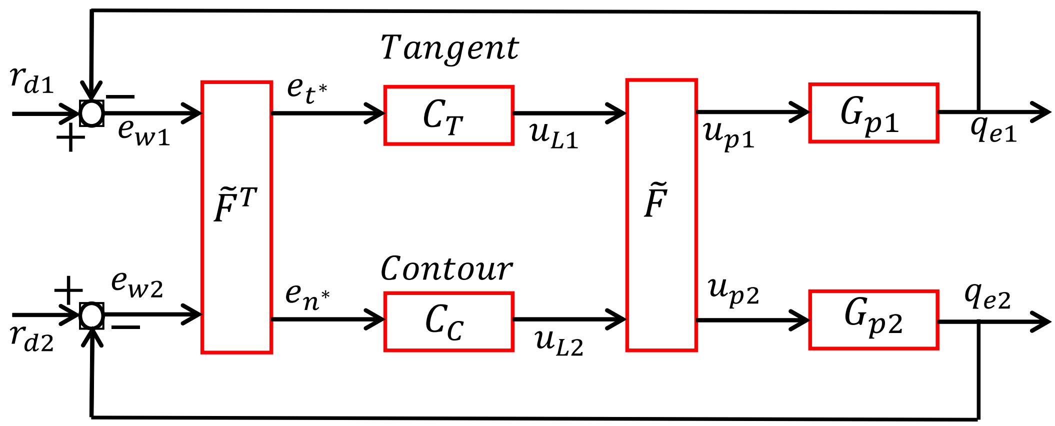

Figure 4.3: Block diagram of the TCC scheme for a biaxial control system

4.2.1 Estimation of contour error

In biaxial feed drive systems, the contour error can be defined by using local and fixed frameworks [65] as shown in Fig. 4.2. Tracking error is the difference between the actual position and desired position for each axis given as

$$\mathbf{e}_w = \begin{bmatrix} e_{w1} & e_{w2} \end{bmatrix}^{\mathrm{T}} = \mathbf{r}_d - \mathbf{q}_e, \tag{4.16}$$

where $\mathbf{r}_d$ is the desired reference position vector and $\mathbf{q}_e$ is the actual table position vector. Contour error e_c is the minimum distance between the reference contour and actual contour. Real-time contour error can be estimated using the modified reference adjustment method [62]. This method decouples the tracking error to tangent and normal components. This is achieved by introducing local coordinate framework $\sum_F$ to the point $\mathbf{r}_d$ and formulate directional vectors $\mathbf{t}_r$ and $\mathbf{n}_r$. The vectors $\mathbf{t}_r$ and $\mathbf{n}_r$ are computed as follows:

$$\mathbf{t}_r = \begin{bmatrix} t_{r1} & t_{r2} \end{bmatrix}^{\mathrm{T}} = \frac{\dot{\mathbf{r}}_d}{\|\dot{\mathbf{r}}_d\|}, \dot{\mathbf{r}}_d \neq 0, \tag{4.17}$$

$$\mathbf{n}_r = \begin{bmatrix} n_{r1} & n_{r2} \end{bmatrix}^{\mathrm{T}} = \frac{\dot{\mathbf{t}}_r}{\|\dot{\mathbf{t}}_r\|}, \ddot{\mathbf{r}}_d \neq 0. \tag{4.18}$$

The transformed tracking error vector from local coordinate is given as

$$\mathbf{e}_L = \begin{bmatrix} e_t & e_n \end{bmatrix}^{\mathrm{T}} = \mathbf{F}^{\mathrm{T}}\mathbf{e}_w, \tag{4.19}$$

$$\mathbf{F} = \begin{bmatrix} t_{r1} & n_{r1} \\ t_{r2} & n_{r2} \end{bmatrix}. \tag{4.20}$$

The normal component e_n can be considered as an approximate estimate of e_c. However, when dealing with complex shapes that have high curvature, the estimate may become unrealistic. To reduce the estimation error, tangential error e_t value is assumed to be the same as the distance between desired position $\mathbf{r}_d$ and point $\mathbf{r}_s$. Furthermore, it is assumed that the velocity along the contour matches the desired velocity. The time required to traverse along e_t is given as

$$t_d = \frac{e_t}{\|\dot{\mathbf{r}}_d\|}, \dot{\mathbf{r}}_d \neq 0. \tag{4.21}$$

A new local coordinate frame $\sum_{\tilde{\mathbf{F}}}$ is attached at $\mathbf{r}_s$ and instantaneous time $\tilde{t} = t - t_d$ which formulate the vectors $\tilde{\mathbf{t}}_r$ and $\tilde{\mathbf{n}}_r$ are given as

$$\tilde{\mathbf{t}}_r = \begin{bmatrix} \tilde{t}_{r1} & \tilde{t}_{r2} \end{bmatrix}^{\mathrm{T}} = \mathbf{t}_r(\tilde{t}), \tag{4.22}$$

$$\tilde{\mathbf{n}}_r = \begin{bmatrix} \tilde{n}_{r1} & \tilde{n}_{r2} \end{bmatrix}^{\mathrm{T}} = \mathbf{n}_r(\tilde{t}). \tag{4.23}$$

The corresponding error vector components from transformed $\sum_{\tilde{\mathbf{F}}}$ local coordinate framework is given as

$$\mathbf{e}_{\tilde{L}} = \begin{bmatrix} e_{\tilde{t}} & e_{\tilde{n}} \end{bmatrix}^{\mathrm{T}} = \tilde{\mathbf{F}}^{\mathrm{T}}\mathbf{e}_w, \tag{4.24}$$

$$\tilde{\mathbf{F}} = \mathbf{F}(\tilde{t}). \tag{4.25}$$

Transforming the error vector $\mathbf{e}_{\tilde{L}}$ into a new local coordinate frame $\sum_{\mathbf{F}^*}$, the transformed error vector becomes

$$\mathbf{e}_{L^*} = \begin{bmatrix} e_{t^*} & e_{n^*} \end{bmatrix}^{\mathrm{T}} = \tilde{\mathbf{F}}^{\mathrm{T}}\mathbf{e}_w + \mathbf{h}^*, \tag{4.26}$$

$$\mathbf{h}^* = \begin{bmatrix} 0 & h_{n^*} \end{bmatrix} = \mathbf{J}\tilde{\mathbf{h}}, \tag{4.27}$$

$$\tilde{\mathbf{h}} = \tilde{\mathbf{F}}^{\mathrm{T}}[\mathbf{r}_d(\tilde{t}) - \mathbf{r}_d(t)]. \tag{4.28}$$

where $\mathbf{J} = \text{diag}\{0, 1\}$. On this design the normal component e_{n^*} is considered as an accurate estimate of the contour error.

4.3 Design of simple adaptive contouring control

4.3.1 Preliminaries

Compound generated tracker (CGT) solution and a plant with ASPR property are required for SAC implementation [55]. In addition, SAC requires a stable reference model. A reference model is given as

$$\dot{\mathbf{x}}_m = \mathbf{A}_m \mathbf{x}_m + \mathbf{B}_m \mathbf{u}_m, \tag{4.29}$$

$$\mathbf{y}_m = \mathbf{C}_m \mathbf{x}_m + \mathbf{D}_m \mathbf{u}_m, \tag{4.30}$$

where $\mathbf{x}_m \in R^{n_m}$, $\mathbf{y}_m \in R^m$, and $\mathbf{u}_m \in R^m$ are the state, output, and input vectors, respectively. $\mathbf{A}_m$, $\mathbf{B}_m$, $\mathbf{C}_m$, and $\mathbf{D}_m$ correspond to system matrix, input matrix, output matrix, and feed through matrix, respectively.

Reference model input $\mathbf{u}_m$ is assumed to be bounded and piece-wise continuous such that $\dot{u}_m$, $\dot{\mathbf{x}}_m$, and $\mathbf{y}_m$ are also bounded. The plant (4.9) has a relative degree of 3, hence it is not ASPR. A plant is known to be ASPR when the following conditions are met; plant should have a relative degree of 0 or 1, plant should be minimum-phase, and the highest frequency gain of the plant must be positive. Therefore, other methods are required to make the plant ASPR.

Perfect tracking is achieved when $\mathbf{y}_p = \mathbf{y}_m$ for $t \geq 0$, there exists an ideal model with state $\mathbf{x}_p^*$, input $\mathbf{u}_p^*$, and output $\mathbf{y}_p^*$ vectors, given in the following state space representation:

$$\dot{\mathbf{x}}_p^* = \mathbf{A}_p^* \mathbf{x}_p^* + \mathbf{B}_p^* \mathbf{u}_p^*, \tag{4.31}$$

$$\mathbf{y}_p^* = \mathbf{C}_p^* \mathbf{x}_p^* + \mathbf{D}_p^* \mathbf{u}_p^*, \tag{4.32}$$

where $\mathbf{A}_p^*$, $\mathbf{B}_p^*$, $\mathbf{C}_p^*$, and $\mathbf{D}_p^*$ are the ASPR plant matrices with appropriate dimensions. Since $\mathbf{x}_m$ and $\mathbf{u}_m$ are of arbitrary in nature, by selecting the stable and correct coefficients of the characteristic equation, the CGT condition can be satisfied [37]. The ideal output is identical to output of the reference model given as

$$\mathbf{y}_p^* = \mathbf{y}_m, \tag{4.33}$$

$$\begin{bmatrix} \mathbf{C}_p^* & \mathbf{D}_p^* \end{bmatrix} \begin{bmatrix} \mathbf{x}_p^* \\ \mathbf{u}_p^* \end{bmatrix} = \begin{bmatrix} \mathbf{C}_m & \mathbf{D}_m \end{bmatrix} \begin{bmatrix} \mathbf{x}_m \\ \mathbf{u}_m \end{bmatrix}, \tag{4.34}$$

with tracking error defined as $\mathbf{e}_w = \mathbf{y}_m - \mathbf{y}_p$, and the following control input was proposed [37]:

$$\mathbf{u}_v = \begin{bmatrix} u_{v1} & u_{v2} \end{bmatrix}^{\mathrm{T}} = \mathbf{K}_{ew}\mathbf{e}_w + \mathbf{K}_{xm}\mathbf{x}_m + \mathbf{K}_{um}\mathbf{u}_m, \tag{4.35}$$

$$\mathbf{u}_v = \mathbf{K}_w\mathbf{r}, \tag{4.36}$$

with

$$\mathbf{K}_w = \begin{bmatrix} \mathbf{K}_{ew} & \mathbf{K}_{xm} & \mathbf{K}_{um} \end{bmatrix}, \tag{4.37}$$

$$\mathbf{r} = \begin{bmatrix} \mathbf{e}_w^{\mathrm{T}} & \mathbf{x}_m^{\mathrm{T}} & \mathbf{u}_m^{\mathrm{T}} \end{bmatrix}^{\mathrm{T}}. \tag{4.38}$$

$\mathbf{K}_w$ is a matrix with appropriate dimensions. The adaptive gain matrix is a combination of "proportional" and "integral" terms; $\mathbf{K}_w = \mathbf{K}_{pw} + \mathbf{K}_{Iw}$ and their adaptation laws are given as

$$\mathbf{K}_{pw} = \mathbf{e}_w\mathbf{r}^{\mathrm{T}}\mathbf{\Gamma}_{pw}, \tag{4.39}$$

$$\dot{\mathbf{K}}_{Iw} = \mathbf{e}_w\mathbf{r}^{\mathrm{T}}\mathbf{\Gamma}_{Iw} - \zeta\mathbf{K}_{Iw}. \tag{4.40}$$

$\mathbf{\Gamma}_{pw}$ and $\mathbf{\Gamma}_{Iw}$ are block diagonal matrices. $\mathbf{\Gamma}_{pw}$ contains the matrices $\mathbf{\Gamma}_{Pew}, \mathbf{\Gamma}_{Pxm}$, and $\mathbf{\Gamma}_{Pum}$. $\mathbf{\Gamma}_{Iw}$ contains matrices $\mathbf{\Gamma}_{Iew}, \mathbf{\Gamma}_{Ixm}$, and $\mathbf{\Gamma}_{Ium}$, respectively. In addition, these matrices are positive semi-definite and positive definite, respectively, used to adjust the adaption rate of the control gains. The integral adaptive gain is needed for stability and asymptotic tracking of the adaptive system [38]. The stability proofs in [37] show that the proportional gain affects the rate of convergence of the system towards perfect tracking. The term ζ in (4.40) is used to avoid divergence of the integral gains in the presence of disturbances.

4.3.2 Contouring control

The coordinate conversion and deconversion is required to establish contouring control using the Tangent-contouring control (TCC) scheme [71]. The matrix $\tilde{\mathbf{F}}$ in (4.25) is used for conversion and its transpose is used for deconversion as shown in Fig. 4.3. The conversed control input is computed as

$$\mathbf{u}_L = \begin{bmatrix} u_{L1} & u_{L2} \end{bmatrix}^{\mathrm{T}} = \mathbf{K}_{eL}\tilde{\mathbf{F}}_{ew}^{\mathrm{T}}\mathbf{e}_w + \mathbf{K}_{xL}\tilde{\mathbf{F}}_{xm}^{\mathrm{T}}\mathbf{x}_m + \mathbf{K}_{uL}\tilde{\mathbf{F}}_{um}^{\mathrm{T}}\mathbf{u}_m = \mathbf{K}\boldsymbol{\Lambda}\mathbf{r}, \tag{4.41}$$

where $\mathbf{K}_{eL} \in R^{m\times m}$, $\mathbf{K}_{xL} \in R^{m\times n_m}$, and $\mathbf{K}_{uL} \in R^{m\times m}$ are matrices with appropriate dimensions. $\tilde{\mathbf{F}}_{ew}$, $\tilde{\mathbf{F}}_{xm}$, and $\tilde{\mathbf{F}}_{um}$ are block diagonal matrices with $\tilde{\mathbf{F}}$ repeated $m/2$, $n_m/2$, and $m/2$ times, respectively. The deconversion control input to the plant is given as follows:

$$\mathbf{u}_p = \begin{bmatrix} u_{p1} & u_{p2} \end{bmatrix}^{\mathrm{T}} = \boldsymbol{\Lambda}^{\mathrm{T}}\mathbf{u}_L = \mathbf{K}\boldsymbol{\Lambda}^{\mathrm{T}}\boldsymbol{\Lambda}\mathbf{r}, \tag{4.42}$$

$$\mathbf{u}_p = \mathbf{K}_{eL}\mathbf{e}_w + \mathbf{K}_{xL}\mathbf{x}_m + \mathbf{K}_{uL}\mathbf{u}_m, \tag{4.43}$$

with

$$\boldsymbol{\Lambda} = \begin{bmatrix} \tilde{\mathbf{F}}_{ew}^{\mathrm{T}} & \tilde{\mathbf{F}}_{xm}^{\mathrm{T}} & \tilde{\mathbf{F}}_{um}^{\mathrm{T}} \end{bmatrix}, \tag{4.44}$$

$$\mathbf{K} = \begin{bmatrix} \mathbf{K}_{eL} & \mathbf{K}_{xL} & \mathbf{K}_{uL} \end{bmatrix} = \mathbf{K}_{pL} + \mathbf{K}_{IL}, \tag{4.45}$$

$\boldsymbol{\Lambda}$ is the block diagonal matrix with appropriate dimensions. The terms $\mathbf{K}_{xL}\mathbf{x}_m$ and $\mathbf{K}_{uL}\mathbf{u}_m$ in (4.43) are used in the contouring control input only because of their important contribution to the performance of the adaptive system, expressed by the negative terms in the derivative of the Lyapunov function [40]. The "proportional" and "integral" terms of the conversed adaptive laws as

$$\mathbf{K}_{pL} = \mathbf{e}_{L^*}\mathbf{r}^{\mathrm{T}}\boldsymbol{\Lambda}^{\mathrm{T}}\boldsymbol{\Gamma}_{pL}, \tag{4.46}$$

$$\dot{\mathbf{K}}_{IL} = \mathbf{e}_{L^*}\mathbf{r}^{\mathrm{T}}\boldsymbol{\Lambda}^{\mathrm{T}}\boldsymbol{\Gamma}_{IL} - \zeta\mathbf{K}_{IL}, \tag{4.47}$$

$\boldsymbol{\Gamma}_{pL}$ and $\boldsymbol{\Gamma}_{IL}$ are block diagonal matrices. $\boldsymbol{\Gamma}_{pL}$ is positive semi-definite matrix contains matrices $\boldsymbol{\Gamma}_{PeL}, \boldsymbol{\Gamma}_{PxL}$, and $\boldsymbol{\Gamma}_{PuL}$, respectively. $\boldsymbol{\Gamma}_{IL}$ is positive definite contains matrices $\boldsymbol{\Gamma}_{IeL}, \boldsymbol{\Gamma}_{IxL}$, and $\boldsymbol{\Gamma}_{IuL}$, respectively.

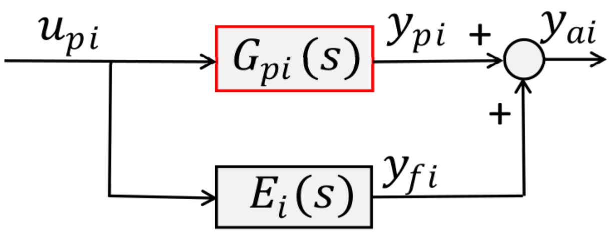

Figure 4.4: PFC design

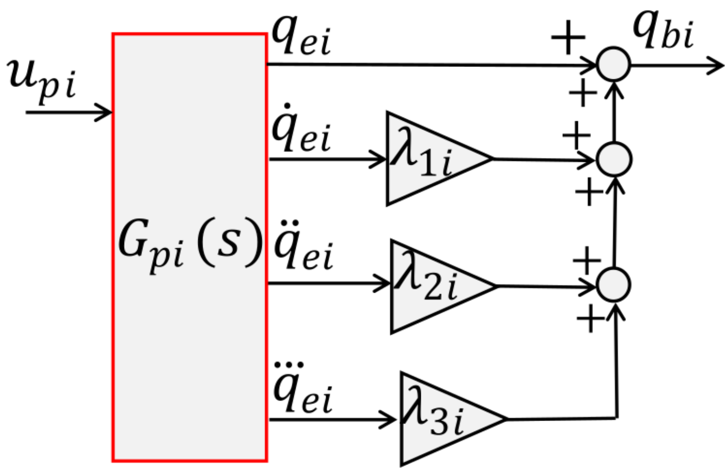

Figure 4.5: Jerk-based AOS design

4.3.3 ASPR property

A typical approach of attaining ASPR property is to introduce the PFC design to the plant as shown in Fig. 4.4 [41]. The stable compensator $E_i(s)$ is added parallel to the plant $G_{pi}(s)$ using the same control input u_{pi} of the i^{th} drive axis. The plant becomes augmented with transfer function $G_{fi}(s) = G_{pi}(s) + E_i(s)$ and the augmented output $y_{ai} = \{G_{pi}(s) + E_i(s)\}u_{pi}$. The relative degree of $E_i(s)$ can be designed with relative degree of 1 which will also make augmented plant have a relative degree of 1. PFC can be designed as a first-order transfer function given as

$$E_i(s) = \frac{D_i}{s + \alpha_i}, D_i, \alpha_i > 0. \tag{4.48}$$

$E_i(s)$ brings a difference between the original and augmented plant, the gain D_i and pole α_i is selected to make the augmented plant $G_{fi} \approx G_{pi}$. It is important that the condition

$G_{fi}(s) \approx G_{pi}(s)$ holds to ensure tracking. The augmented tracking error from PFC design is given by

$$\mathbf{e}_{af} = \begin{bmatrix} e_{af1} & e_{af2} \end{bmatrix}^{\mathrm{T}} = \mathbf{y}_m - (\mathbf{y}_p + \mathbf{y}_f) = \mathbf{e}_w - \mathbf{y}_f, \tag{4.49}$$

where $\mathbf{y}_f$ is the PFC output and from tracking error definition $\mathbf{e}_w = \mathbf{y}_m - \mathbf{y}_p$. The $\mathbf{e}_{af}$ is used for the tracking control. For the contouring, the transformed augmented output error vector $\mathbf{e}_{Lf^*} = \begin{bmatrix} e_{Lf1^*} & e_{Lf2^*} \end{bmatrix}^{\mathrm{T}}$ is computed as follows

$$\mathbf{e}_{Lf^*} = \tilde{\mathbf{F}}^{\mathrm{T}}\mathbf{e}_w + \mathbf{h}^* - \tilde{\mathbf{F}}^{\mathrm{T}}\mathbf{y}_f. \tag{4.50}$$

The error terms $\mathbf{e}_w$ and $\mathbf{e}_{L^*}$ are replaced by $\mathbf{e}_{af}$ and $\mathbf{e}_{Lf^*}$ in (4.36-4.47), respectively.

Another approach for the ASPR property is the jerk-based AOS as shown in Fig. 4.5. This method introduces a third order polynomial $H_i(s) = 1 + \lambda_{1i}s + \lambda_{2i}s^2 + \lambda_{3i}s^3$ for the i^{th} axis to the plant. The augmented plant becomes

$$G_{ai}(s) = \frac{(c_i s + k_i)H_i(s)}{Q_i(s)}, \tag{4.51}$$

where, the values of λ_{1i}, λ_{2i}, and λ_{3i} are constants selected to make the polynomials Hurwitz stable. Expanding the augmented plant (4.51) becomes

$$G_{ai}(s) = G_{pi}(s) + \lambda_{1i}sG_{pi}(s) + \lambda_{2i}s^2G_{pi}(s) + \lambda_{3i}s^3G_{pi}(s), \tag{4.52}$$

this brings to the augmented output signal of

$$\mathbf{q}_b = \mathbf{q}_e + \lambda_1\dot{\mathbf{q}}_e + \lambda_2\ddot{\mathbf{q}}_e + \lambda_3\dddot{\mathbf{q}}_e. \tag{4.53}$$

where $\lambda_1 = \mathrm{diag}\{\lambda_{11}, \lambda_{12}\}$, $\lambda_2 = \mathrm{diag}\{\lambda_{21}, \lambda_{22}\}$, and $\lambda_3 = \mathrm{diag}\{\lambda_{31}, \lambda_{32}\}$. Jerk-based AOS requires the reference model to have at least the same order as the plant and in turn the vector $H(s)$ is applied to the reference model. This leads to an augmented reference output signal given as

$$\mathbf{q}_m = \mathbf{y}_m + \lambda_1\dot{\mathbf{y}}_m + \lambda_2\ddot{\mathbf{y}}_m + \lambda_3\dddot{\mathbf{y}}_m, \tag{4.54}$$

and the augmented output error is defined as

$$\mathbf{e}_a = \begin{bmatrix} e_{a1} & e_{a2} \end{bmatrix}^{\mathrm{T}} = \mathbf{q}_b - \mathbf{q}_m. \tag{4.55}$$

The $\mathbf{e}_a$ formulation is used for the tracking approach. For the contouring approach, the transformed augmented output error requires higher-order derivatives of $\mathbf{e}_{L^*}$ to define the AOS. These derivatives are computed as follows:

$$\dot{\mathbf{e}}_{L^*} = \dot{\tilde{\mathbf{F}}}^{\mathrm{T}}\mathbf{e}_w + \tilde{\mathbf{F}}^{\mathrm{T}}\dot{\mathbf{e}}_w + \dot{\mathbf{h}}^*, \tag{4.56}$$

$$\ddot{\mathbf{e}}_{L^*} = \ddot{\tilde{\mathbf{F}}}^{\mathrm{T}}\mathbf{e}_w + 2\dot{\tilde{\mathbf{F}}}^{\mathrm{T}}\dot{\mathbf{e}}_w + \tilde{\mathbf{F}}^{\mathrm{T}}\ddot{\mathbf{e}}_w + \ddot{\mathbf{h}}^*, \tag{4.57}$$

$$\dddot{\mathbf{e}}_{L^*} = \dddot{\tilde{\mathbf{F}}}^{\mathrm{T}}\mathbf{e}_w + 3\ddot{\tilde{\mathbf{F}}}^{\mathrm{T}}\dot{\mathbf{e}}_w + 3\dot{\tilde{\mathbf{F}}}^{\mathrm{T}}\ddot{\mathbf{e}}_w + \tilde{\mathbf{F}}^{\mathrm{T}}\dddot{\mathbf{e}}_w + \dddot{\mathbf{h}}^*. \tag{4.58}$$

The transformed augmented output error is given as

$$\mathbf{e}_{La^*} = \mathbf{e}_{L^*} + \lambda_1\dot{\mathbf{e}}_{L^*} + \lambda_2\ddot{\mathbf{e}}_{L^*} + \lambda_3\dddot{\mathbf{e}}_{L^*}. \tag{4.59}$$

The error terms $\mathbf{e}_w$ and $\mathbf{e}_{L^*}$ are replaced by $\mathbf{e}_a$ and $\mathbf{e}_{La^*}$ in (4.36-4.47), respectively.

4.3.4 State observer

Jerk-based AOS requires the higher-order derivatives of the table positions which are velocity, acceleration, and jerk. Using discrete derivation method to obtain these signals may produce unreliable results when the signals contain noise. Kinematic model using Taylor series with Kalman filter design can be used to estimate the higher-order derivatives [57]. The kinematic model is given in the discrete-state space model as

$$\mathbf{q}_p(k+1) = \underbrace{\begin{bmatrix} 1 & 0 & T_s & 0 & T_s^2/2 & 0 & T_s^3/6 & 0 \\ 0 & 1 & 0 & T_s & 0 & T_s^2/2 & 0 & T_s^3/6 \\ 0 & 0 & 1 & 0 & T_s & 0 & T_s^2/2 & 0 \\ 0 & 0 & 0 & 1 & 0 & T_s & 0 & T_s^2/2 \\ 0 & 0 & 0 & 0 & 1 & 0 & T_s & 0 \\ 0 & 0 & 0 & 0 & 0 & 1 & 0 & T_s \\ 0 & 0 & 0 & 0 & 0 & 0 & 1 & 0 \\ 0 & 0 & 0 & 0 & 0 & 0 & 0 & 1 \end{bmatrix}}_{\mathbf{\Phi}_k} \mathbf{q}_p(k), \tag{4.60}$$

$$\mathbf{y}(k) = \underbrace{\begin{bmatrix} 1 & 0 & 0 & 0 & 0 & 0 & 0 & 0 \\ 0 & 1 & 0 & 0 & 0 & 0 & 0 & 0 \end{bmatrix}}_{\mathbf{C}_k} \mathbf{q}_p(k), \tag{4.61}$$

where T_s is the sampling time of the control loop at the k^{th} sample. $\mathbf{\Phi}_k$ is the kinematic state transition matrix. $\mathbf{C}_k$ is the state measurement matrix. $\mathbf{q}_p$ and $\mathbf{y}$ are the state vector and measured values at the k^{th} sample, respectively. The state observer is designed to use table position measurements and state vector estimate $\hat{\mathbf{q}}_p$ by two iterative steps of the Kalman filter procedure as

$$\hat{\mathbf{q}}_p^-(k) = \mathbf{\Phi}_k \hat{\mathbf{q}}_p(k-1), \tag{4.62}$$

$$\mathbf{P}_k^-(k) = \mathbf{\Phi}_k \mathbf{P}_k(k-1) \mathbf{\Phi}_k^{\mathrm{T}} + \mathbf{Q}_k, \tag{4.63}$$

where $\mathbf{P}_k, \mathbf{P}_k^-$, and $\hat{\mathbf{q}}_p^-$ are the current predicted estimate uncertainty matrix, prior predicted estimate uncertainty matrix, and prior state vector estimate at the k^{th} sample, respectively. $\mathbf{Q}_k$ is the constant process noise covariance matrix is obtained as

$$\mathbf{Q}_k = \mathbf{\Phi}_k \mathbf{J}_k \mathbf{\Phi}_k^{\mathrm{T}}, \mathbf{J}_k = \mathrm{diag}\{0, 0, 0, 0, 0, 0, \sigma_{j1}^2, \sigma_{j2}^2\}, \tag{4.64}$$

where σ_{j1}^2 and σ_{j2}^2 are the random variance in jerk for each axis, respectively. Equations (4.60 - 4.63) and (4.64) summaries the prediction step which is essential for the process, and followed by correction step which is given as

$$\mathbf{K}_k(k) = \mathbf{P}_k^-(k)\mathbf{H}_k^{\mathrm{T}}(\mathbf{H}_k\mathbf{P}_k^-(k)\mathbf{H}_k^{\mathrm{T}} + \mathbf{R}_k)^{-1}, \tag{4.65}$$

$$\hat{\mathbf{q}}_p(k) = \hat{\mathbf{q}}_p^-(k) + \mathbf{K}_k(k)[\mathbf{y}(k) - \mathbf{H}_k\hat{\mathbf{q}}_p^-(k)], \tag{4.66}$$

$$\mathbf{P}_k(k) = \mathbf{P}_k^-(k) - \mathbf{K}_k(k)\mathbf{H}_k\mathbf{P}_k^-(k), \tag{4.67}$$

where $\mathbf{K}_k$ is the Kalman gain matrix at the k^{th} sample. $\mathbf{H}_k$ is the constant observation matrix which is the same as $\mathbf{C}_k$. $\mathbf{R}_k$ is the measurement noise covariance matrix. The values $\mathbf{R}_k$, σ_{j1}^2 and σ_{j2}^2 are selected by trial and error manner to achieve best performance. Initial values are also assigned to $\mathbf{P}_k$.

4.3.5 Error dynamics

The perfect tracking occurs when the $\mathbf{y}_p^* = \mathbf{y}_m$ condition is met. The ideal state $\mathbf{x}_p^*$ and input $\mathbf{u}_p^*$ corresponds to linear combination of the state and input of the reference model given by

$$\mathbf{x}_p^* = \mathbf{S}_{11}\mathbf{x}_m + \mathbf{S}_{12}\mathbf{u}_m, \tag{4.68}$$

$$\mathbf{u}_p^* = \mathbf{K}_{xL}^*\mathbf{x}_m + \mathbf{K}_{uL}^*\mathbf{u}_m, \tag{4.69}$$

where $\mathbf{S}_{11}$ and $\mathbf{S}_{12}$ are the time-varying coefficient matrices. $\mathbf{K}_{xL}^*$ and $\mathbf{K}_{uL}^*$ are constant matrices. Derivative of $\mathbf{x}_p^*$ is given by

$$\dot{\mathbf{x}}_p^* = \dot{\mathbf{S}}_{11}\mathbf{x}_m + \mathbf{S}_{11}\dot{\mathbf{x}}_m + \dot{\mathbf{S}}_{12}\mathbf{u}_m + \mathbf{S}_{12}\dot{\mathbf{u}}_m. \tag{4.70}$$

From (4.29), $\dot{\mathbf{x}}_m = \mathbf{A}_m\mathbf{x}_m + \mathbf{B}_m\mathbf{u}_m$, expanding the above equation with addition and subtraction of $\mathbf{A}_p^*\mathbf{x}_p^* + \mathbf{B}_p^*\mathbf{u}_p^*$ it becomes

$$\begin{aligned}\dot{\mathbf{x}}_p^* = {} & \mathbf{A}_p^*\mathbf{x}_p^* + \mathbf{B}_p^*\mathbf{u}_p^* + \Big(\dot{\mathbf{S}}_{11} - \mathbf{A}_p^*\mathbf{S}_{11} + \mathbf{S}_{11}\mathbf{A}_m - \mathbf{B}_p^*\mathbf{K}_x^*\Big)\mathbf{x}_m \\ & + \Big(\mathbf{S}_{11}\mathbf{B}_m - \mathbf{B}_p^*\mathbf{K}_u^* + \dot{\mathbf{S}}_{12} - \mathbf{A}_p^*\mathbf{S}_{12}\Big)\mathbf{u}_m + \mathbf{S}_{12}\dot{\mathbf{u}}_m.\end{aligned} \tag{4.71}$$

The state error is given by $\mathbf{e}_x = \mathbf{x}_p^* - \mathbf{x}_p$ and its derivative is given as

$$\dot{\mathbf{e}}_x = \dot{\mathbf{x}}_p^* - \dot{\mathbf{x}}_p. \tag{4.72}$$

Substituting $\dot{\mathbf{x}}_p^*$ from (4.71), $\dot{\mathbf{x}}_p$ from (4.31), then add and subtract the term $\mathbf{B}_p^*\mathbf{K}_{eL}^*\mathbf{e}_a$ leads to

$$\dot{\mathbf{e}}_x = \mathbf{A}_p^*\mathbf{e}_x + \mathbf{B}_p^*(\mathbf{u}_p^* - \mathbf{u}_p) + \mathbf{B}_p^*\mathbf{K}_{eL}^*\mathbf{e}_a - \mathbf{B}_p^*\mathbf{K}_{eL}^*\mathbf{e}_a + \mathbf{z}, \tag{4.73}$$

where $\mathbf{z}$ contains the rest of the terms, which is considered to vanish upon the following two conditions are satisfied [37]:

$$\big(\mathbf{C}_p^*\mathbf{S}_{11} + \mathbf{D}_p^*\mathbf{K}_{xL} - \mathbf{C}_m\big)\mathbf{x}_m + \big(\mathbf{C}_p^*\mathbf{S}_{12} + \mathbf{D}_p^*\mathbf{K}_{uL}\big)\mathbf{u}_m = 0, \tag{4.74}$$

$$\begin{aligned}&\big(\dot{\mathbf{S}}_{11} + \mathbf{S}_{11}\mathbf{A}_m - \mathbf{A}_p^*\mathbf{S}_{11} - \mathbf{B}_p^*\mathbf{K}_{xL}^*\big)\mathbf{x}_m + \big(\mathbf{S}_{11}\mathbf{B}_m + \dot{\mathbf{S}}_{12} - \mathbf{A}_p^*\mathbf{S}_{12} - \mathbf{B}_p^*\mathbf{K}_{uL}^*\big)\mathbf{u}_m \\ &+\mathbf{S}_{12}\dot{\mathbf{u}}_m = 0,\end{aligned} \tag{4.75}$$

for this case, the conditions (4.74) and (4.75) hold. Substituting the transformed ideal control input $\mathbf{u}_p^*$ from (4.69), control input $\mathbf{u}_p$ from (4.43), and rotation matrix property; $\mathbf{\Lambda}\mathbf{\Lambda}^{\mathrm{T}} = \mathbf{I}$ into (4.73) and defining unknown desired constant matrix with desired values, $\mathbf{K}^* = \begin{bmatrix}\mathbf{K}_{eL}^* & \mathbf{K}_{xL}^* & \mathbf{K}_{uL}^*\end{bmatrix}$, leads to

$$\dot{\mathbf{e}}_x = \mathbf{A}_p^*\mathbf{e}_x - \mathbf{B}_p^*\mathbf{K}_{eL}^*\mathbf{e}_a - \mathbf{B}_p^*[\mathbf{K} - \mathbf{K}^*]\mathbf{r}. \tag{4.76}$$

The augmented output error between ideal model and the plant can also be represented as

$$\mathbf{e}_a = \mathbf{C}_{pc}\mathbf{e}_x + \mathbf{D}_{pc}[\mathbf{K} - \mathbf{K}^*]\mathbf{r}, \tag{4.77}$$

with

$$\mathbf{C}_{pc} = \mathbf{C}_p^*(\mathbf{I} + \mathbf{D}_p^*\mathbf{K}_{eL}^*)^{-1}, \tag{4.78}$$

$$\mathbf{D}_{pc} = \mathbf{D}_p^*(\mathbf{I} + \mathbf{D}_p^*\mathbf{K}_{eL}^*)^{-1}, \tag{4.79}$$

$$\mathbf{C}_p^* = \begin{bmatrix}1 & 0 & \lambda_{11} & 0 & \lambda_{21} & 0 & \lambda_{31} & 0\\ 0 & 1 & 0 & \lambda_{12} & 0 & \lambda_{22} & 0 & \lambda_{32}\end{bmatrix}. \tag{4.80}$$

The state error derivative from (4.76) can also be defined as

$$\dot{\mathbf{e}}_x = \mathbf{A}_{pc}\mathbf{e}_x - \mathbf{B}_{pc}[\mathbf{K} - \mathbf{K}^*]\mathbf{r}, \tag{4.81}$$

with

$$\mathbf{A}_{pc} = \mathbf{A}_p^* - \mathbf{B}_p^*\mathbf{K}_{eL}^*\mathbf{C}_{pc}, \tag{4.82}$$

$$\mathbf{B}_{pc} = \mathbf{B}_p^*\mathbf{K}_{eL}^*\mathbf{D}_{pc} - \mathbf{B}_p^*. \tag{4.83}$$

The transformed state error is given as $\mathbf{x}_L = \mathbf{N}^{\mathrm{T}}\boldsymbol{\Lambda}^{\mathrm{T}}\mathbf{N}\mathbf{e}_x$, $\mathbf{N}$ represents the transformation matrix, whose derivative is given as

$$\dot{\mathbf{x}}_L = \mathbf{N}^{\mathrm{T}}\boldsymbol{\Lambda}^{\mathrm{T}}\mathbf{N}\dot{e}_x + \mathbf{N}^{\mathrm{T}}\dot{\boldsymbol{\Lambda}}^{\mathrm{T}}\mathbf{N}\mathbf{e}_x. \tag{4.84}$$

By substituting the state error derivative from (4.84), this brings to

$$\dot{\mathbf{x}}_L = \mathbf{A}_{pc}\mathbf{x}_L - \mathbf{N}^{\mathrm{T}}\boldsymbol{\Lambda}^{\mathrm{T}}\mathbf{N}\mathbf{B}_{pc}[\mathbf{K} - \mathbf{K}^*]\mathbf{r} + \mathbf{N}^{\mathrm{T}}\dot{\boldsymbol{\Lambda}}^{\mathrm{T}}\mathbf{N}\mathbf{e}_x. \tag{4.85}$$

Hence, using the transformed error dynamics, the stability can be analysed.

4.3.6 Stability analysis

Lyapunov function candidate is defined as

$$V = \mathbf{x}_L^{\mathrm{T}}\mathbf{P}\mathbf{x}_L + \mathrm{tr}\left\{\mathbf{S}^{\mathrm{T}}(\mathbf{K}_{IL} - \mathbf{K}^*)\boldsymbol{\Gamma}_{IL}^{-1}(\mathbf{K}_{IL} - \mathbf{K}^*)^{\mathrm{T}}\mathbf{S}\right\}, \tag{4.86}$$

where $\mathbf{P}$ and $\boldsymbol{\Gamma}_{IL}$ are the positive definite symmetric matrix and positive definite matrix, respectively. $\mathbf{S}$ is the non-singular matrix. The derivative of V is given as

$$\dot{V} = \dot{x}_L^{\mathrm{T}}\mathbf{P}\mathbf{x}_L + \mathbf{x}_L^{\mathrm{T}}\mathbf{P}\dot{\mathbf{x}}_L + 2\mathrm{tr}\left\{\mathbf{S}^{\mathrm{T}}(\mathbf{K}_{IL} - \mathbf{K}^*)\boldsymbol{\Gamma}_{IL}^{-1}\dot{\mathbf{K}}_{IL}^{\mathrm{T}}\mathbf{S}\right\}. \tag{4.87}$$

Substituting $\dot{\mathbf{x}}_L$ from (4.85), $\dot{\mathbf{K}}_{IL}$ from (4.47) with $\mathbf{e}_{L^*}$ is replaced by $\mathbf{e}_{La^*}$, and $\mathbf{K}_{IL} = \mathbf{K} - \mathbf{e}_{La^*}\mathbf{r}^{\mathrm{T}}\mathbf{\Lambda}^{\mathrm{T}}\mathbf{\Gamma}_{pL}$ into $\dot{V}$, it becomes

$$
\begin{aligned}
&\dot{V} = \mathbf{x}_L^{\mathrm{T}}(\mathbf{A}_{pc}^{\mathrm{T}}\mathbf{P} + \mathbf{P}\mathbf{A}_{pc})\mathbf{x}_L \\
&-\mathbf{N}^{\mathrm{T}}\mathbf{N}\mathbf{B}_{pc}^{\mathrm{T}}[\mathbf{K} - \mathbf{K}^*]^{\mathrm{T}}\mathbf{\Lambda}\mathbf{r}^{\mathrm{T}}\mathbf{P}\mathbf{x}_L \\
&-\mathbf{x}_L^{\mathrm{T}}\mathbf{P}\mathbf{N}^{\mathrm{T}}\mathbf{\Lambda}^{\mathrm{T}}\mathbf{N}\mathbf{B}_{pc}[\mathbf{K} - \mathbf{K}^*]\mathbf{r} \\
&-2\mathbf{S}^{\mathrm{T}}\mathbf{S}\mathbf{e}_{La^*}^{\mathrm{T}}\mathbf{r}\mathbf{\Lambda}\mathbf{\Gamma}_{pL}\mathbf{e}_{La^*}\mathbf{r}^{\mathrm{T}}\mathbf{\Lambda}^{\mathrm{T}} \\
&-2\zeta\mathbf{S}^{\mathrm{T}}\mathbf{S}[\mathbf{K}_{IL} - \mathbf{K}^*]^{\mathrm{T}}\mathbf{\Gamma}_{IL}^{-1}[\mathbf{K}_{IL} - \mathbf{K}^*] \\
&-2\zeta\mathbf{S}^{\mathrm{T}}\mathbf{S}[\mathbf{K}_{IL} - \mathbf{K}^*]^{\mathrm{T}}\mathbf{\Gamma}_{IL}^{-1}\mathbf{K}^* \\
&+2\mathbf{S}^{\mathrm{T}}\mathbf{S}[\mathbf{K} - \mathbf{K}^*]^{\mathrm{T}}\mathbf{e}_{La^*}\mathbf{r}^{\mathrm{T}}\mathbf{\Lambda}^{\mathrm{T}} \\
&+\mathbf{N}\dot{\mathbf{\Lambda}}\mathbf{N}^{\mathrm{T}}\mathbf{e}_x^{\mathrm{T}}\mathbf{P}\mathbf{N}^{\mathrm{T}}\mathbf{\Lambda}^{\mathrm{T}}\mathbf{N}\mathbf{e}_x \\
&+\mathbf{N}\mathbf{\Lambda}\mathbf{N}^{\mathrm{T}}\mathbf{e}_x\mathbf{P}\mathbf{N}^{\mathrm{T}}\dot{\mathbf{\Lambda}}^{\mathrm{T}}\mathbf{N}\mathbf{e}_x.
\end{aligned} \tag{4.88}
$$

The last two terms are eliminated by the rotation matrix property $\mathbf{\Lambda}^{\mathrm{T}}\dot{\mathbf{\Lambda}} + \dot{\mathbf{\Lambda}}^{\mathrm{T}}\mathbf{\Lambda} = \mathbf{0}$. With the choice of $\mathbf{K} = \mathbf{K}^*$ the second, third, and seventh terms are eliminated. The first term satisfies the passivity relation for “strict positive realness” condition [37] :

$$\mathbf{P}\mathbf{A}_{pc} + \mathbf{A}_{pc}^{\mathrm{T}}\mathbf{P} = -\mathbf{Q} - \mathbf{L}^{\mathrm{T}}\mathbf{L} < 0, \tag{4.89}$$

$$\mathbf{P}\mathbf{B}_{pc} = \mathbf{C}_{pc}^{\mathrm{T}}(\mathbf{S}^{\mathrm{T}}\mathbf{S}) - \mathbf{L}^{\mathrm{T}}\mathbf{W}, \tag{4.90}$$

$$\mathbf{D}_{pc} + \mathbf{D}_{pc}^{\mathrm{T}} = \mathbf{W}^{\mathrm{T}}\mathbf{W} \tag{4.91}$$

where $\mathbf{L}$ and $\mathbf{Q}$ are the positive definite matrices and positive-definite symmetric matrix $(\mathbf{S}^{\mathrm{T}}\mathbf{S})$ exists, which makes the product $(\mathbf{S}^{\mathrm{T}}\mathbf{S})\mathbf{C}_{pc}\mathbf{B}_{pc}$ positive definite symmetric whenever $\mathbf{C}_{pc}\mathbf{B}_{pc}$ is positive definite but not symmetric [38]. Using $\mathbf{e}_{La^*} = \mathbf{C}_{pc}\mathbf{x}_L + \mathbf{C}_{pc}\mathbf{h}_r$, $\mathbf{h}_r = \left[\mathbf{h}^{*\mathrm{T}}, \dot{\mathbf{h}}^{*\mathrm{T}}, \ddot{\mathbf{h}}^{*\mathrm{T}}, \dddot{\mathbf{h}}^{*\mathrm{T}}\right]^{\mathrm{T}}$, Lyapunov candidate derivative becomes

$$
\begin{aligned}
\dot{V} &= -\mathbf{x}_L^{\mathrm{T}}\mathbf{Q}\mathbf{x}_L - \mathbf{x}_L^{\mathrm{T}}\mathbf{L}^{\mathrm{T}}\mathbf{L}\mathbf{x}_L \\
&-2\mathbf{C}_{pc}(\mathbf{S}^{\mathrm{T}}\mathbf{S})[\mathbf{K}-\mathbf{K}^*]^{\mathrm{T}}\boldsymbol{\Lambda}\mathbf{r}^{\mathrm{T}}\mathbf{x}_L \\
&+2\mathbf{L}\mathbf{W}^{\mathrm{T}}[\mathbf{K}-\mathbf{K}^*]^{\mathrm{T}}\boldsymbol{\Lambda}\mathbf{r}^{\mathrm{T}}\mathbf{x}_L \\
&-2\mathbf{S}^{\mathrm{T}}\mathbf{S}\mathbf{e}_{La^*}^{\mathrm{T}}\mathbf{r}\boldsymbol{\Lambda}\boldsymbol{\Gamma}_{pL}\mathbf{e}_{La^*}\mathbf{r}^{\mathrm{T}}\boldsymbol{\Lambda}^{\mathrm{T}} \\
&-2\zeta\mathbf{S}^{\mathrm{T}}\mathbf{S}[\mathbf{K}_{IL}-\mathbf{K}^*]^{\mathrm{T}}\boldsymbol{\Gamma}_{IL}^{-1}[\mathbf{K}_{IL}-\mathbf{K}^*] \\
&-2\zeta\mathbf{S}^{\mathrm{T}}\mathbf{S}[\mathbf{K}_{IL}-\mathbf{K}^*]^{\mathrm{T}}\boldsymbol{\Gamma}_{IL}^{-1}\mathbf{K}^* \\
&+2\mathbf{S}^{\mathrm{T}}\mathbf{S}[\mathbf{K}-\mathbf{K}^*]^{\mathrm{T}}\mathbf{r}^{\mathrm{T}}\boldsymbol{\Lambda}\mathbf{C}_{pc}\mathbf{x}_L \\
&+2\mathbf{S}^{\mathrm{T}}\mathbf{S}[\mathbf{K}-\mathbf{K}^*]^{\mathrm{T}}\mathbf{r}^{\mathrm{T}}\boldsymbol{\Lambda}\mathbf{C}_{pc}\mathbf{h}_r. \qquad (4.92)
\end{aligned}
$$

The second and seventh terms are cancel each other and with the choice of $\mathbf{K}=\mathbf{K}^*$ which is required for implementation [37], rearranging the equation (4.92) becomes

$$
\begin{aligned}
\dot{V} &= -\mathbf{x}_L^{\mathrm{T}}\mathbf{Q}\mathbf{x}_L - \mathbf{x}_L^{\mathrm{T}}\mathbf{L}^{\mathrm{T}}\mathbf{L}\mathbf{x}_L - 2\mathbf{S}^{\mathrm{T}}\mathbf{S}\mathbf{e}_{La^*}^{\mathrm{T}}\mathbf{r}\boldsymbol{\Lambda}\boldsymbol{\Gamma}_{pL}\mathbf{e}_{La^*}\mathbf{r}^{\mathrm{T}}\boldsymbol{\Lambda}^{\mathrm{T}} \\
&-2\zeta\mathbf{S}^{\mathrm{T}}\mathbf{S}[\mathbf{K}_{IL}-\mathbf{K}^*]^{\mathrm{T}}\boldsymbol{\Gamma}_{IL}^{-1}[\mathbf{K}_{IL}-\mathbf{K}^*] - 2\zeta\mathbf{S}^{\mathrm{T}}\mathbf{S}[\mathbf{K}_{IL}-\mathbf{K}^*]^{\mathrm{T}}\boldsymbol{\Gamma}_{IL}^{-1}\mathbf{K}^*. \qquad (4.93)
\end{aligned}
$$

For simplicity, by introducing the non-negative constants $\beta_1, \beta_2, \beta_3, .., \beta_6$ leads to

$$
\begin{aligned}
\dot{V} &\leq -\beta_1\|\mathbf{x}_L\|^2 - \beta_2\|\mathbf{e}_{La^*}\|^2\|\tilde{\mathbf{F}}_{ew}^{\mathrm{T}}\mathbf{e}_a\|^2 - \beta_3\|\mathbf{e}_{La^*}\|^2\|\tilde{\mathbf{F}}_{xm}^{\mathrm{T}}\mathbf{x}_m\|^2 \\
&-\beta_4\|\mathbf{e}_{La^*}\|^2\|\tilde{\mathbf{F}}_{um}^{\mathrm{T}}\mathbf{u}_m\|^2 - \beta_5\|[\mathbf{K}_{IL}-\mathbf{K}^*]\|^2 - \beta_6\|[\mathbf{K}_{IL}-\mathbf{K}^*]\|. \qquad (4.94)
\end{aligned}
$$

Thus, $\dot{V}$ becomes negative semi-definite. The quadratic form of V guarantees that $\mathbf{x}_L$, $\mathbf{e}_{La}^*$, $\mathbf{e}_a$ and $\mathbf{K}_{IL}$ are bounded. Since V in (4.86) is lower bounded and $\dot{V}$ is negative semi-definite, to apply the Barbalat's lemma requires $\dot{V}$ to be uniformly continuous. The derivative of $\dot{V}$ is

$$
\begin{aligned}
\ddot{V} &= -2\dot{\mathbf{x}}_L^{\mathrm{T}}(\mathbf{Q}+\mathbf{L}^{\mathrm{T}}\mathbf{L})\mathbf{x}_L - 4\mathbf{S}^{\mathrm{T}}\mathbf{S}\mathbf{e}_{La^*}^{\mathrm{T}}\mathbf{r}\boldsymbol{\Lambda}\boldsymbol{\Gamma}_{pL}\dot{\mathbf{e}}_{La^*}\mathbf{r}^{\mathrm{T}}\boldsymbol{\Lambda}^{\mathrm{T}} \\
&-4\mathbf{S}^{\mathrm{T}}\mathbf{S}\mathbf{e}_{La^*}^{\mathrm{T}}\dot{\mathbf{r}}\boldsymbol{\Lambda}\boldsymbol{\Gamma}_{pL}\mathbf{e}_{La^*}\mathbf{r}^{\mathrm{T}}\boldsymbol{\Lambda}^{\mathrm{T}} - 4\zeta\mathbf{S}^{\mathrm{T}}\mathbf{S}\dot{\mathbf{K}}_{IL}^{\mathrm{T}}\boldsymbol{\Gamma}_{IL}^{-1}[\mathbf{K}_{IL}-\mathbf{K}^*] \\
&-2\zeta\mathbf{S}^{\mathrm{T}}\mathbf{S}\dot{\mathbf{K}}_{IL}^{\mathrm{T}}\boldsymbol{\Gamma}_{IL}^{-1}\mathbf{K}^*. \qquad (4.95)
\end{aligned}
$$

The regressor $\mathbf{r}$ contains vector signals $\mathbf{e}_a$, $\mathbf{x}_m$, and $\mathbf{u}_m$. Reference control input signal u_m and its derivative are assumed uniformly bounded and piece-wise continuous, thus $\mathbf{x}_m$ and $\dot{\mathbf{x}}_m$ are bounded from (4.29). Hence, $\mathbf{r}$ is bounded as $\mathbf{e}_a$ is bounded as well.

The derivative of $\mathbf{x}_L$ from (4.85) is bounded as $\dot{\mathbf{\Lambda}}^{\mathrm{T}} = \mathbf{U}^{\mathrm{T}}\mathbf{\Lambda}^{\mathrm{T}}$, here $\mathbf{U}$ is the skew-symmetric matrix and as $\mathbf{x}_L$ is bounded from (4.93) at $\mathbf{K} = \mathbf{K}^*$. The derivative of $\mathbf{e}_{La^*}$: $\dot{\mathbf{e}}_{La^*} = \mathbf{C}_{pc}\dot{\mathbf{x}}_L + \mathbf{C}_{pc}\dot{\mathbf{h}}_r$, $\dot{\mathbf{h}}_r$ is bounded by the reference model piece-wise continuous assumption, therefore $\dot{\mathbf{e}}_{La^*}$ is bounded as $\dot{\mathbf{x}}_L$ and $\dot{\mathbf{h}}_r$ are bounded. As $\mathbf{e}_{La^*}$ and its derivative are bounded, thus makes $\mathbf{e}_a$ and $\dot{\mathbf{e}}_a$ bounded. The derivative of regressor vector $\mathbf{r}$ is also bounded as $\dot{\mathbf{e}}_a$, $\dot{\mathbf{x}}_m$, and $\dot{\mathbf{u}}_m$ are bounded. This shows that $\ddot{V}$ is bounded, hence $\dot{V}$ is uniformly continuous, and from the Barbalat's lemma,

$$\lim_{t\to\infty} \mathbf{x}_L(t) = 0$$

is shown.

4.4 Simulation and experiment

4.4.1 Conditions

Simulation and experiments are conducted to verify the effectiveness of the proposed contouring control. The butterfly reference trajectory shown in Fig. 4.6 is used as the tracking reference. The trajectory is obtained by

$$\begin{aligned} y_{m1} &= 4\sin(\theta)\left(\mathbf{e}^{\cos(\theta)} - 2\cos(4\theta) + \sin(\frac{\theta}{12})^5\right), \\ y_{m2} &= 4\cos(\theta)\left(\mathbf{e}^{\cos(\theta)} - 2\cos(4\theta) + \sin(\frac{\theta}{12})^5\right), \theta \in [0, 2\pi]. \end{aligned} \tag{4.96}$$

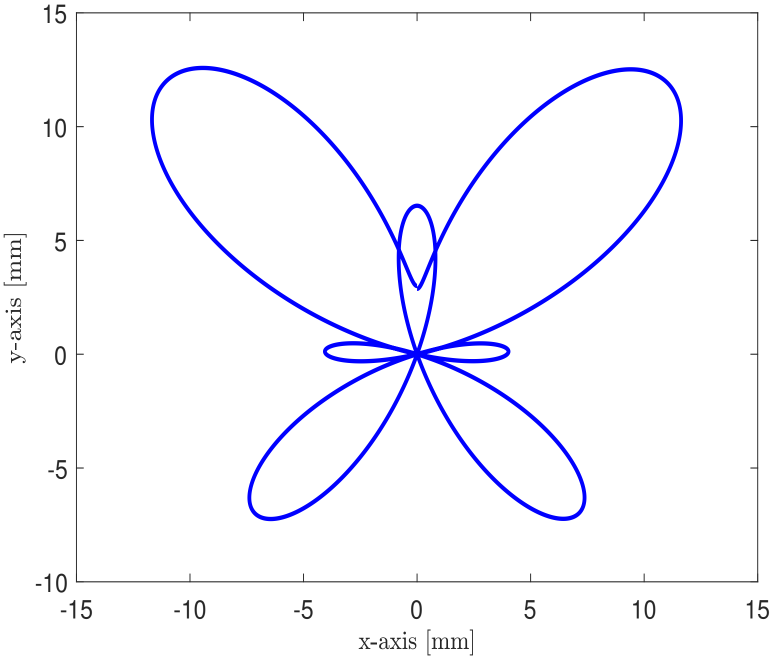

Figure 4.6: Reference butterfly trajectory

The reference model is selected as a fifth order given as

$$
\dot{\mathbf{x}}_m = \begin{bmatrix} 0 & 0 & 1 & 0 & 0 & 0 & 0 & 0 & 0 & 0 \\ 0 & 0 & 0 & 1 & 0 & 0 & 0 & 0 & 0 & 0 \\ 0 & 0 & 0 & 0 & 1 & 0 & 0 & 0 & 0 & 0 \\ 0 & 0 & 0 & 0 & 0 & 1 & 0 & 0 & 0 & 0 \\ 0 & 0 & 0 & 0 & 0 & 0 & 1 & 0 & 0 & 0 \\ 0 & 0 & 0 & 0 & 0 & 0 & 0 & 1 & 0 & 0 \\ 0 & 0 & 0 & 0 & 0 & 0 & 0 & 0 & 1 & 0 \\ 0 & 0 & 0 & 0 & 0 & 0 & 0 & 0 & 0 & 1 \\ 2p & 0 & -8p^3 & 0 & 8p^3 & 0 & -8p^4 & 0 & p^5 & 0 \\ 0 & 2p & 0 & -8p^3 & 0 & 8p^3 & 0 & -8p^4 & 0 & p^5 \end{bmatrix} \mathbf{x}_m
$$
$$
+ \begin{bmatrix} 0 & 0 & 0 & 0 & 0 & 0 & 0 & 0 & 1/10^{-4} & 0 \\ 0 & 0 & 0 & 0 & 0 & 0 & 0 & 0 & 0 & 1/10^{-4} \end{bmatrix}^{\mathrm{T}} \mathbf{u}_m, \tag{4.97}
$$

Table 4.1: Plant parameters

Parameter	1^{st}axis	2^{nd}axis
L_{li}	0.01 m	0.01 m
J_{mi}	1.46×10^{-4} kgm^2	1.54×10^{-4} kgm^2
m_{ei}	88.08 Ns^2/m	97.9 Ns^2/m
c_i	535.20 Ns/m	796 Ns/m
k_i	36.58 N/m	45.56 N/m
c_{ei}	172.81 Ns/m	192.08 Ns/m
c_{ai}	384.38 Ns/m	766.35 Ns/m

where p is the negative pole that is selected to make $\mathbf{A}_m$ matrix Hurwitz stable. For the reference model, states vectors $\mathbf{x}_m$, and derivatives in (4.29) are known, and hence the control variable $\mathbf{u}_m$ is available. The reference state vector, denoted by $\mathbf{x}_m$, is a component of the control laws as described in (4.36) and (4.43). It contains higher-order derivatives of the desired trajectory. These derivatives can have high peak values that may cause distortions. To prevent distortions, the reference state vector $\mathbf{x}_m$ is replaced by $\mathbf{\Theta}_m\mathbf{x}_m$ in the regressor vector $\mathbf{r}$, where $\mathbf{\Theta}_m = \text{diag}\{\rho^0, \rho^0 ..., \rho^{n_m-1}, \rho^{n_m-1}\} \in R^{n_m \times n_m}$. All the diagonal terms in $\mathbf{\Theta}_m$ must be positive, and since $\mathbf{x}_m$ is bounded, $\mathbf{\Theta}_m\mathbf{x}_m$ is also bounded. The ASPR imposing methods; parallel feedforward compensation (PFC) and jerk-based augmented output signal which contains the velocity, acceleration, and jerk signals (AOS-v-a-j) are paired with SACC and results are compared. The equivalent mass of an actuator is given as

$$m_{ai} = \frac{4\pi^2 J_{mi}}{L_{li}^2}, \tag{4.98}$$

where J_{mi} is the motor actuator inertia and L_{li} is the lead of the ball nut of the i^{th} axis. The plant parameters and controller values are given in Tables 4.1 and 4.2, respectively.

4.4.2 Experimental setup

An industrial feed drive system shown in Fig. 2.3 with ball-screw mechanism powered by an AC servo motor was employed. The actual position is measured by a rotary encoder attached to a drive motor with the equivalent sensor resolution for linear motion as 76.29 nm at a 0.35

Table 4.2: Control parameters

Parameter	Values
p	-2
ρ	10^{-4}
ζ	$\text{diag}\{10^{-3}, 10^{-3}\}$
D_1, D_2	10^{-4}
α_1, α_2	2.5
$\mathbf{\Gamma}_{Pxm}, \mathbf{\Gamma}_{PxL}$	$\text{diag}\{10^3, 10^3, 10, 10, 10^{-1}, 10^{-1}, 10^{-3}, 10^{-3}, 10^{-5}, 10^{-5}\}$,
$\mathbf{\Gamma}_{Ixm}, \mathbf{\Gamma}_{IxL}$	$\text{diag}\{10^3, 10^3, 10, 10, 10^{-1}, 10^{-1}, 10^{-3}, 10^{-3}, 10^{-5}, 10^{-5}\}$,
$\mathbf{\Gamma}_{Pum}, \mathbf{\Gamma}_{PuL}$	$\text{diag}\{10^{-5}, 10^{-5}\}$
$\mathbf{\Gamma}_{Ium}, \mathbf{\Gamma}_{IuL}$	$\text{diag}\{10^{-5}, 10^{-5}\}$
λ_1,λ_2,λ_3	$\text{diag}\{10^{-4}, 10^{-4}\}\text{s}$, $\text{diag}\{10^{-7}, 10^{-7}\}\text{s}^2$, $\text{diag}\{10^{-13}, 10^{-13}\}\text{s}^3$

ms sampling time for each drive axis. A power analyzer (HIOKI 3390) connected to the motor driver measures energy consumption at a 50 ms data interval update. The industrial feed drive is operated by a computer with Ubuntu operating system using C/C++ programming environment. The adaptation scaling factors on the adaptive gains are assigned by trial and error manner until the best tracking performance is achieved. The AOS-v-a-j approach requires the Kalman filter design in (4.60-4.67) implemented with the values of σ_{ji}^2 and R_{ki} selected as 10^{15} and 0.0002 same for each axis, respectively.

4.4.3 Simulation results

Figure 4.7 shows the simulation results comparing the tracking and contouring performance of two different ASPR imposition methods: PFC and AOS-v-a-j. The results show that AOS-v-a-j is able to achieve lower tracking and contouring errors than PFC, when both methods are used under the same conditions. Furthermore, comparing the performance of AOS-v-a-j with SACC to that of AOS-v-a-j with SAC, AOS-v-a-j is able to achieve lower tracking and contouring errors simultaneously under similar conditions. These results demonstrate the superior performance of AOS-v-a-j with SACC in terms of reducing tracking and contouring errors. The adaptive

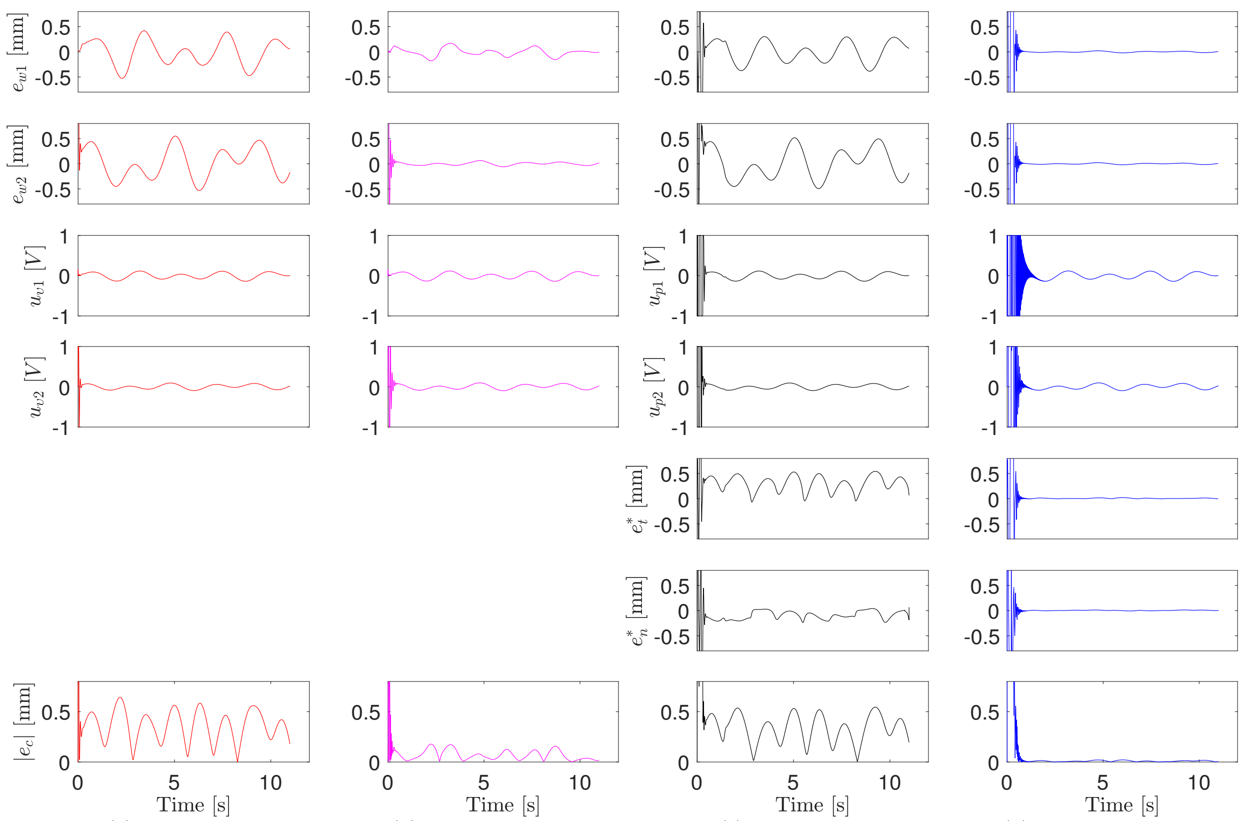

Figure 4.7: Simulation results

gains profiles are shown in Fig. 4.8 for PFC with SAC, AOS-v-a-j with SAC, PFC with SACC, and AOS-v-a-j with SACC, respectively, under the same assigned adaptation scaling factors. These results show PFC with SAC, AOS-v-a-j with SAC, and PFC with SACC, fail to attain sufficient adaptation for precisely tracking the trajectory as compared to AOS-v-a-j with SACC. Referring to equations (4.56-4.58), higher-order derivatives of $\tilde{\mathbf{F}}$ amplifies the adaptation scaling factors making faster transient response, and smaller steady state error is achieved for AOS-v-a-j with SACC. Moreover, lack of improvement on contouring accuracy for PFC with SACC is caused by the transformed PFC output signal $\tilde{\mathbf{F}}^{\mathrm{T}}\mathbf{y}_f$ in (4.50). Since the PFC output signal is different from that of the actual plant, the transformed augmented output error used as an adaptation signal in the control input is altered. For clarity, the summary of the steady state SACC contour error results after convergence are shown in Table 4.3.

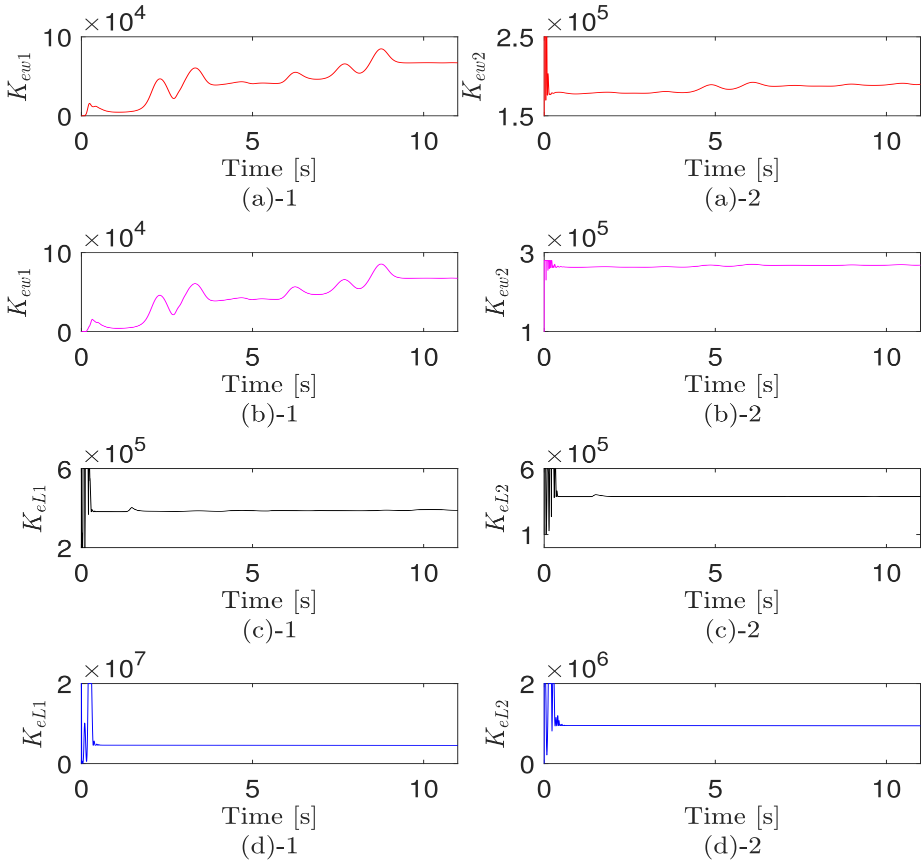

Figure 4.8: Controller gain profiles in simulation; (a) PFC with SAC, (b) AOS-v-a-j with SAC, (c) PFC with SACC, and (d) AOS-v-a-j with SACC

4.4.4 Experimental results

Experiments were conducted to evaluate the tracking error, contour error, and energy saving capability of the proposed contouring approach using the butterfly trajectory given in (4.96). Three specific cases were investigated. The first case aims to confirm the effectiveness of the AOS-v-a-j with SACC in contouring by comparing its performance to that of the AOS-v-a-j with SAC, PFC with SAC, and PFC with SACC under similar conditions. The second case was to confirm the contouring performance of AOS-v-a-j with SACC compared to PFC with SACC when performed under similar conditions. Finally, the third case aimed to confirm the effectiveness of SACC compared to SAC when subjected to high adaptive gains.

Table 4.3: Summary of SACC contour error results

	Tangential and normal errors [mm]			
	Maximum		Average	
Controller	$\lvert e_t^* \rvert$	$\lvert e_n^* \rvert$	$\lvert e_t^* \rvert$	$\lvert e_n^* \rvert$
PFC	0.5444	0.2367	0.3086	0.0927
AOS-v-a-j	0.0209	0.0131	0.0075	0.0052

4.4.4.1 Tracking performance

Selecting the same positive definite matrices $\mathbf{\Gamma}_{pL}$, $\mathbf{\Gamma}_{IL}$, $\mathbf{\Gamma}_{pw}$, and $\mathbf{\Gamma}_{Iw}$, experiments were conducted to compare the tracking and contouring performance of two different ASPR imposition methods: PFC and AOS-v-a-j with SAC and SACC, interchangeably as shown in Fig. 4.9. The performance of AOS-v-a-j with SACC was compared to that of AOS-v-a-j with SAC, it was found that AOS-v-a-j with SACC was able to simultaneously achieve lower tracking and contouring errors under similar conditions. Moreover, the steady-state control input for AOS-v-a-j with SACC was smoother than that of PFC with SACC under similar conditions. These results demonstrate the superior performance of AOS-v-a-j with SACC in terms of reducing tracking and contouring errors while achieving smoother control input. The same experiment design was repeated 5 times for each control scheme in which energy consumption was measured and control input variance was calculated using

$$\sigma^2 = \sum_{i=1}^{2} \left(\frac{\sum_{j=1}^{N_u} (u_{ij} - \mu_i)^2}{N_u} \right), \tag{4.99}$$

where u_{ij} represents the control input value at the j^{th} sampling instant of the i^{th} axis, N_u is the total number of samples ($j = 1, 2, ..., N_u$) and μ_i is the average of all control values of the i^{th} axis. Fig. 4.10 shows the trial results of the tracking performance, control input variance, and energy consumption comparisons between PFC and AOS-v-a-j using either SAC or SACC. PFC with SACC reduced the mean tracking error of the 1$^{\text{st}}$ axis by about 32% when compared to PFC with SAC. However, for the 2$^{\text{nd}}$ axis, the mean tracking error increased by about 50%. Using AOS-v-a-j with SACC demonstrated superiority on which the tracking error was reduced

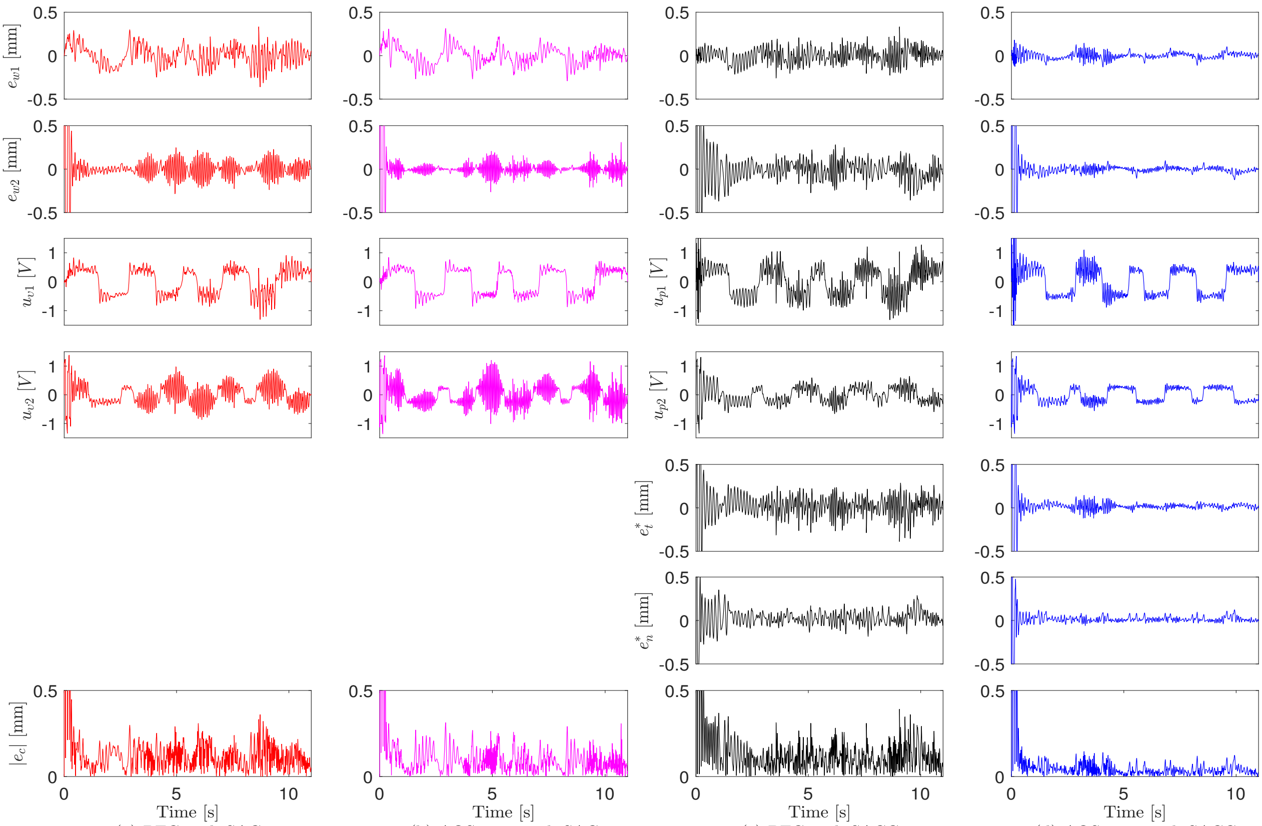

(a) PFC with SAC (b) AOS-v-a-j with SAC (c) PFC with SACC (d) AOS-v-a-j with SACC

Figure 4.9: Experimental results

by about 60% and 5% on the 1st and 2nd axes, respectively when compared to AOS-v-a-j with SAC.

When comparing PFC with SACC to PFC with SAC, it was found that the control input variance increased by approximately 10%, and a 2% increase in average energy consumption. On the other hand, AOS-v-a-j with SACC showed a 6% reduction in control input variance compared to AOS-v-a-j with SAC, and energy consumption was reduced by about 7% on average.

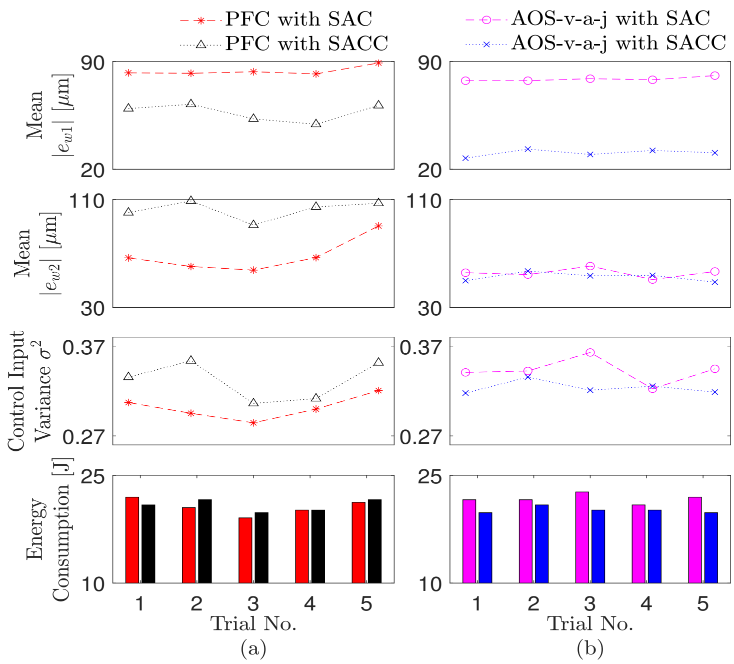

Figure 4.10: Case I experimental results

4.4.4.2 Contouring performance

Using the butterfly trajectory, both designed contouring controllers with ASPR imposing methods: PFC and AOS-v-a-j are compared with each other using identical positive definite matrices for adaptive gains. Fig. 4.11 shows the comparisons of the absolute mean values of the tangent error e_{t^*}, normal error e_{n^*}, contour error e_c, control input variance σ^2, and energy consumption for the trial runs. The results demonstrated that AOS-v-a-j with SACC reduce by about 45.90%, 46.35%, and 45.92% for tangent, normal, and contour errors, respectively when compared to PFC with SACC. In terms of energy saving, AOS-v-a-j with SACC reduce by about 3.11% of energy consumption and by about 2.42% of control input variance when compared to PFC with SACC. AOS-v-a-j with SACC was superior in terms of accuracy and energy saving compared to PFC with SACC.

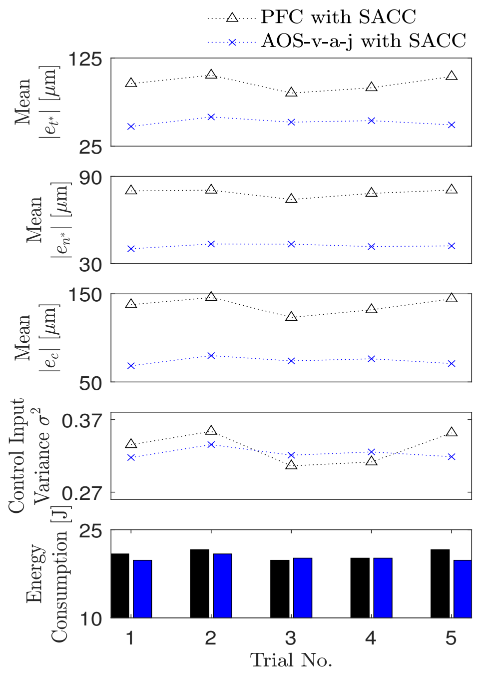

Figure 4.11: Case II experimental results

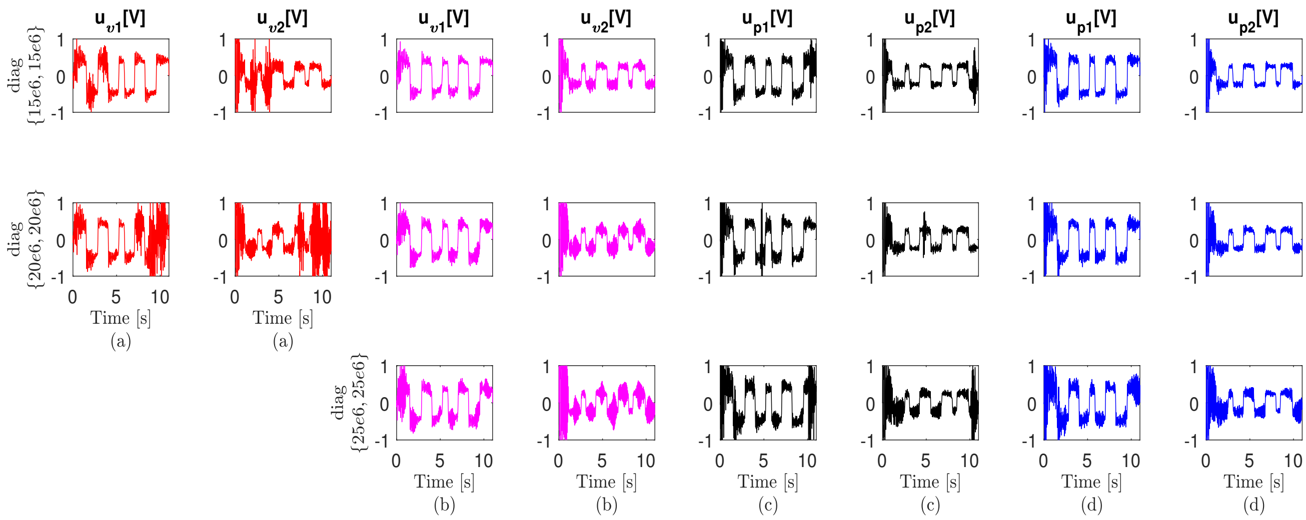

Figure 4.12: Case III experimental results; (a) PFC with SAC, (b) AOS-v-a-j with SAC, (c) PFC with SACC, and (d) AOS-v-a-j with SACC

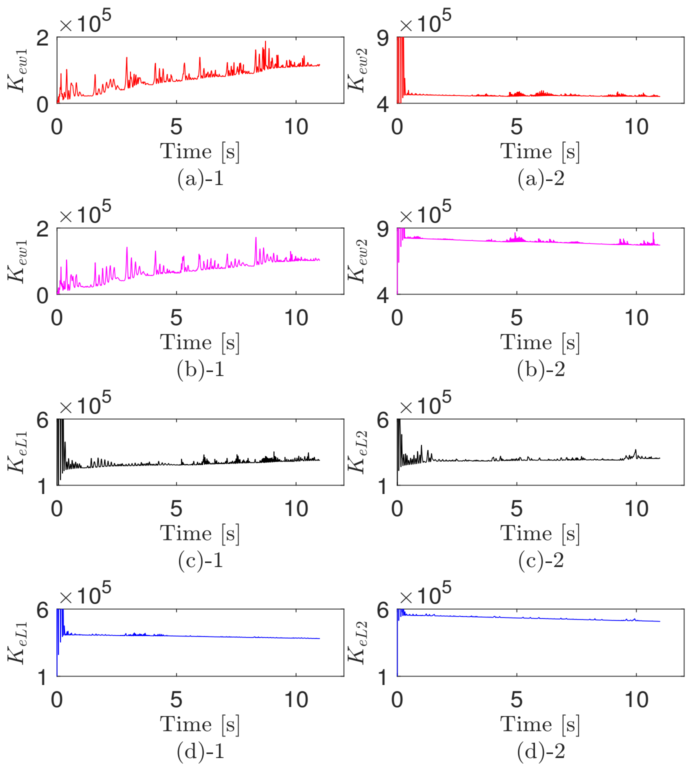

Figure 4.13: Experimental controller gains profiles; (a) PFC with SAC, (b) AOS-v-a-j with SAC, (c) PFC with SACC, and (d) AOS-v-a-j with SACC

4.4.4.3 Effects of adaptation scaling

The performance of SAC and SACC can be increased by the use of high adaptation scaling factors [72]. The adaptation scaling factors matrices used for cases I and II are given as $\mathbf{\Gamma}_{Pew} = \mathbf{\Gamma}_{Iew} = \mathbf{\Gamma}_{PeL} = \mathbf{\Gamma}_{IeL} = \text{diag}\{10e6, 10e6\}$. On the case III, adaptation scaling factors are increased to $\text{diag}\{15e6, 15e6\}$, $\text{diag}\{20e6, 20e6\}$, and $\text{diag}\{25e6, 25e6\}$ with the purpose of evaluating the effectiveness of PFC with SAC, PFC with SACC, AOS-v-a-j with SAC, and AOS-v-a-j with SACC. Fig. 4.12 shows the control input for both axes. As a result, it can be concluded that AOS-v-a-j with SAC, PFC with SACC, and AOS-v-a-j with SACC are more effective, unlike PFC with SAC shows instability at high adaptation scaling factors. In addition, AOS-v-a-j with SACC is shown to be more superior achieving smoother control input.

4.5 Discussion

Figs. 4.8 and 4.13 show the controller gain profiles for both simulation and experiment results, which exhibit similar behavior. Moreover, both simulation and experiment performances reached the same conclusion regarding the comparison of tracking and contouring performances for both ASPR imposing methods under the same operating parameters, as shown in Figs. 4.7 and 4.10. In addition, controller gains for all the controllers are initialized to zero, which requires time for controller gains to settle to reasonable values. Hence, the transient state is unsatisfactory. This tendency is observed in both Figs. 4.7 and 4.10. Predominantly the proposed contouring approach, AOS-v-a-j with SACC demonstrated superiority in terms of tracking error reduction, contouring accuracy, and smoother control input when compared to PFC with SACC, and AOS-v-a-j with SAC as shown on the cases I, II, and III. Furthermore, AOS-v-a-j is related to the original plant output making the augmented output error proper to generate the desired control input unlike PFC which has an independent plant. Fig. 4.13 shows the behavior of controller gains for all the approaches. The proposed approach of AOS-v-a-j with SACC attains higher controller gains compared to AOS-v-a-j with SAC under similar assigned adaptation scaling factors. Higher controller gains are achieved by the derivatives of rotation matrix $\tilde{\mathbf{F}}$ on the formulation (4.56 - 4.59). On the SAC theory, controller gains behavior is known to increase only if needed [37]. From these results it can be seen the AOS-v-a-j with SACC after transient state, the controller gains decrease on both axes unlike PFC with SAC, PFC with SACC, and AOS-v-a-j with SAC.

PFC with SACC achieves better tracking performance on the 1$^{\text{st}}$ axis and lower tracking on the 2$^{\text{nd}}$ axis as compared to PFC with SAC as shown on Fig. 4.10 case I (a). This is influenced by the effects of transformed PFC output signal $\tilde{\mathbf{F}}^{\mathrm{T}}\mathbf{y}_f$ to the transformed augmented output error $\mathbf{e}_{Lf^*}$ in (4.49 - 4.50), which is used as adaptation signal. TCC requires the mismatch of both axes to be small enough [71, 73] which is not the case for PFC with SACC under the presence of PFC output $\mathbf{y}_f$. As the PFC output signal is different from that of the actual plant, further mismatch between augmented output of both axes occurs.

Actually, energy consumption may be influenced by many factors, including the controller design, controller gains, trajectory generation, and the complexity of the trajectory. Therefore, there are cases in which high contouring accuracy may lead to increased energy consumption, as shown in [74, 75]. Furthermore, on Fig. 4.10 shows the results of the both tracking and contouring performances for PFC and AOS type controllers. The large difference between the two axes are due to using the same adaptation scaling factors for updating gains while the axes model parameters are different and the reason it was selected the same adaptation scaling parameters is to investigate the performances of tracking cases and contouring cases.

4.6 Summary

Simple adaptive contouring control proposed in this chapter which combines simple adaptive control and tangent-contouring control using the modified reference adjustment method in a parametric trajectory. This allows the designed adaptive contouring controller to address the estimated contour error directly and increase contouring accuracy with low control input variance of the biaxial feed drive system. Approaches that achieve the almost strictly positive real property have been described; the parallel feedforward compensation approach and the jerk-based augmented output signal. Simulation and experiments were conducted using simple adaptive contouring control with the almost strictly positive real property imposed methods. The proposed approach has shown to achieve better contouring accuracy with lower control input variance compared to the parallel feedforward compensation approach. The results have shown that the proposed method have higher contouring accuracy by about 45% compared to PFC under the same tracking conditions.

Chapter 5

Combined simple adaptive and integral terminal sliding control

In this chapter a novel approach of combining simple adaptive and integral terminal adaptive control is proposed for industrial feed drive systems. The adaptive control law is designed from a fractional power integral terminal sliding mode control configuration using a simple adaptive control-like technique. This formulation allows the proposed controller to mitigate the plant parameters estimation difficulties while benefiting from the inclusion of fractional power signals in the adaptive control law. Simulation and experiments were conducted using the proposed approach compared to conventional approaches. The proposed approach has shown to achieve higher tracking accuracy compared to the conventional approaches under the same tracking conditions. Experimental results show that the proposed approach can reduce by about 58.6% and 73% for axis 1 and 2, respectively as compared to simple adaptive control only.

This chapter is organized as follows: Section 5.1 presents the related works followed by a dynamic model of the plant is presented described in Section 5.2. Controller design is described in section 5.3, followed by simulation and experiment in section 5.4. Section 5.5 discusses results, followed by concluding remarks in section 5.6

5.1 Related works

In modern manufacturing, feed drives are widely used because of their simple structure, high transmission accuracy and low sensitivity to variations [46, 76, 77]. In order to attain high productivity and precision, the control system of feed drives must have good transient and steady tracking performances. However, feed drives experience tracking errors caused by ball-screw assembly and face disturbances which may deteriorate the overall system performance. Cascade Proportional/Proportional-Integral (P/PI) controller is widely applied in most machine control algorithm. The cascade P/PI control consists of a PI controlled inner velocity loop with a P controller in the outer position loop, but its performance is limited.

In recent years, nonlinear control techniques including model predictive control [10], sliding mode control [11], model-reference adaptive control [12], and robust control [13] have been applied in the feed drives to achieve high-performance in different situations. Among these control methods, sliding mode control is one of the most efficient methods to improve the disturbance rejection and robustness properties of the feed drive system. Sliding mode control has the ability to switch the control law very fast to drive the system states from any initial states onto a user-specified sliding surface, and to maintain the states on the surface for all subsequent time. This results in a system that is insensitive to parametric uncertainties and external disturbances. However, conventional linear sliding mode cannot converge in finite-time, which hinders its application in practical engineering. Wu *et al.* [78] proposed a terminal sliding mode (TSM) control, a nonlinear term was introduced into the sliding mode surface to make the system tracking error reach the equilibrium point in finite-time. However, TSM control has singularity problem near the equilibrium point. Chui [79] proposed integral terminal sliding mode (ITSM) control with fractional calculus concept to the relative degree one systems. The design allows to eliminate reaching time to the sliding hyperplane and the convergence of both tracking error and integral error is accomplished in a finite-time. However, the equivalent control law of ITSM control requires thorough knowledge of the controlled plant parameters and dynamics, which are difficult to obtain.

In real applications, the parameters of a plant are not always accessible and may be time-varying. This necessitates using adaptive control strategies to adjust to these changes in real-time to ensure optimal performance. One effective solution is using SAC developed by Sobel *et* *al.* [80]. SAC is a direct adaptive control technique that updates the controller gains without requiring the estimation of unknown plant parameters or mathematical models of the system. Adaptive law of SAC only requires the reference model and tracking error information. In addition, SAC algorithm is ease to implementation. However, it requires that the plant should satisfy “almost strictly positive real (ASPR)” property. Note that ASPR conditions are not satisfied by most systems in the real world. Hence, Barkana and Kaufman [41, 81] introduce a parallel feedforward compensator (PFC) that satisfies the ASPR property. Yasser *et al.* [82] proposed adaptive sliding mode control using SAC with PFC to construct an equivalent control input and a modified sliding surface with a sign function is used to construct a corrective control input, eliminating the need for prior knowledge of the plant for calculating the control law. Mokhtari *et al.* [58] proposed simple adaptive synergetic control for nonlinear systems without requiring knowledge of the system parameters and dynamics using SAC with PFC. Adaptive synergetic control law is derived from the desired manifold of the synergetic control theory. These works [58, 82] show that adaptive control law can be derived using the SAC algorithm. However, using PFC for ASPR property brings augmented feedback, degrading overall performance due to parallel structures.

For feed drive actuation, SAC applications have employed [53, 54, 68, 69, 83]. These methods use augmented output signals (AOS) for ASPR property. These approaches use higher-order output derivatives with assigned constant relative gains to the signals and the augmented output is used as the feedback. These approaches have shown a significant improvement in tracking control compared to PFC.

The chapter proposes simple terminal adaptive sliding mode control for the feed drive systems. This is accomplished by using SAC to construct the equivalent control for fractional ITSM control which will remove the problem of unknown plant parameters and dynamics. Augmented output signal with terminal sliding surface is used to derive the adaptive control law with a switching corrective control input gain to counteract the disturbances.

5.2 Dynamic model for feed drive system

The dynamics of a typical feed drive system is represented by the following decoupled second order system:

$$m_i\ddot{\theta}_i + h_i\dot{\theta}_i + d_i = f_{ai}, \tag{5.1}$$

where m_i, θ_i, h_i, d_i, and f_{ai} are the equivalent mass of the table, the position of the table, the viscous friction coefficient, the bounded input disturbances, and the driving force to the i^{th} drive axis, respectively. The dynamic equation of the feed drive dynamics can be written in the following form:

$$\ddot{\theta}_i = -m_i^{-1}h_i\dot{\theta}_i + m_i^{-1}u_i - \delta_i, \delta_i = m_i^{-1}d_i \tag{5.2}$$

where $u_i = f_{ai}$ is the control input and δ_i is total disturbance which is assumed globally bounded, such that there exists a constant $\bar{\delta}_i \in \mathbb{R}^+$ that satisfy

$$|\delta_i| \leq \bar{\delta}_i, |d_i| \leq \bar{d}_i. \tag{5.3}$$

5.3 Controller design

5.3.1 Integral terminal sliding mode control

Fractional ITSM control was first introduced in [79], which it uses a sliding surface that employs fractional power to achieve desired trajectory in a finite-time. The sliding mode $s_{ti} = 0$ can be reached from anywhere in the phase plane in finite-time. The tracking error is defined as $e_{vi} = \theta_{di} - \theta_i$, with θ_{di} as desired position. Using sliding function $e_{zi} = \dot{e}_{vi} + \omega_i e_{vi}$, where $\omega_i > 0$ a design constant. The fractional integral terminal sliding variable is described as

$$s_{ti} = e_{zi} + \varphi_i e_{Izi}, \tag{5.4}$$

with

$$\dot{e}_{Izi} = e_{zi}^{\frac{q_i}{p_i}}, \tag{5.5}$$

$$e_{zi}^{\frac{q_i}{p_i}} = |e_{zi}|^{\frac{q_i}{p_i}} \operatorname{sign}(e_{zi}), \tag{5.6}$$

where $\varphi_i > 0$ is a design constant. p_i and q_i are odd integers selected to satisfy the condition: $p_i > q_i$. On the surface $s_{ti} = 0$, the integrator (5.5) is defined as:

$$\dot{e}_{Izi} = -\varphi_i^{\frac{q_i}{p_i}} e_{Izi}^{\frac{q_i}{p_i}}. \tag{5.7}$$

From solving the error dynamic (5.7), the time for convergence of e_{Izi} is obtained as:

$$t_{fi} = \frac{|e_{Izi}(0)|^{1-\frac{q_i}{p_i}}}{\varphi_i^{\frac{q_i}{p_i}}\left(1 - \frac{q_i}{p_i}\right)} = \frac{|e_{zi}(0)|^{1-\frac{q_i}{p_i}}}{\varphi_i^{\frac{q_i}{p_i}}\left(1 - \frac{q_i}{p_i}\right)}. \tag{5.8}$$

Meanwhile, the time spent for the convergence of the state error e_{zi} is also t_{fi}. The time derivative of s_{ti} in (5.4) is written as

$$\dot{s}_{ti} = \ddot{\theta}_{di} + m_i^{-1} h_i \dot{\theta}_i + \delta_i - m_i^{-1} u_i + \omega_i \dot{e}_{vi} + \varphi_i e_{zi}^{\frac{q_i}{p_i}}, \tag{5.9}$$

for the system in (5.2) the control law is given by

$$u_i = u_{0i} + u_{1i}, \tag{5.10}$$

where u_{0i} is equivalent control and u_{1i} is a discontinuous control for the rejection of δ_i. The equivalent control law is achieved by considering the ideal closed-loop dynamics $\dot{s}_{ti} + \kappa_i s_{ti} = 0$ when $\delta_i = 0$ and $u_{1i} = 0$. The equivalent control vector u_{0i} becomes

$$u_{0i} = m_i(\ddot{\theta}_{di} + m_i^{-1} h_i \dot{\theta}_i + \omega_i \dot{e}_{vi} + \varphi_i e_{zi}^{\frac{q_i}{p_i}} + \kappa_i s_{ti}), \tag{5.11}$$

where $\kappa_i > 0$ is the design constant. For $|\delta_i| > 0$, the time derivative of s_{ti} from (5.9) and using the control laws (5.10) and (5.11), it becomes

$$\dot{s}_{ti} = \delta_i - m_i^{-1} u_{1i}, \tag{5.12}$$

the discontinuous control is selected as

$$u_{1i} = \alpha_{si} \mathrm{sign}(s_{ti}), \alpha_{si} \geq m_i(\bar{\delta}_i + \eta_i) \tag{5.13}$$

where α_{si} is the switching gain. The reaching condition [45]:

$$s_{ti}\dot{s}_{ti} = s_{ti}(\delta_i - m_i^{-1} u_{1i}), s_{ti}\dot{s}_{ti} \leq -\eta_i |s_{ti}|, \tag{5.14}$$

where η_i is the positive constant specifying the converging rate of s_{ti}, respectively. Note that the control law in (5.11) requires the knowledge of the plant parameters.

5.3.2 Simple adaptive control

The design of the SAC law does not necessitate the knowledge of system parameters. The implementation of SAC requires a solution from the Compound generated tracker (CGT) and a plant with the ASPR property [55]. Furthermore, a stable reference model is a prerequisite for SAC. A reference model is given by

$$\dot{\mathbf{x}}_{mi} = \mathbf{A}_{mi}\mathbf{x}_{mi} + \mathbf{b}_{mi} u_{mi}, \tag{5.15}$$

$$y_{mi} = \mathbf{c}_{mi}^{\mathrm{T}} \mathbf{x}_{mi}, \tag{5.16}$$

where $\mathbf{x}_{mi} \in R^{n_m}$, $y_{mi} \in R$, and $u_{mi} \in R$ are the state vector, output, and input, respectively. $\mathbf{A}_{mi}$, $\mathbf{b}_{mi}$, and $\mathbf{c}_{mi}$ correspond to the reference system matrix, input vector, and output vector, respectively. u_{mi} in the reference model is assumed bounded and piece-wise continuous, such that $\dot{u}_{mi}$, $\dot{\mathbf{x}}_{mi}$, and y_{mi} are bounded as well. Neglecting the disturbances, the plant in (5.1) has a relative degree of 2, hence not ASPR. A plant is known to be ASPR when the following conditions are met; plant should have a relative degree of 0 or 1, plant should be minimum-phase and the highest frequency gain of the denominator must be positive. The aim of the control is to realize the following relation:

$$\lim_{t\to\infty} e_{wi} = \lim_{t\to\infty} \{y_{mi} - \theta_i\} = 0$$

perfectly. Ideal model exists with state $\mathbf{x}_i^*$, input u_i^*, and output y_i^* vectors, given in the following state space representation:

$$\dot{\mathbf{x}}_i^* = \mathbf{A}_i \mathbf{x}_i^* + \mathbf{b}_i u_i^*, \tag{5.17}$$

$$y_i^* = \mathbf{c}_i^{\mathrm{T}} \mathbf{x}_i^*, \tag{5.18}$$

where $\mathbf{A}_i$ is the ASPR plant matrix, and $\mathbf{b}_i$ and $\mathbf{c}_i$ vectors with appropriate dimensions, respectively. Since $\mathbf{x}_{mi}$ and u_{mi} are of arbitrary in nature, by selecting the stable and correct coefficients of the characteristic equation, the CGT condition can be satisfied [37]. The ideal output is identical to output of the reference model given as $y_i^* = y_{mi}$. The ideal control input is given as linear combination of $\mathbf{x}_{mi}$ and u_{mi}:

$$u_i^* = {\mathbf{k}_{xi}^*}^{\mathrm{T}} \mathbf{x}_{mi} + k_{ui}^* u_{mi}, \tag{5.19}$$

where $\mathbf{k}_{xi}^*$ and k_{ui}^* are unknown constant vector and scalar desired values, respectively. The tracking error is defined as $e_{wi} = y_{mi} - \theta_i$, and the following control input was proposed [37]:

$$u_{vi} = k_{ewi} e_{wi} + \mathbf{k}_{xmi}^{\mathrm{T}} \mathbf{x}_{mi} + k_{umi} u_{mi}, \tag{5.20}$$

$$u_{vi} = \mathbf{k}_{vi}^{\mathrm{T}} \mathbf{v}_i, \tag{5.21}$$

with

$$\mathbf{k}_{vi} = \begin{bmatrix} k_{ewi} & \mathbf{k}_{xmi}^{\mathrm{T}} & k_{umi} \end{bmatrix}^{\mathrm{T}}, \tag{5.22}$$

$$\mathbf{v}_i = \begin{bmatrix} e_{wi} & \mathbf{x}_{mi}^{\mathrm{T}} & u_{mi} \end{bmatrix}^{\mathrm{T}}. \tag{5.23}$$

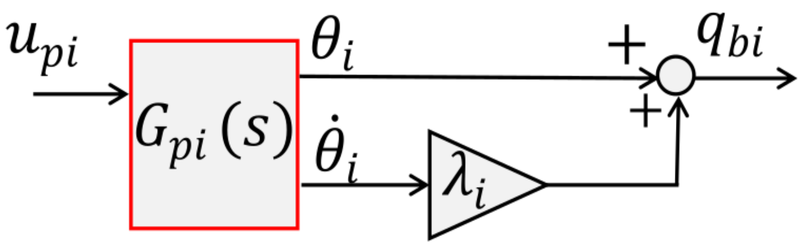

Figure 5.1: Velocity-based AOS

The adaptive gain vector $\mathbf{k}_{vi}$ is a combination of "proportional" and "integral" terms; $\mathbf{k}_{vi} = \mathbf{k}_{pvi} + \mathbf{k}_{Ivi}$ and their adaptation laws are given as

$$\mathbf{k}_{pvi} = \mathbf{\Gamma}_{pvi}\mathbf{v}_i e_{wi}, \tag{5.24}$$

$$\dot{\mathbf{k}}_{Ivi} = \mathbf{\Gamma}_{Ivi}\mathbf{v}_i e_{wi}, \tag{5.25}$$

where $\mathbf{\Gamma}_{pvi}$ and $\mathbf{\Gamma}_{Ivi}$ are positive definite matrices. In addition, these matrices are positive definite used to adjust the adaption rate of the control gains. The proportional term in (5.24) adds immediate penalty for large errors, and leads the system very quickly towards small tracking errors and the integral gain given in (5.25) is used to guarantee convergence [40].

5.3.3 Sufficiency of ASPR condition

The plant in (5.1) is without ASPR. Harada and Uchiyama [53] proposed the use of velocity signal for the ASPR property. This method augments the plant with the linear polynomial $H_i(s) = 1 + \lambda_i s$ of the i^{th} drive axis to the plant, where s is the variable of Laplace transform. The transfer function with the AOS signal provides the ASPR property as

$$G_{ai}(s) = \frac{1 + \lambda_i s}{m_i s^2 + c_i s} \tag{5.26}$$

as shown on Fig. 5.1. The relative gain λ_i is assigned a constant positive value which makes the augmented plant to be with a relative degree of 1. The augmented plant becomes

$$G_{ai}(s) = G_{pi}(s) + \lambda_i s G_{pi}(s). \tag{5.27}$$

The augmented output signal considered is given as

$$q_{bi} = \theta_i + \lambda_i \dot{\theta}_i, \tag{5.28}$$

where $\lambda_i > 0$ is a design constant and θ_i is the table position to the i^{th} drive axis. Velocity-based AOS requires the reference model to have at least the same order as the plant and in turn the linear polynomial $H_i(s)$ is applied to the reference model. This leads to the augmented reference output signal given as

$$q_{mi} = y_{mi} + \lambda_i \dot{y}_{mi}, \tag{5.29}$$

and the augmented output error is defined as

$$e_{ai} = e_{wi} + \lambda_i \dot{e}_{wi} = \mathbf{c}_i^{\mathrm{T}} \mathbf{e}_{xi}, \tag{5.30}$$

where $\mathbf{c}_i = \begin{bmatrix} 1 & \lambda_i \end{bmatrix}^{\mathrm{T}}$ and the state error $\mathbf{e}_{xi} = \mathbf{x}_i^* - \mathbf{x}_i$, $\mathbf{x}_i = \begin{bmatrix} \theta_i & \dot{\theta}_i \end{bmatrix}$. The error term e_{wi} is replaced by e_{ai} in (5.21-5.25), respectively for SAC implementation. The derivative of $\mathbf{e}_{xi}$; $\dot{\mathbf{e}}_{xi} = \dot{\mathbf{x}}_i^* - \dot{\mathbf{x}}_i$ and using (5.1) in state space and (5.17), and neglecting the disturbances. It becomes

$$\dot{\mathbf{e}}_{xi} = \mathbf{A}_i \mathbf{e}_{xi} + \mathbf{b}_i (u_i^* - u_{pi}). \tag{5.31}$$

It is worth noting that the system model, described in (5.18), is considered "strictly passive" and its transfer function is referred to as "strictly real" if it satisfies the satisfies the Kalman–Yakubovich–Popov conditions [37]:

$$\mathbf{P}_i(\mathbf{A}_i - \mathbf{b}_i k_{ai}^* \mathbf{c}_i^{\mathrm{T}}) + (\mathbf{A}_i - \mathbf{b}_i k_{ai}^* \mathbf{c}_i^{\mathrm{T}})^{\mathrm{T}} \mathbf{P}_i = -\mathbf{Q}_i, \tag{5.32}$$

$$\mathbf{b}_i^{\mathrm{T}} \mathbf{P}_i = \mathbf{c}_i^{\mathrm{T}} \mathbf{W}_i, \tag{5.33}$$

where $\mathbf{P}_i$ and $\mathbf{Q}_i$, are positive definite symmetric matrices, and $\mathbf{W}_i$ is the positive-definite matrix, and k_{ai}^* is the positive definite gain, respectively. In addition, the product $\mathbf{c}_i^{\mathrm{T}} \mathbf{b}_i$ is positive definite symmetric.

5.3.4 Simple adaptive integral terminal sliding mode control

To develop adaptive control law for the augmented system (5.27). Consider fractional integral terminal sliding variable using augmented output error in (5.30) defined as

$$s_{ai} = e_{ai} + \beta_i e_{Iai}, \tag{5.34}$$

and its derivative is given by

$$\dot{s}_{ai} = \dot{e}_{ai} + \beta_i e_{ai}^{\frac{q_i}{p_i}}, \tag{5.35}$$

with

$$e_{ai}^{\frac{q_i}{p_i}} = |e_{ai}|^{\frac{q_i}{p_i}} \operatorname{sign}(e_{ai}) \tag{5.36}$$

where $\beta_i > 0$, p_i, and q_i are defined below (5.6). The ideal augmented closed-loop dynamics of $\dot{s}_{ai} + \gamma_i s_{ai} = 0$, with $\gamma_i > 0$ is selected for determining the equivalent control. Using (5.19), (5.30), and (5.31) with ideal augmented closed-loop dynamics brings to

$$u_{pi} = (\mathbf{c}_i^{\mathrm{T}} \mathbf{A}_i^{-1} \mathbf{b}_i)^{-1} e_{ai} + {\mathbf{k}_{xi}^*}^{\mathrm{T}} \mathbf{x}_{mi} + k_{ui}^* u_{mi} + (\mathbf{c}_i^{\mathrm{T}} \mathbf{b}_i)^{-1} \mathbf{\Lambda}_i^{\mathrm{T}} \mathbf{e}_{ti}, \tag{5.37}$$

where $\mathbf{\Lambda}_i = \begin{bmatrix} \beta_i & \gamma_i \end{bmatrix}^{\mathrm{T}}$ and $\mathbf{e}_{ti} = \begin{bmatrix} e_{ai}^{q_i/p_i} & s_{ai} \end{bmatrix}^{\mathrm{T}}$. Define $k_{ai} = (\mathbf{c}_i^{\mathrm{T}} \mathbf{A}_i^{-1} \mathbf{b}_i)^{-1} \in R$, $\mathbf{k}_{xi} = \mathbf{k}_{xi}^* \in R^{n_m}$. $k_{ui} = k_{ui}^* \in R$, and $\mathbf{k}_{ti} = (\mathbf{c}_i^{\mathrm{T}} \mathbf{b}_i)^{-1} \mathbf{\Lambda}_i^{\mathrm{T}} \in R^{n_e}$. The equivalent control law is given as

$$u_{pi} = k_{ai} e_{ai} + \mathbf{k}_{xi}^{\mathrm{T}} \mathbf{x}_{mi} + k_{ui} u_{mi} + \mathbf{k}_{ti}^{\mathrm{T}} \mathbf{e}_{ti}, \tag{5.38}$$

$$u_{pi} = \mathbf{k}_i^{\mathrm{T}} \mathbf{r}_i, \tag{5.39}$$

with

$$\mathbf{k}_i = \begin{bmatrix} k_{ai} & \mathbf{k}_{xi}^{\mathrm{T}} & k_{ui} & \mathbf{k}_{ti}^{\mathrm{T}} \end{bmatrix}^{\mathrm{T}}, \tag{5.40}$$

$$\mathbf{r}_i = \begin{bmatrix} e_{ai} & \mathbf{x}_{mi}^{\mathrm{T}} & u_{mi} & \mathbf{e}_{ti}^{\mathrm{T}} \end{bmatrix}^{\mathrm{T}}. \tag{5.41}$$

According to the SAC theory [37], $\mathbf{k}_i$ gain can be estimated using combination of "proportional" and "integral" adaptation laws; $\mathbf{k}_i = \mathbf{k}_{pi} + \mathbf{k}_{Ii}$. Adaptation laws are given as

$$\mathbf{k}_{pi} = \mathbf{\Gamma}_{pi}\mathbf{r}_i e_{ai}, \tag{5.42}$$

$$\dot{\mathbf{k}}_{Ii} = \mathbf{\Gamma}_{Ii}\mathbf{r}_i e_{ai}, \tag{5.43}$$

where $\mathbf{\Gamma}_{pi}$ and $\mathbf{\Gamma}_{Ii}$ are diagonal matrices. Furthermore, these matrices are positive definite used to adjust the adaption rate of the control gains. The nominal control term u_{0i} from (5.11) can be estimated as

$$u_{0i} \cong u_{pi} = \mathbf{k}_i^{\mathrm{T}}\mathbf{r}_i. \tag{5.44}$$

The following Lyapunov candidate is considered for proofing stability of the equivalent control input is given as

$$L_i = \mathbf{e}_{xi}^{\mathrm{T}}\mathbf{P}_i\mathbf{e}_{xi} + \mathrm{tr}\left\{\mathbf{W}_i[\mathbf{k}_{Ii} - \mathbf{k}_i^*]^{\mathrm{T}}\mathbf{\Gamma}_{Ii}^{-1}[\mathbf{k}_{Ii} - \mathbf{k}_i^*]\right\}, \tag{5.45}$$

where $\mathbf{P}_i$ is the positive definite matrix and $\mathbf{\Gamma}_{Ii}^{-1}$ is the positive definite scaling matrix and $\mathbf{k}_i^* = \begin{bmatrix} k_{ai}^* & \mathbf{k}_{xi}^{*\,\mathrm{T}} & k_{ui}^* & \mathbf{k}_{ti}^{*\,\mathrm{T}} \end{bmatrix}^{\mathrm{T}}$ is unknown constant matrix with desired values. Using (5.19) and (5.39), the state error in (5.31) can be given as

$$\dot{\mathbf{e}}_{xi} = \left(\mathbf{A}_i - \mathbf{b}_i k_{ai}^*\mathbf{c}_i^{\mathrm{T}}\right)\mathbf{e}_{xi} - \mathbf{b}_i[\mathbf{k}_i - \mathbf{k}_i^*]^{\mathrm{T}}\mathbf{r}_i - \mathbf{b}_i\mathbf{k}_{ti}^{*\,\mathrm{T}}\mathbf{e}_{ti}. \tag{5.46}$$

The derivative of L_i is given as

$$\dot{L}_i = \dot{\mathbf{e}}_{xi}^{\mathrm{T}}\mathbf{P}_i\mathbf{e}_{xi} + \mathbf{e}_{xi}^{\mathrm{T}}\mathbf{P}_i\dot{\mathbf{e}}_{xi} + 2\mathrm{tr}\left\{\mathbf{W}_i[\mathbf{k}_{Ii} - \mathbf{k}_i^*]^{\mathrm{T}}\mathbf{\Gamma}_{Ii}^{-1}\dot{\mathbf{k}}_{Ii}\right\}. \tag{5.47}$$

Substituting (5.43) and (5.46) into (5.47) with $\mathbf{k}_{Ii} = \mathbf{k}_i - \mathbf{\Gamma}_{pi}\mathbf{r}_i e_{ai}$ from (5.42), and using passivity relations from (5.33), $\dot{L}_i$ with (5.30) becomes

$$\dot{L}_i = -\mathbf{e}_{xi}^{\mathrm{T}}\mathbf{Q}_i\mathbf{e}_{xi} - 2e_{ai}^{\mathrm{T}}\mathbf{W}_i e_{ai}\mathbf{r}_i^{\mathrm{T}}\mathbf{\Gamma}_{pi}\mathbf{r}_i - 2\mathbf{e}_{ti}^{\mathrm{T}}\mathbf{k}_{ti}^*\mathbf{W}_i\mathbf{c}_i^{\mathrm{T}}\mathbf{e}_{xi}. \tag{5.48}$$

For simplification, (5.48) is written as

$$\dot{L}_i = -\mathbf{e}_{si}^{\mathrm{T}}\mathbf{\Omega}_i\mathbf{e}_{si} - 2e_{ai}^{\mathrm{T}}\mathbf{W}_i e_{ai}\mathbf{r}_i^{\mathrm{T}}\mathbf{\Gamma}_{pi}\mathbf{r}_i. \tag{5.49}$$

with

$$\mathbf{e}_{si} = \begin{bmatrix} \mathbf{e}_{xi} \\ \mathbf{e}_{ti} \end{bmatrix}^{\mathrm{T}}, \mathbf{\Omega}_i = \begin{bmatrix} \mathbf{Q}_i & \mathbf{k}_{ti}^{*\,\mathrm{T}} \mathbf{W}_i \mathbf{c}_i \\ \mathbf{k}_{ti}^{*} \mathbf{W}_i \mathbf{c}_i^{\mathrm{T}} & \mathbf{0} \end{bmatrix}, \tag{5.50}$$

where $\mathbf{\Omega}_i$ is the positive semi-definite matrix. Introducing the non-negative constant ξ_1, and positive constants ξ_2, ξ_3, ξ_4, ξ_5, and ξ_6 to (5.49), this can be written as

$$\dot{L}_i \leq -\xi_1||\mathbf{e}_{si}||^2 - \xi_2||e_{ai}||^4 - \xi_3||e_{ai}||^2\Big(\xi_4||\mathbf{x}_{mi}||^2 + \xi_5||u_{mi}||^2 + \xi_6||\mathbf{e}_{ti}||^2\Big). \tag{5.51}$$

Thus, $\dot{L}_i$ becomes negative semi-definite. The quadratic form of L_i guarantees that $\mathbf{e}_{xi}$, $\mathbf{e}_{ti}$, e_{ai} and $\mathbf{k}_{Ii}$ are bounded. Since L_i in (5.45) is lower bounded and $\dot{L}_i$ is negative semi-definite, to apply the Barbalat's lemma requires $\dot{L}_i$ to be uniformly continuous. The derivative of $\dot{L}_i$ is

$$\ddot{L}_i = -2\dot{\mathbf{e}}_{si}^{\mathrm{T}}\mathbf{\Omega}_i\mathbf{e}_{si} - 4\dot{e}_{ai}^{\mathrm{T}}\mathbf{W}_i e_{ai}\mathbf{r}_i^{\mathrm{T}}\mathbf{\Gamma}_{pi}\mathbf{r}_i - 4e_{ai}^{\mathrm{T}}\mathbf{W}_i e_{ai}\dot{\mathbf{r}}_i^{\mathrm{T}}\mathbf{\Gamma}_{pi}\mathbf{r}_i. \tag{5.52}$$

The regressor $\mathbf{r}_i$ contains vector signals e_{ai}, $\mathbf{x}_{mi}$, u_{mi}, and $\mathbf{e}_{ti}$. Reference control input signal u_{mi} and its derivative are assumed uniformly bounded and piece-wise continuous, thus $\mathbf{x}_{mi}$ and $\dot{\mathbf{x}}_{mi}$ are bounded from (5.15). Hence, $\mathbf{r}_i$ is bounded as e_{ai} and $\mathbf{e}_{ti}$ are bounded as well.

The derivative of $\mathbf{e}_{xi}$ is bounded from (5.46), as the signals $\mathbf{e}_{xi}$, $\mathbf{r}_i$, $\mathbf{k}_{Ii}$, and $\mathbf{e}_{ti}$ are bounded with $\mathbf{k}_i = \mathbf{\Gamma}_{pi}\mathbf{r}_i e_{ai} + \mathbf{k}_{Ii}$. The derivative of e_{ai}: $\dot{e}_{ai} = \mathbf{c}_i^{\mathrm{T}}\dot{\mathbf{e}}_{xi}$, is bounded as $\dot{\mathbf{e}}_{xi}$ is bounded. The derivative of $\mathbf{e}_{ti}$: $\dot{\mathbf{e}}_{ti} = \begin{bmatrix} {}^{q_i}\!/_{p_i} e_{ai}^{({}^{q_i}\!/_{p_i}-1)}\dot{e}_{ai} & \dot{s}_{ai} \end{bmatrix}^{\mathrm{T}}$ is bounded as e_{ai} and $\dot{e}_{ai}$ are bounded, and $\dot{s}_{ai}$ from (5.35) is bounded. Therefore, $\dot{\mathbf{e}}_{si}$ and derivative of regressor vector $\mathbf{r}_i$ are bounded as the signals $\dot{\mathbf{e}}_{xi}$ and $\dot{\mathbf{e}}_{ti}$, $\dot{e}_{ai}$, $\dot{\mathbf{x}}_{mi}$, $\dot{u}_{mi}$, and $\dot{\mathbf{e}}_{ti}$ are bounded, respectively. This shows that $\ddot{L}_i$ is bounded, hence $\dot{L}_i$ is uniformly continuous, and from the Barbalat's lemma,

$$\lim_{t\to\infty} \mathbf{e}_{si}(t) = 0$$

is shown.

The overall proposed control input from (5.13) and (5.44) is given as

$$u_{pi} = \mathbf{k}_i^{\mathrm{T}}\mathbf{r}_i + \alpha_{ti}\mathrm{sign}(s_{ai}). \tag{5.53}$$

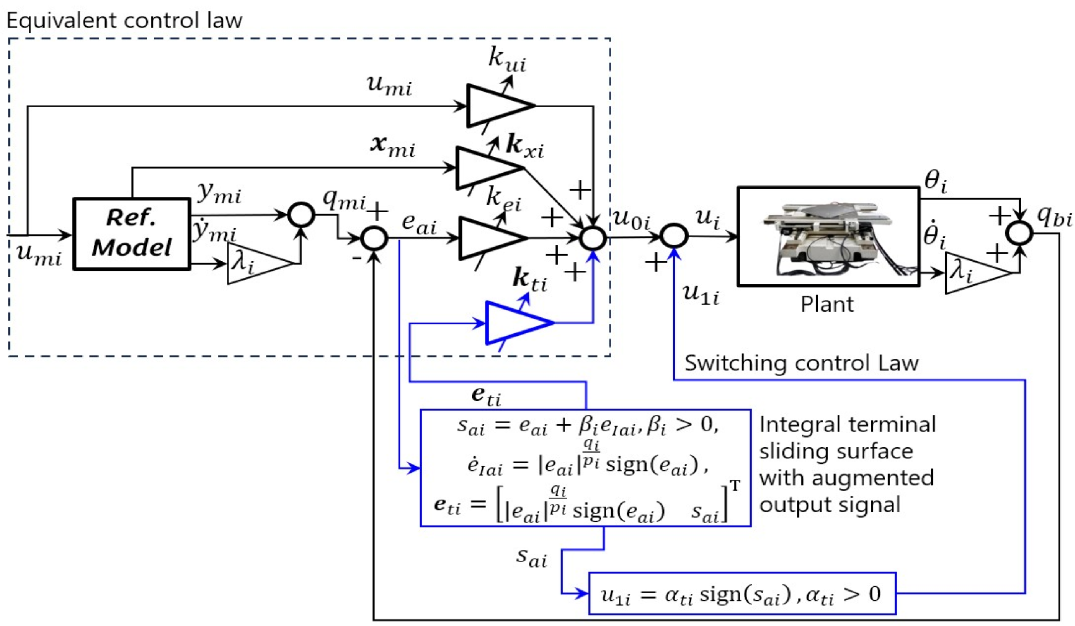

Figure 5.2: Schematic of the proposed approach (AITSMC)

where $\alpha_{ti} > 0$ is a switching gain aims to ensure robustness against disturbances. The overall control schematic is shown in Fig. 5.2 and the adaptive control law does not require the information of the plant parameters.

For tuning the control parameters, some simple rules are considered as follows: The control parameters λ_i and β_i from (5.30) and (5.34) are selected with small values, and they are gradually increased while, simultaneously, the matrices termed as $\boldsymbol{\Gamma}_{pi}$ and $\boldsymbol{\Gamma}_{Ii}$ from (5.42) and (5.43) are also increased gradually on the diagonal elements until satisfactory performance is obtained. It is important to note that the integral gain is essential for ensuring the stability of the control system's adaptation and for accelerating convergence. The proportional gain, on the other hand, enhances plant performance and aids in achieving precise output tracking by immediately penalizing large errors [37]. Then, switching gain α_{ti} from (5.53) is selected by trial and error manner to balance robustness and chattering. Its worth noting larger λ_i puts emphasize on the error derivative, speeding up the response and reducing settling time, but may cause high-frequency oscillations or instability if too large. Similarly, a larger β_i reduces settling time by eliminating steady-state error. However, if it is too large, it can make the system sluggish or unstable due to excessive past error accumulation.

The stability analysis of the overall system is achievable by considering the following Lyapunov candidate function

$$V_i = \frac{s_{ai}^2}{2}, \tag{5.54}$$

taking the derivative of V_i and using (5.31),(5.37), (5.44), and (5.53) gives

$$\begin{aligned}
\dot{V}_i &= s_{ai}\dot{s}_{ai} = s_{ai}\left(\dot{e}_{ai} + \beta_i e_{ai}^{\frac{q_i}{p_i}}\right), \\
&= s_{ai}\left(\mathbf{c}_i^{\mathrm{T}}\dot{\mathbf{e}}_{xi} + \beta_i e_{ai}^{\frac{q_i}{p_i}}\right), \\
&= s_{ai}\Bigg(\mathbf{c}_i^{\mathrm{T}}\Big\{\mathbf{A}_i\mathbf{e}_{xi} + \mathbf{b}_i\big[u_i^* - u_{0i} - u_{1i} + d_i\big]\Big\} + \beta_i e_{ai}^{\frac{q_i}{p_i}}\Bigg), \\
&= s_{ai}\Bigg(\mathbf{c}_i^{\mathrm{T}}\Big\{\mathbf{A}_i\mathbf{e}_{xi} + \mathbf{b}_i\Big[{\mathbf{k}_{xi}^*}^{\mathrm{T}}\mathbf{x}_{mi} + k_{ui}^* u_{mi} - (\mathbf{c}_i^{\mathrm{T}}\mathbf{b}_i)^{-1}\mathbf{A}_i\mathbf{c}_i^{\mathrm{T}}\mathbf{e}_{xi} - {\mathbf{k}^*}_{xi}^{\mathrm{T}}\mathbf{x}_{mi} - k_{ui}^* u_{mi} \\
&\quad -(\mathbf{c}_i^{\mathrm{T}}\mathbf{b}_i)^{-1}\beta_i e_{ai}^{\frac{q_i}{p_i}} - (\mathbf{c}_i^{\mathrm{T}}\mathbf{b}_i)^{-1}\gamma_i s_{ai} - \alpha_{ti}\mathrm{sign}(s_{ai})\Big] + \mathbf{b}_i d_i\Big\} + \beta_i e_{ai}^{\frac{q_i}{p_i}}\Bigg), \\
&= s_{ai}\Bigg(\mathbf{c}_i^{\mathrm{T}}\mathbf{A}_i\mathbf{e}_{xi} - \mathbf{c}_i^{\mathrm{T}}\mathbf{b}_i(\mathbf{c}_i^{\mathrm{T}}\mathbf{b}_i)^{-1}\mathbf{c}_i^{\mathrm{T}}\mathbf{A}_i\mathbf{e}_{xi} - \mathbf{c}_i^{\mathrm{T}}\mathbf{b}_i(\mathbf{c}_i^{\mathrm{T}}\mathbf{b}_i)^{-1}\beta_i e_{ai}^{\frac{q_i}{p_i}} - \mathbf{c}_i^{\mathrm{T}}\mathbf{b}_i(\mathbf{c}_i^{\mathrm{T}}\mathbf{b}_i)^{-1}\gamma_i s_{ai} \\
&\quad -\mathbf{c}_i^{\mathrm{T}}\mathbf{b}_i\alpha_{ti}\mathrm{sign}(s_{ai}) + \mathbf{c}_i^{\mathrm{T}}\mathbf{b}_i d_i + \beta_i e_{ai}^{\frac{q_i}{p_i}}\Bigg), \\
&= s_{ai}\Big(-\gamma_i s_{ai} - \mathbf{c}_i^{\mathrm{T}}\mathbf{b}_i\alpha_{ti}\mathrm{sign}(s_{ai}) + \mathbf{c}_i^{\mathrm{T}}\mathbf{b}_i d_i\Big), \\
&= -s_{ai}\gamma_i s_a + s_{ai}\Big(\mathbf{c}_i^{\mathrm{T}}\mathbf{b}_i\big[d_i - \alpha_{ti}\mathrm{sign}(s_{ai})\big]\Big),
\end{aligned} \tag{5.55}$$

and from (5.3), this brings to

$$\leq -s_{ai}^2\gamma_i - (\alpha_{ti} - \bar{d}_i)|s_{ai}|\mathbf{c}_i^{\mathrm{T}}\mathbf{b}_i, \tag{5.56}$$

if α_{ti} and γ_i are chosen such that $\alpha_{ti} > \bar{d}_i$ and $\gamma_i > 0$. Furthermore, when $s_{ai} \neq 0$ then the expression (5.56) becomes $\dot{V}_i < 0$ meaning that the terminal sliding variable s_{ai} converges to the TSM surface $s_{ai} = 0$ in a finite-time [84]. Thus, on the TSM surface, the closed-loop error dynamics will enjoy the finite-time convergence characteristic. This completes the proof.

In order to reduce chattering which is caused by discontinuous sign function, $\alpha_{ti}\text{sign}(s_{ai})$ in robust term (5.53) is replaced by the continuous function $r_{si}(s_{ai})$ defined as follows [85]:

$$r_{si}(s_{ai}) = \frac{\alpha_{ti}s_{ai}}{|s_{ai}| + \epsilon_i}, \epsilon_i = \epsilon_{0i} + \epsilon_{1i}|e_{ai}|, \;\; i(=1,2), \tag{5.57}$$

where ϵ_{0i} and ϵ_{1i} are two positive constants.

5.4 Simulation and experiment

5.4.1 Conditions

Comparative simulation and experiment are carried out to confirm the effectiveness of the controllers as follows:

i. Simple adaptive control with velocity-based AOS (SAC)
ii. Adaptive sliding mode control based on simple adaptive control-like technique (ASMC) proposed in [82]
iii. Continuous non-singular fast terminal sliding mode controller based on time delay estimation (CNTSMC) proposed in [86].
iv. Proposed approach of combined simple adaptive and integral terminal sliding mode control (AITSMC).

The control law for SAC is given in (5.21) and ASMC control law is defined as follows:

$$u_{ai} = k_{ai}e_{ai} + \mathbf{k}_{xi}^{\mathrm{T}}\mathbf{x}_{mi} + k_{ui}u_{mi} + r_{si}(s_{si}), \tag{5.58}$$

with

$$r_{si}(s_{si}) = \frac{\alpha_{si}s_{si}}{|s_{si}| + \epsilon_i}, \tag{5.59}$$

$$\epsilon_i = \epsilon_{0i} + \epsilon_{1i}|e_{ai}|, \tag{5.60}$$

$$s_{si} = \psi_i e_{ai} + \dot{e}_{ai}, \;\; i(=1,2), \tag{5.61}$$

where $\alpha_{si}, \psi_i, \epsilon_{0i}, \epsilon_{1i} > 0$. The control law for CNTSMC design is based on time delay estimation to ensure the controller remains model-free given as

$$u_{ai} = \hat{M}_i u_{pi} + u_{ai(t-L)} - \hat{M}_i \ddot{\theta}_{i(t-L)}, \tag{5.62}$$

with

$$u_{pi} = \ddot{\theta}_{di} + c_{2i}^{-1}\phi_{2i}^{-1}\left[(1 + c_{1i}\phi_{1i}|e_{vi}|^{(\phi_{1i}-1)})\mathrm{sig}(\dot{e}_{vi})^{(2-\phi_{2i})} + \nu_{1i}s_{ci} + \nu_{2i}\mathrm{sig}(s_{ci})^{\phi_{3i}}\right], \tag{5.63}$$

$$s_{ci} = e_{vi} + c_{1i}\mathrm{sig}(e_{vi})^{\phi_{1i}} + c_{2i}\mathrm{sig}(\dot{e}_{vi})^{\phi_{2i}}. \tag{5.64}$$

where $\hat{M}_i$, c_{1i}, c_{2i}, ν_{1i}, ν_{2i} are positive constants, and ϕ_{1i}, ϕ_{2i}, ϕ_{3i} are control parameters satisfying $\phi_{1i} > \phi_{2i}$, $1 < \phi_{2i} < 2$ and $0 < \phi_{3i} < 1$. The notation $\mathrm{sig}(\cdot)^a = |\cdot|^a\mathrm{sign}(\cdot)$ is used for simplicity and L is the delayed time.

The heart-shaped reference trajectory shown in Fig.5.3 is used as the tracking reference. The trajectory is obtained by

$$\begin{cases} r_{d1} = 10\sin^3\left(\frac{\pi t}{2}\right) \text{ [mm]} \\ r_{d2} = 7\cos\left(\frac{\pi t}{2}\right) - \frac{5}{2}\cos(\pi t) - \cos\left(\frac{3\pi t}{2}\right) \text{ [mm]}. \end{cases} \tag{5.65}$$

The reference model is selected as

$$\dot{\mathbf{x}}_{mi} = \begin{bmatrix} 0 & 1 & 0 \\ 0 & 0 & \iota_i \\ \tau_i & -3\tau_i^2 & 3\iota_i^2\tau_i^3 \end{bmatrix}\mathbf{x}_{mi} + \begin{bmatrix} 0 \\ 0 \\ 1/10^{-3} \end{bmatrix} u_{mi}, \tag{5.66}$$

where τ_i and ι_i are the negative pole and positive value that are selected to make $\mathbf{A}_{mi}$ matrix Hurwitz stable, respectively. For the reference model, states vectors $\mathbf{x}_{mi}$ and derivatives in (5.66) are known, and hence the control variable u_{mi} is available. Plant and control parameters are given in Tables 5.1 and 5.2, respectively used in simulation. The external disturbance of $d_i = 30$ N is applied to evaluate the performance for each axis. The adaptation scaling factors on the adaptive gains are assigned by trial and error manner until the best tracking performance is achieved for SAC and then the same adaptation scaling factors are used on for the rest of

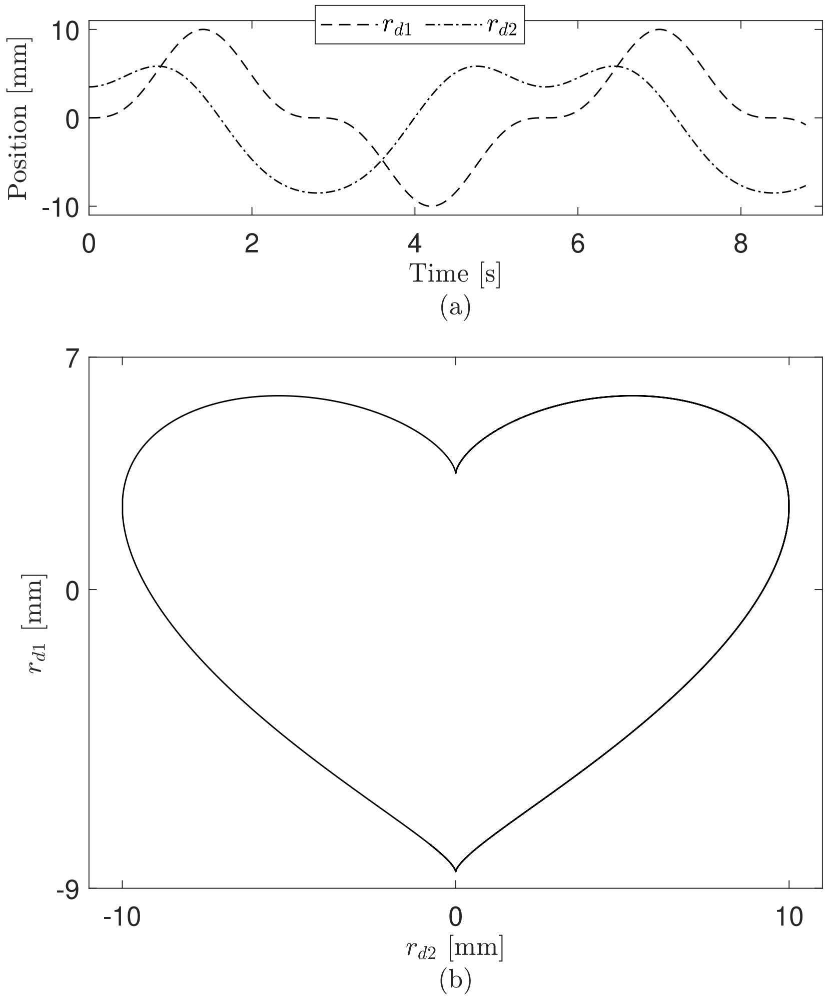

Figure 5.3: Heart-shaped reference trajectory

the controllers. Followed by using the same adaptation coefficients for the rest of the adaptive controllers. Adaptive controller gains are initialized to zero. This initialization allows for a fair comparison across the controllers, as it ensures that each controller starts from the same baseline.

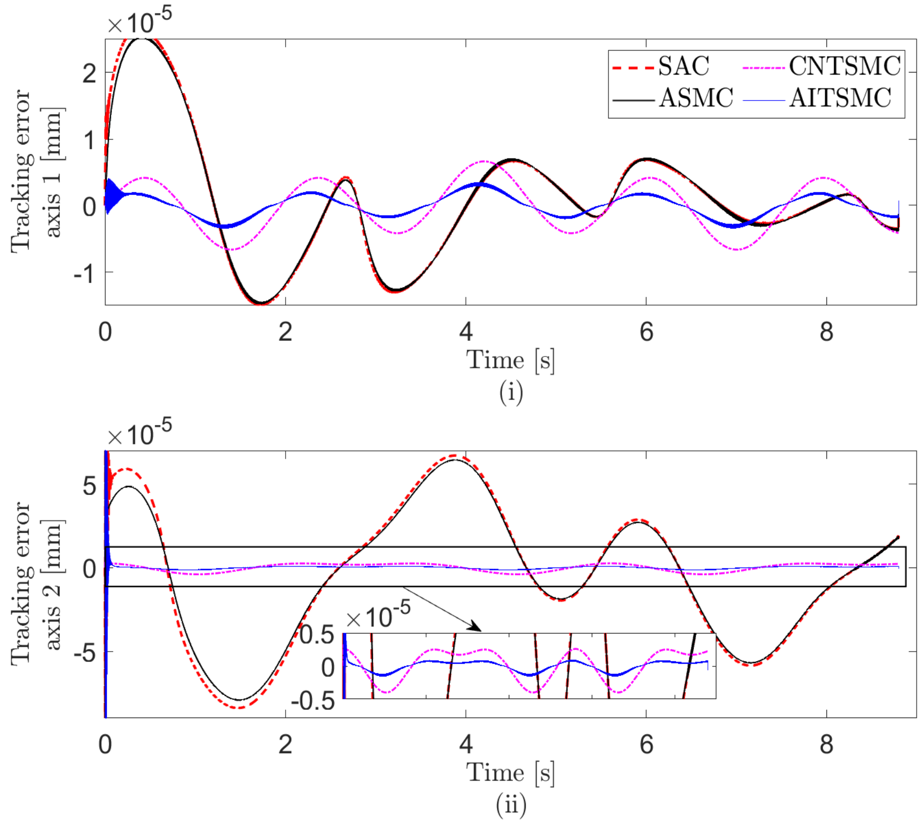

Figure 5.4: Simulation results of tracking error

Table 5.1: Plant parameters

Par.	Unit	1^{st}axis	2^{nd}axis
m_i	$\mathrm{Ns^2m^{-1}}$	86.72	99.65
c_i	$\mathrm{Nsm^{-1}}$	558.62	795.5

5.4.2 Experimental setup

Industrial feed drive system shown in Fig. 2.3 with ball-screw mechanism powered by an AC servo motor was employed. The actual position is measured by attached laser rotary encoder with linear equivalent resolution of 76.29 nm at a 0.35 ms sampling time. The industrial feed drive is operated by a computer with Ubuntu operating system using C/C++ programming environment. The energy consumption was measured using a HIOKI 3390 power analyzer,

Table 5.2: Simulation control parameters

Parameter	1^{st}axis values	2^{nd}axis values
τ_i	-2	-2
ι_i	10^{-3}	10^{-3}
p_i	7	7
q_i	5	5
λ_i	$10^{-3.5}$[s]	$10^{-3.5}$[s]
ψ_i	10^2	10^2
β_i	10	10
$\mathbf{\Gamma}_{pvi}, \mathbf{\Gamma}_{Ivi}$	$\text{diag}\{10^{17}, 10^6, 10^6, 10^{11}, 10^9\}$	$\text{diag}\{10^{16}, 10^6, 10^2, 10, 10^2\}$
$\mathbf{\Gamma}_{pi}, \mathbf{\Gamma}_{Ii}$	$\text{diag}\{10^{17}, 10^6, 10^6, 10^{11}, 10^9, 10^{15.5}, 10^{14.5}\}$	$\text{diag}\{10^{16}, 10^6, 10^2, 10, 10^2, 10^{13.7}, 10^{13.8}\}$
α_{si}	$20e3$	$30e3$
α_{ti}	$20e5$	$50e4$
ϵ_{0i}	0.1	0.1
ϵ_{1i}	10	10
$\hat{M}_i$	70	100
c_{1i}, c_{2i}	$10^5, 0.005$	$10^5, 0.005$
ν_{1i}, ν_{2i}	$10^7, 10^3$	$10^7, 10^3$
$\phi_{1i}, \phi_{2i}, \phi_{3i}$	$2, 1.5, 0.5$	$2, 1.5, 0.5$

which was connected to the motor driver. The data was updated at intervals of 50 milliseconds, and these values were used for the measurements. The adaptation scaling factors on the adaptive gains are assigned by trial and error manner until the best tracking performance is achieved and the control parameters are given in Table 5.3.

5.4.3 Simulation results

Figure 5.4 shows the tracking performance results of the controllers: SAC, ASMC, CNTSMC, and the proposed one. Results show the proposed approach is capable of reducing the tracking error because of the extra control inputs as compared to SAC. The control input $\mathbf{k}_{ti}^{\mathrm{T}}\mathbf{e}_{ti}$ from (5.39) and $r_{si}(s_{si})$ from (5.57) provides an extra inputs to accelerate the convergence and minimize the tracking error. CNTSMC out performs both SAC and ASMC because of its fast finite-time tracking error convergence property. Proposed approach is superior to CNTSMC

Table 5.3: Experimental control parameters

Parameter	1^{st}axis values	2^{nd}axis values
τ_i	-2	-2
ι_i	10^{-3}	10^{-3}
p_i	7	7
q_i	5	5
λ_i	$10^{-3.5}$[s]	$10^{-3.5}$[s]
ψ_i	10^2	10^2
β_i	10^{-1}	10
$\mathbf{\Gamma}_{pvi}, \mathbf{\Gamma}_{Ivi}$	$\text{diag}\{10^7, 10^4, 10^3, 10^2, 10^4\}$	$\text{diag}\{10^6, 10^3, 10^2, 10, 10^3\}$
$\mathbf{\Gamma}_{pi}, \mathbf{\Gamma}_{Ii}$	$\text{diag}\{10^7, 10^4, 10^3, 10^2, 10^4, 10^5, 10^5\}$	$\text{diag}\{10^6, 10^3, 10^2, 10, 10^3, 10^4, 10^4\}$
α_{si}	10	10
α_{ti}	300	300
ϵ_{0i}	0.1	0.1
ϵ_{1i}	10	10
$\hat{M}_i$	0.7	1
c_{1i}, c_{2i}	$10, 0.08$	$10, 0.08$
ν_{1i}, ν_{2i}	$12, 10$	$12, 10$
$\phi_{1i}, \phi_{2i}, \phi_{3i}$	$2, 1.5, 0.5$	$2, 1.5, 0.5$

in tracking accuracy because of adaptive nature from SAC-like design and finite-time tracking error convergence property. Furthermore, as the proposed method achieves low tracking error, switching gain α_{ti} to address disturbances can be selected high.

5.4.4 Experimental results

Following the trajectory shown in Fig. 5.3. The results are shown in Fig. 5.5, for which SAC, ASMC, and CNTSMC are considered as the conventional approaches. The proposed approach reduces the tracking error more effectively than conventional approaches. However, as seen in Fig. 5.5 (b)-(i) and (b)-(ii), and Fig. 5.7, it requires a higher control input to achieve this level of performance. ASMC and the proposed approach have auxiliary control input compared to SAC. CNTSMC auxiliary control input is based on time-delay estimation approach. For repeatability purposes, Fig. 5.6 illustrates the steady-state mean tracking error results after 1

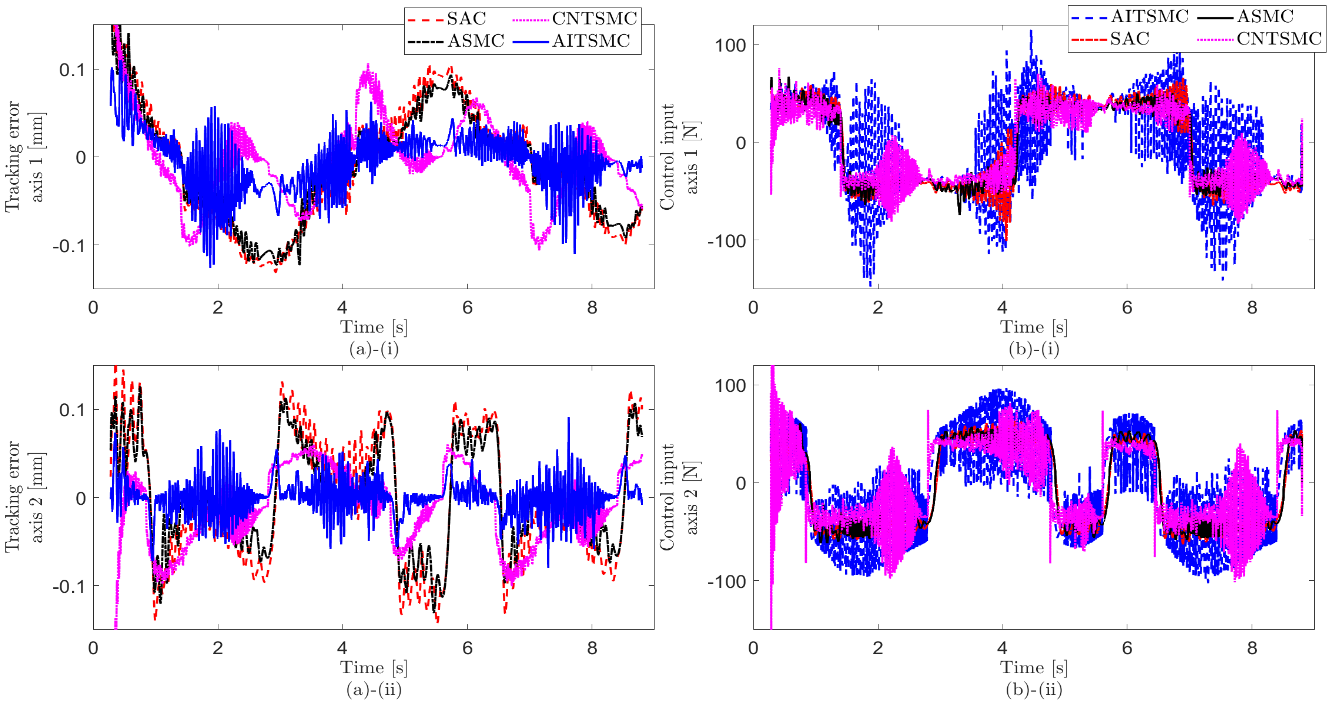

Figure 5.5: Experimental tracking control performance

second from the experimental 10 runs using a heart-shaped trajectory. This result shows the efficiency of the proposed controller in comparison to conventional approaches. The proposed approach managed to reduced the mean tracking error by about 58.6% and 73% for axes 1 and 2, respectively as compared to SAC and by about 52.7% and 61.8% for axes 1 and 2, respectively when compared to ASMC. In addition, the proposed approach when compared to CNTSMC managed to reduce the tracking error by about 35.03% and 52.5% for axes 1 and 2, respectively. CNTSMC results to a lower absolute mean tracking error by about 36.26% and 43.08% compared to ASMC, and by 27.2% and 19.6% compared to SAC for axes 1 and 2, respectively. ASMC achieves lower mean tracking error by about 12.4% and 29.2% for axes 1 and 2, respectively as compared to SAC.

Figure 5.7 shows the measured energy on all controllers for the 10 trial runs on axes 1 and 2. Compared to CNTSMC, ASMC, and SAC, the proposed controller requires extra energy by about 30.6% and 28.9%, 20% and 11.9%, and 16% and 11.1% for axes 1 and 2, respectively. CNTSMC achieved smoother control input with reduced energy by 17.3% and 20.1%, and 13.2% and 19.3% for axes 1 and 2, respectively, compared to SAC and ASMC approaches. In addition,

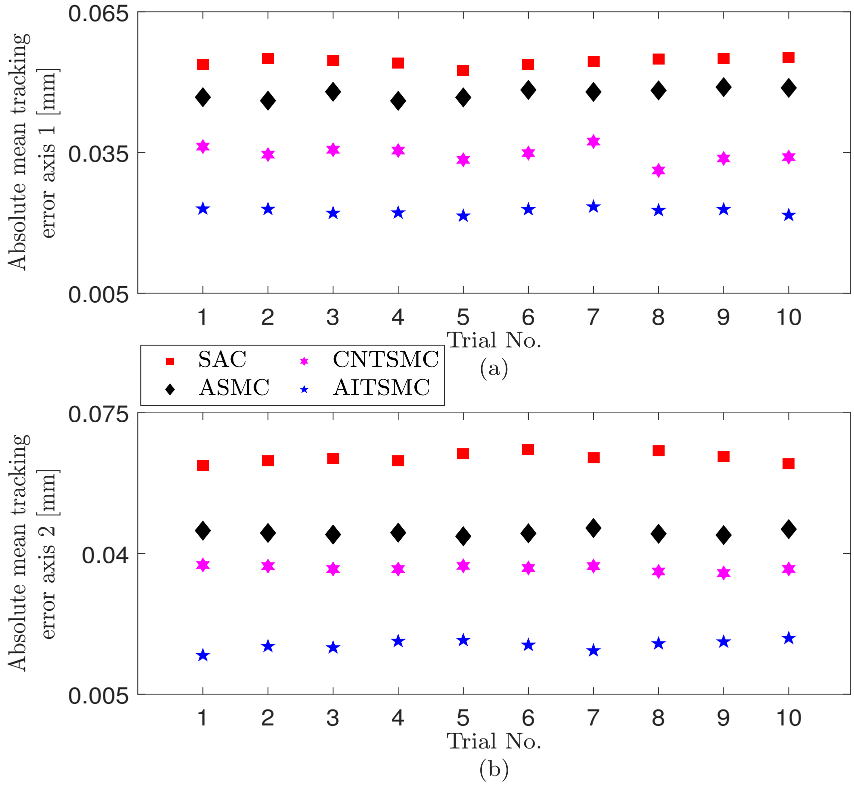

Figure 5.6: Experimental repeatability performance

ASMC managed to achieve reduced energy consumption by about 4.8% and 0.9% for axes 1 and 2, respectively compared to SAC. The controller gains are shown in Fig. 5.8 for the adaptive controllers on the augmented tracking error controller gains. The proposed approach achieved lower controller gains k_{ai}, $\mathbf{k}_{xi}$, and k_{ui} as compared to ASMC and SAC because of smaller tracking errors. There are high oscillations around times 2 seconds, 4 seconds, and 7 seconds for the proposed controller in Fig. 5.8 when tracking errors are smaller because the proportional gain is high. The supplementary control inputs for ASMC and proposed compared to SAC controller further penalize the tracking errors to smaller values and there controller gains for the proposed approach are shown in Fig. 5.9. In addition, the proposed approach (c) performs better than SAC, ASMC, and CNTSMC on overall performance as shown in Fig. 5.10 as e_{ci} is the contour error calculated as in [87].

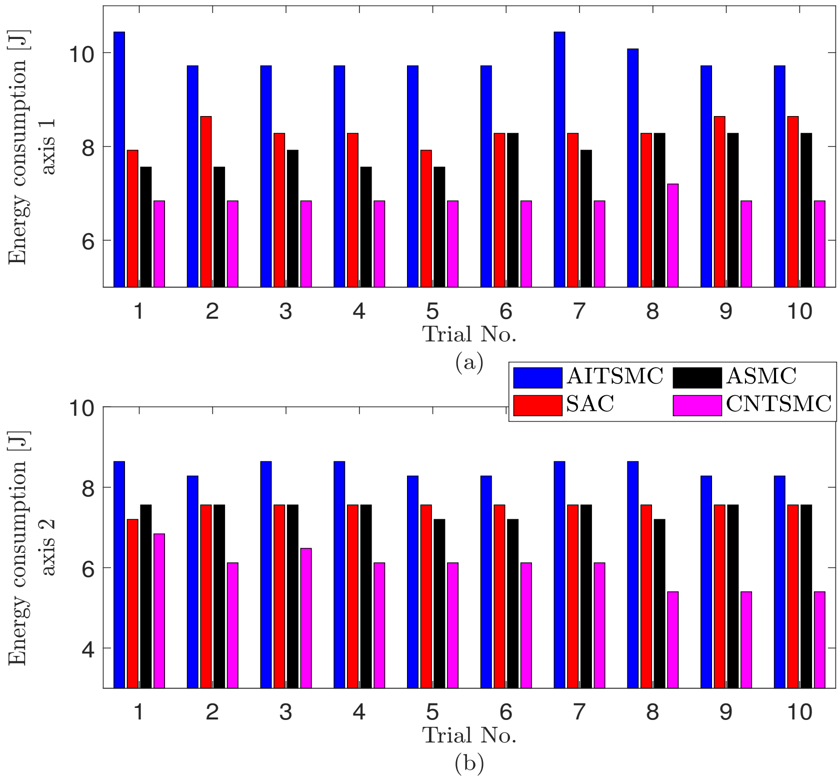

Figure 5.7: Experimental energy consumption

5.5 Discussion

Primarily, the proposed approach demonstrated superiority regarding tracking error reduction compared to SAC, ASMC, and CNTSMC as shown in Figs. 5.5, 5.6, and 5.10, respectively. CNTSMC achieves lower energy consumption magnitude compared to the rest of the controllers because of non-linear term $c_{2i}\text{sig}(\dot{e}_{vi})^{\phi_{2i}}$ in (5.62) ensures the control action is gradual, improving the smoothness of control inputs and the other non-linear term $c_{1i}\text{sig}(e_{vi})^{\phi_{1i}}$ provides additional control effort, allowing the controller to respond more aggressively to larger errors, hence it outperforms ASMC and SAC. ASMC achieves smoother control input because of the corrective control input $r_{si}(s_{si})$ as shown in (5.58), which improves the effectiveness of the control system. Because ASMC has an extra control input, it achieves lower tracking errors than SAC. The proposed approach achieves superior performance in terms of tracking accuracy compared to

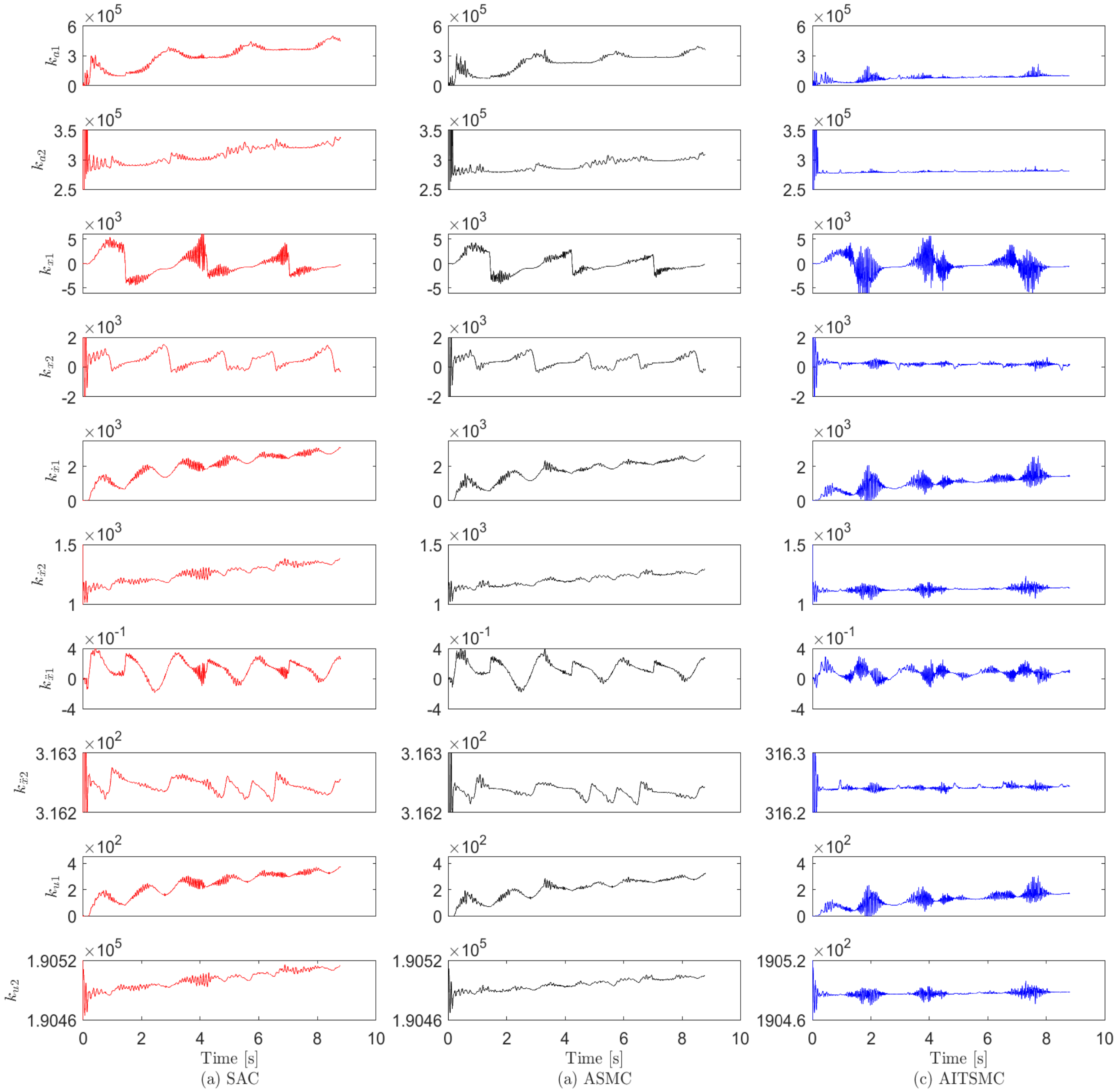

Figure 5.8: Controller gains ($k_{ai}, \mathbf{k}_{xi}, k_{ui}$)

CNTSMC because of the proportional and integral adaptation laws (5.42-5.43) which contain non-linear terms of sliding variable and augmented tracking errors for finite-time convergence. The auxiliary control inputs, which are $\mathbf{k}_{ti}^{\mathrm{T}}\mathbf{e}_{ti}$ and $r_{si}(s_{ai})$ compared to SAC as shown in (5.53) and (5.57) adds robustness to the design. The signals $\mathbf{e}_{ti}$ and s_{ai} are related to tracking errors.

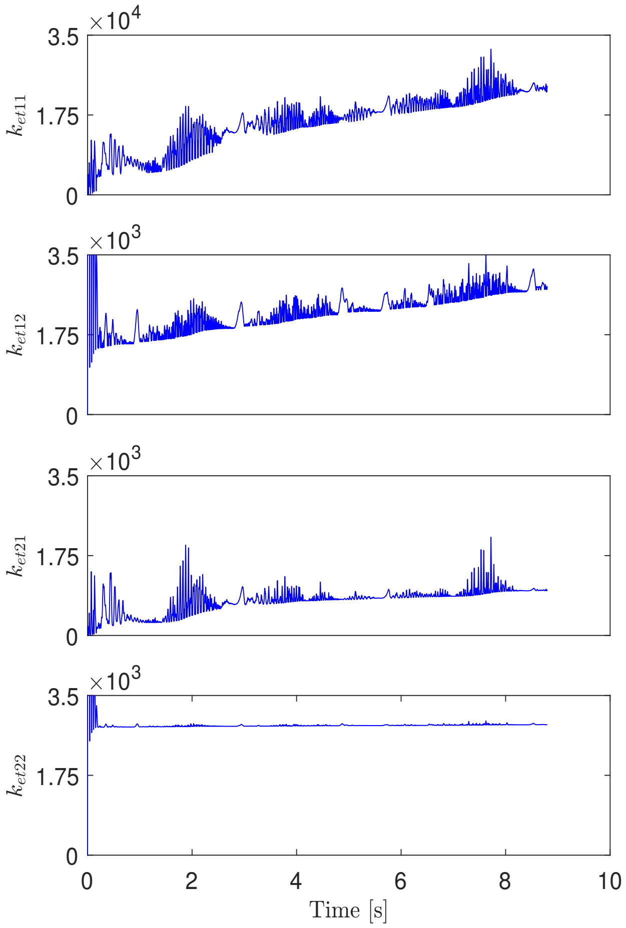

Figure 5.9: Controller gains ($\mathbf{k}_{ti}$)

In addition, the signals possess fractional power, which introduces non-linearity into the control action. This allows different control input responses from different error magnitudes. If $|e_{ai}| > 1$, the auxiliary control input response to the tracking error will be less aggressive, unlike when the augmented tracking error is less than 1 because $|e_{ai}|^{\frac{q_i}{p_i}}$ grows slower when $|e_{ai}| > 1$. The rate at which the signals increase or decrease is determined by the fractional power. This is specifically configured with odd numbers of p_i and q_i, under the condition that p_i is greater than q_i. Therefore, this design may prevent the controller from over reacting to large errors and causing the system to become unstable. Furthermore, when the error is small $|e_{ai}| < 1$, the controller response will be more aggressive, which can reduce the error more quickly. However, as shown in Figs. 5.5 and 5.7, energy consumption may increase.

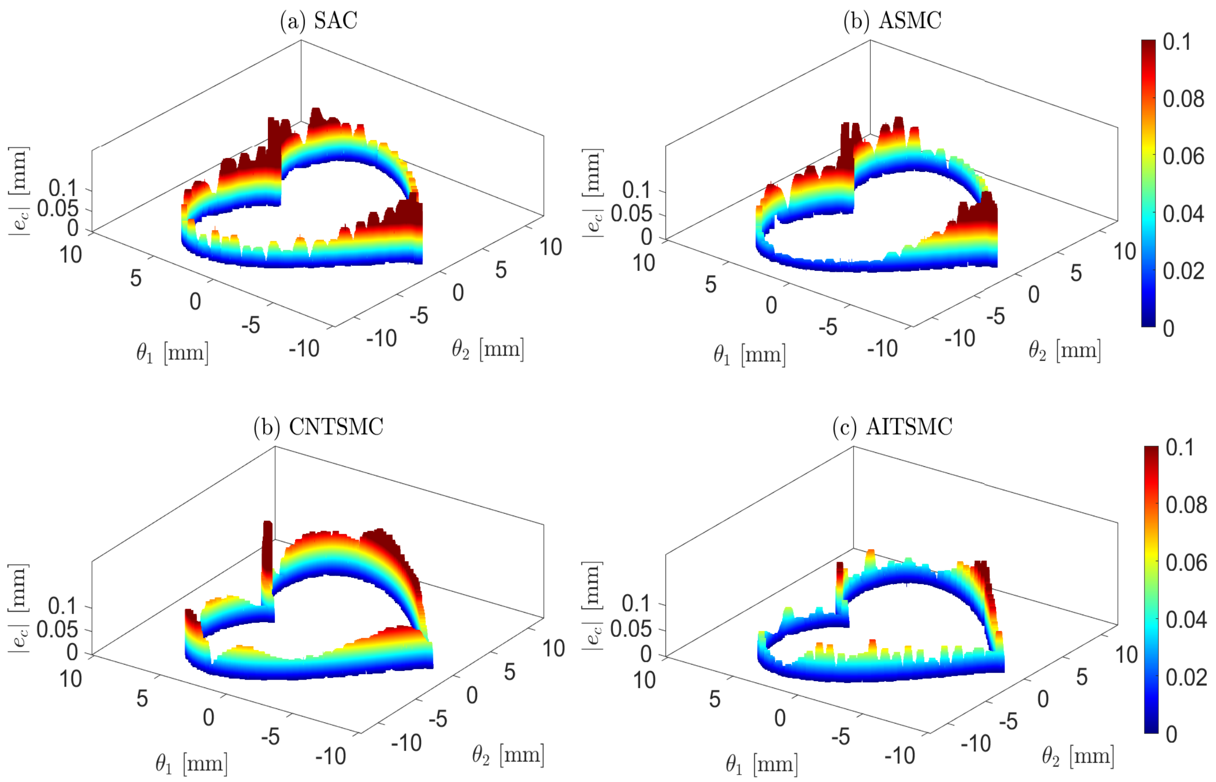

Figure 5.10: Experimental contouring performance

One such source is mechanical vibrations, which can be triggered by imperfections in the mechanical components, misalignment, or even external vibrations as shown in Fig. 5.11, with the peaks around the lower frequencies (below 500 Hz). Another significant contributor to these disturbances is friction. This includes nonlinear and variable forces that are particularly noticeable at low velocities or during changes in direction. Disturbances can also arise from electrical noise present in the drive's control electronics. Additionally, thermal effects can lead to disturbances. For instance, changes in temperature can cause thermal expansion or contraction, which in turn can impact the positioning accuracy of the system. Estimating these disturbances may pose a unique challenge, especially when using a model-free approach in experiments. This is primarily due to the absence of a predefined plant model, which would otherwise help to effectively quantify and isolate the disturbances.

From the SAC theory [39], the adaptive controller gains $\mathbf{k}_{xmi}$ and k_{umi} from (5.21) perform

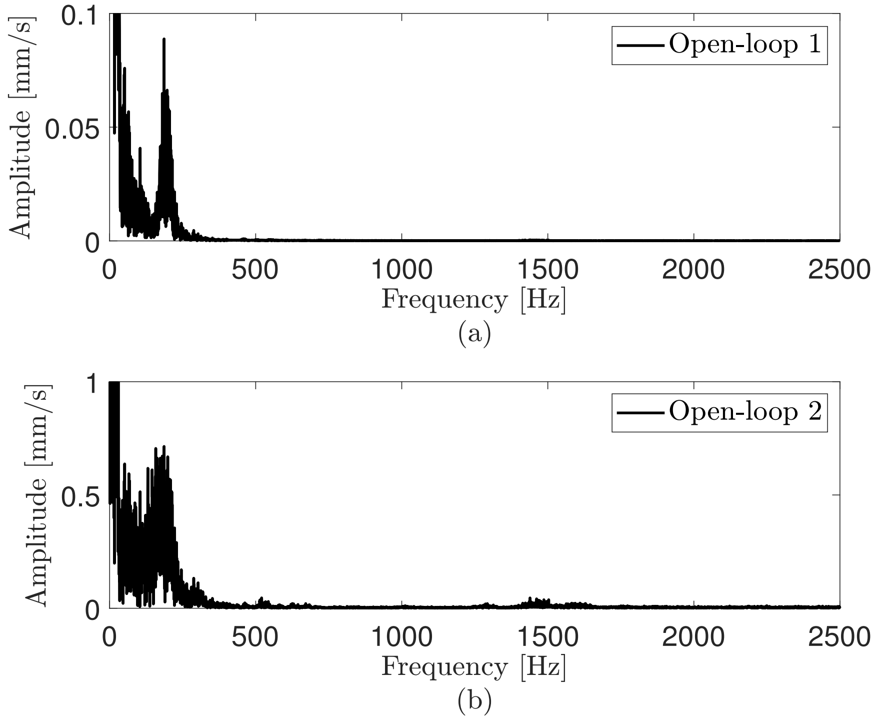

Figure 5.11: FFT for open-loop excited experiments

gradient steepest descent towards minimizing the tracking error, and therefore k_{ewi} is included for stability concerns which is related to tracking error [38]. The auxiliary input signal $\mathbf{e}_{ti}$ in the proposed approach control law is a function of the augmented tracking error as given in (5.37), which is used to calculate the auxiliary adaptive control gain $\mathbf{k}_{ti}$. Therefore, the auxiliary control input contributes to stability of the system as shown in the stability analysis.

5.6 Summary

In this chapter, a novel approach is presented that combines simple adaptive and integral terminal sliding mode control for industrial feed drive systems application. The design of the adaptive control law is derived from a fractional power of the integral terminal sliding surface, which is based on velocity-based augmented output signal. The mode control configuration employs a technique similar to simple adaptive control. This unique formulation enables the proposed controller to overcome challenges associated with estimating plant parameters when using integral terminal sliding mode control. To validate the effectiveness of the proposed method, simulations and experiments were conducted. The results are compared with conventional methods. The proposed approach outperforms the conventional methods, achieving superior tracking accuracy. This shows the proposed controller can be used in enhancing the performance of industrial feed drive systems.

Chapter 6

Conclusions and future works

6.1 Conclusions

Ball-screw feed drive systems are crucial parts in the manufacturing industry and are widely used because of their simple structure, high transmission accuracy and low sensitivity to variations. Industrial machine operations are currently driven by ball-screw feed drive systems the need for high tracking accuracy and energy-saving efficiency. This can be achieved by constructing feedback control law that is simple to implement and ensures high tracking accuracy with minimum effort. Simple adaptive control is a direct type of model referencing adaptive control which enables to construct the adaptive control system regardless of the plant order. To implement the SAC algorithm, it requires the almost strictly positive real property adhered for stability of the control system and to achieve model output following by feed-forward compensation using the command generator tracker concept. Despite the SAC advantages of lack of dependence on plant parameter estimates, the main constraint is the requirement of the ASPR-ness of the plant.

In the Chapter 2, preliminaries of simple adaptive control for ASPR plants are described to set precedent for the following chapters. Furthermore, the recent new concept of terminal at tractor inclusion to sliding mode and its shortcoming is also discussed and dynamics of a ball-screw feed drive systems used for simulation studies.

To enhance the effectiveness of the SAC to feed drive systems which does not satisfy the ASPR property, the jerk-based augmented output signal feedback for ASPR property is proposed in Chapter 3. The jerk-based augmented output signal uses the position, velocity, acceleration, and jerk information to achieve the ASPR property. High tracking accuracy is achieved by assigning maximum allowable value on the higher-order derivatives of position. The stability of the proposed SAC algorithm is shown. The effectiveness of the proposed approach is shown on simulations and verified on experiments. The proposed approach achieves higher tracking accuracy and less energy consumption as compared to the widely known approach of parallel feedfoward compensator.

Chapter 4 extends the idea from Chapter 3 to contouring control which is highly recommended for feed drive applications. This chapter proposes simple adaptive contouring control (SACC) using jerk-based augmented output signal for the ASPR property. The ASPR property guarantees the stability of the controlled system even when adaptive gains are high. SACC is designed by following the tangent-contour control scheme while using the SAC technique to enhance the contouring accuracy. The simulation analysis and experimental validation are provided to show the effectiveness of the proposed technique. The proposed contouring approach achieves lower contour error and energy consumption by about 45%, and 3% respectively, as compared to the most common parallel feedforward compensation approach.

A modified SAC algorithm made of integral terminal sliding mode control procedures is proposed for industrial feed drive systems in Chapter 5. The adaptive control law is designed from a fractional power integral terminal sliding mode control configuration using a simple adaptive control-like technique. This formulation allows the proposed controller to mitigate the plant parameters estimation difficulties while benefiting from the inclusion of fractional power signals in the adaptive control law. Simulation and experiments were conducted using the proposed approach compared to conventional approaches. The proposed approach has shown to achieve higher tracking accuracy compared to the conventional approaches under the same tracking conditions. Experimental results show that the proposed approach can reduce by about 58.6% and 73% for axis 1 and 2, respectively as compared to simple adaptive control only.

In summary, the proposals in this thesis addresses the requirement of ASPR-ness for the feed drive systems with the objective to achieve high tracking and contouring accuracy. In the context of the energy consumption by industrial machines, the energy saving capabilities of the proposed controllers relative to the conventional approaches might seem relatively small. However, given that industrial activities are continuous, even minor percentage reductions can accumulate to significant energy savings over a period. For instance, an industrial machine running around the clock can realize notable annual energy and cost savings with a mere small percentage enhancement in energy savings. Additionally, when you factor in the hundreds of machines working concurrently, the aggregate impact can be considerably larger. The suggested schemes for adaptive control design of feed drive systems can be useful for plants with little or no information on plants order and plants parameters.

6.2 Future works

The main objective of this thesis is to improve the tracking and contouring accuracy of the feed drive systems with capability of reducing the energy consumption for the feed drive systems to contribute in energy resource shortage and environmental effects. In the future the following scenarios can be further explored to contribute to knowledge and industrial applications as follows:

- Feed drive systems are highly affected by friction which is nonlinear in nature and its not yet clear that adaptive control techniques proposed in this thesis can compensate them adequately or needs further formulations to ensure and achieve higher tracking accuracy and energy-saving capabilities, this concept can be further explored and clarified for industrial applications and narrowing the knowledge gap for future developments.
- In the jerk-based augmented output signal for ASPR property approach requires the relative gains assigned to be maximum allowable values to the higher-order derivatives signals and high adaptation scaling factors on the controller gains to achieve high tracking accuracy. This improves the steady-state response significantly. However the transient response sometimes becomes worse because of the overshoots especially on the contouring control. This can be further investigated and reduced or eliminated.
- The scheme proposed in Chapter 5 is limited to tracking accuracy and extra control input effectiveness is less aggressive when tracking error is greater than 1 and might

limit some applications. The formulation can be extended to faster convergent speed when the tracking error and ensures that the tracking error converges to zero within a limited time. In addition, extension to contouring control which is highly recommended for general contour applications in the industry. Furthermore, the switching gain which is the robust part of the simple adaptive terminal sliding mode control to handle disturbances is assigned to be constant can be replaced with the adaptive mechanism that will allow for higher contouring and tracking accuracy.

- This thesis uses the augmented output signals consisting of higher-order derivatives and position of the industrial feed drive system. This enables the extended plant to have the ASPR property and apply the SAC successfully. The allowable maximum value of the augmented output signal can be assigned in the design such that high precision control is expected. However, there might be limited because the relative assigned gains to the higher-order derivative(s) are constant which might hinder further performance. These relative gains can be further adjusted to be adaptive in nature.

Bibliography

[1] L. Lv, C. Lu, S. Chen, and W. Wang, “Study on load distribution and fatigue elastic life of ball screw under ultimate conditions,” *Applied Sciences*, vol. 14, no. 5, p. 1966, 2024.

[2] V. Swamy and S. Vidyasagar, “High-efficiency regenerative shock absorbers considering twin ball screws transmission for increasing the vehicles’ driving range using a hybrid approach,” *Proceedings of the Institution of Mechanical Engineers, Part I: Journal of Systems and Control Engineering*, vol. 238, no. 1, pp. 141–157, 2024.

[3] H. Wu, Q. Guan, C. Xi, and D. Zuo, “Construction of dynamic temperature field model of ball screw based on superposition of positive and negative temperature fields,” *Numerical Heat Transfer, Part A: Applications*, vol. 83, no. 4, pp. 343–360, 2023.

[4] C. Li, M. Xu, W. Song, and H. Zhang, “A review of static and dynamic analysis of ball screw feed drives, recirculating linear guideway, and ball screw,” *International Journal of Machine Tools and Manufacture*, vol. 188, p. 104021, 2023.

[5] E. W. Nshama, M. R. Msukwa, and N. Uchiyama, “A trade-off between energy saving and cycle time reduction by pareto optimal corner smoothing in industrial feed drive systems,” *IEEE Access*, vol. 9, pp. 23579–23594, 2021.

[6] Y. Lu, J. Zhao, Z. Zhang, Z. Fu, X. Sun, S. Song, Z. Zhang, and Q. Liu, “Research on a novel integrated control strategy for contour error compensation of biaxial CNC machining,” *The International Journal of Advanced Manufacturing Technology*, vol. 130, no. 1, pp. 385–402, 2024.

[7] P. Waide and C. U. Brunner, “Energy-efficiency policy opportunities for electric motor-driven systems,” *IEA Energy Papers*, vol. 7, 2011. https://doi.org/10.1787/5kgg52gb9gjd-en.

[8] L. Abdullah, Z. Jamaludin, Q. Ahsan, J. Jamaludin, N. A. Rafan, T. Chiew, K. Jusoff, and M. Yusoff, “Evaluation on tracking performance of PID, gain scheduling and classical cascade P/PI controller on xy table ballscrew drive system,” *World Applied Sciences Journal*, vol. 21, no. 1, pp. 1–10, 2013.

[9] Y. Altintas, A. Verl, C. Brecher, L. Uriarte, and G. Pritschow, “Machine tool feed drives,” *CIRP Annals*, vol. 60, no. 2, pp. 779–796, 2011.

[10] V. Leipe, C. Hinze, A. Lechler, and A. Verl, “Model predictive control for compliant feed drives with offset-free tracking behavior,” *Production Engineering*, vol. 17, no. 6, pp. 805–814, 2023.

[11] M. R. Msukwa, E. W. Nshama, and N. Uchiyama, “Adaptive sliding mode control with feedforward compensator for energy-efficient and high-speed precision motion of feed drive systems,” *IEEE Access*, vol. 8, pp. 43571–43581, 2020.

[12] Q.-B. Xiao, M. Wan, Y. Yang, and W.-H. Zhang, “Pre-compensation of contour errors for five-axis machine tools through constructing a model reference adaptive control,” *Mechanism and Machine Theory*, vol. 183, p. 105258, 2023.

[13] A. Accetta, F. Alonge, M. Cirrincione, F. D’Ippolito, M. Pucci, R. Rabbeni, and A. Sferlazza, “Robust control for high performance induction motor drives based on partial state-feedback linearization,” *IEEE Transactions on Industry Applications*, vol. 55, no. 1, pp. 490–503, 2018.

[14] M. Schwenzer, M. Ay, T. Bergs, and D. Abel, “Review on model predictive control: an engineering perspective,” *The International Journal of Advanced Manufacturing Technology*, vol. 117, no. 5, pp. 1327–1349, 2021.

[15] M. A. Stephens, C. Manzie, and M. C. Good, “Model predictive control for reference tracking on an industrial machine tool servo drive,” *IEEE Transactions on Industrial Informatics*, vol. 9, no. 2, pp. 808–816, 2012.

[16] X. Yang, R. Seethaler, C. Zhan, D. Lu, and W. Zhao, “A model predictive contouring error precompensation method,” *IEEE Transactions on Industrial Electronics*, vol. 67, no. 5, pp. 4036–4045, 2019.

[17] J. Li, C. Qi, Y. Li, and Z. Wu, “Prediction and compensation of contour error of CNC systems based on LSTM neural-network,” *IEEE/ASME Transactions on Mechatronics*, vol. 27, no. 1, pp. 572–581, 2021.

[18] R. Xi, H. Zhang, S. Sun, and Y. Wang, “Reduced-order high-gain observer (ROHGO)-based neural tracking control for random nonlinear systems with output delay,” *IEEE Transactions on Systems, Man, and Cybernetics: Systems*, vol. 52, no. 12, pp. 7507–7515, 2022.

[19] K. Sobel, H. Kaufman, and L. Mabius, “Model reference output adaptive control systems without parameter identification,” *18th IEEE Conference on Decision and Control including the Symposium on Adaptive Processes*, pp. 347–351, 1979.

[20] F. Chen, Q. Wu, B. Jiang, and G. Tao, “A reconfiguration scheme for quadrotor helicopter via simple adaptive control and quantum logic,” *IEEE Transactions on Industrial Electronics*, vol. 62, no. 7, pp. 4328–4335, 2015.

[21] A. I. Belkharraz and K. Sobel, “Simple adaptive control for aircraft control surface failures,” *IEEE Transactions on Aerospace and Electronic Systems*, vol. 43, no. 2, pp. 600–611, 2007.

[22] N. Uchiyama, Y. Ogawa, M. Abd El Khalick, and S. Sano, “Energy saving in five-axis machine tools using synchronous and contouring control and verification by machining experiment,” *IEEE Transactions on Industrial Electronics*, vol. 62, no. 9, pp. 5608–5618, 2015.

[23] A. Farrage and N. Uchiyama, “Improvement of motion accuracy and energy consumption for industrial feed drive systems using adaptive sliding mode control,” *ISA Transactions*, vol. 106, pp. 382–391, 2020.

[24] M. Rigacci, R. Sato, and K. Shirase, “Experimental evaluation of mechanical and electrical power consumption of feed drive systems driven by a ball-screw,” *Precision Engineering*, vol. 64, pp. 280–287, 2020.

[25] J. Wu, Z. Liu, G. Yu, and Y. Song, “A study on tracking error based on mechatronics model of a 5-DOF hybrid spray-painting robot,” *Journal of Mechanical Science and Technology*, vol. 36, no. 9, pp. 4761–4773, 2022.

[26] X.-C. Xi, W.-S. Zhao, and A.-N. Poo, “Improving CNC contouring accuracy by robust digital integral sliding mode control,” *International Journal of Machine Tools and Manufacture*, vol. 88, pp. 51–61, 2015.

[27] J. Wu, G. Yu, Y. Gao, and L. Wang, “Mechatronics modeling and vibration analysis of a 2-DOF parallel manipulator in a 5-DOF hybrid machine tool,” *Mechanism and Machine Theory*, vol. 121, pp. 430–445, 2018.

[28] Y. Koren, “Cross-coupled biaxial computer control for manufacturing systems,” *ASME Trans J Dyn Syst Meas Control*, vol. 102, pp. 265–272, 1980.

[29] Z. Li, J. Wang, J. An, Q. Zhang, Y. Zhu, H. Liu, and H. Sun, “Control strategy of biaxial variable gain cross-coupled permanent magnet synchronous linear motor based on MPC-MRAS,” *IEEE Transactions on Industry Applications*, vol. 58, no. 4, pp. 4733–4743, 2022.

[30] N.-T. Hu, L.-Y. Chen, and C.-S. Chen, “Novel cross-coupling position command shaping controller using H_∞ in multiaxis motion systems,” *IEEE Transactions on Industrial Electronics*, vol. 69, no. 12, pp. 13099–13110, 2021.

[31] S.-L. Chen and S.-M. Hsieh, “Iterative learning contouring control: theory and application to biaxial systems,” *Mechatronics*, vol. 89, p. 102932, 2023.

[32] Z. Li, Q. Zhang, J. An, H. Liu, and H. Sun, “Cross-coupling control method of the two-axis linear motor based on second-order terminal sliding mode,” *Journal of Mechanical Science and Technology*, vol. 36, no. 3, pp. 1485–1495, 2022.

[33] Z. Wang, R. Zhou, C. Hu, and Y. Zhu, “Real-time iterative compensation based contouring control method for polar coordinate motion systems,” *IEEE/ASME Transactions on Mechatronics*, vol. 27, no. 5, pp. 3517–3526, 2022.

[34] G.-C. Chiu and M. Tomizuka, “Contouring control of machine tool feed drive systems: a task coordinate frame approach,” *IEEE Transactions on Control Systems Technology*, vol. 9, no. 1, pp. 130–139, 2001.

[35] R. Ke, T. Wang, J. Dong, and L. Cao, "Tangential velocity tracking-based task coordinate frame approach for contouring control of biaxial motion systems," *The International Journal of Advanced Manufacturing Technology*, vol. 124, no. 10, pp. 3489–3504, 2023.

[36] J. Broussard and M. O'Brien, "Feedforward control to track the output of a forced model," *IEEE Transactions on Automatic Control*, vol. 25, no. 4, pp. 851–853, 1980.

[37] H. Kaufman, I. Barkana, and K. Sobel, *Direct adaptive control algorithms: theory and applications*. Springer Science & Business Media, 2012.

[38] I. Barkana, "Classical and simple adaptive control for nonminimum phase autopilot design," *Journal of Guidance, Control, and Dynamics*, vol. 28, no. 4, pp. 631–638, 2005.

[39] I. Barkana, "Gain conditions and convergence of simple adaptive control," *International Journal of Adaptive Control and Signal Processing*, vol. 19, no. 1, pp. 13–40, 2005.

[40] I. Bar-Kana and H. Kaufman, "Simple adaptive control of large flexible space structures," *IEEE Transactions on Aerospace and Electronic Systems*, vol. 29, no. 4, pp. 1137–1149, 1993.

[41] I. Bar-Kana, "Parallel feedforward and simplified adaptive control," *Internat J Adapt Control Signal Process*, vol. 1, no. 2, pp. 95–109, 1987.

[42] I. Rusnak and I. Barkana, "SPR and ASPR untangled," *IFAC Proceedings Volumes*, vol. 42, no. 6, pp. 126–131, 2009.

[43] I. Barkana, "Robustness and perfect tracking in simple adaptive control," *International Journal of Adaptive Control and Signal Processing*, vol. 30, no. 8-10, pp. 1118–1151, 2016.

[44] T. Yang, Y. Deng, H. Li, Z. Sun, H. Cao, and Z. Wei, "Fast integral terminal sliding mode control with a novel disturbance observer based on iterative learning for speed control of PMSM," *ISA Transactions*, vol. 134, pp. 460–471, 2023.

[45] Y. Pan, C. Yang, L. Pan, and H. Yu, "Integral sliding mode control: performance, modification, and improvement," *IEEE Transactions on Industrial Informatics*, vol. 14, no. 7, pp. 3087–3096, 2017.

[46] H. Yang, Z. Wang, T. Zhang, and F. Du, "A review on vibration analysis and control of machine tool feed drive systems," *The International Journal of Advanced Manufacturing Technology*, vol. 107, pp. 503–525, 2020.

[47] A. Dumanli and B. Sencer, "Data-driven iterative trajectory shaping for precision control of flexible feed drives," *IEEE/ASME Transactions on Mechatronics*, vol. 26, no. 5, pp. 2735–2746, 2020.

[48] Z. Zhang, Z. Yang, S. Xiong, S. Chen, S. Liu, and X. Zhang, "Simple adaptive control-based reconfiguration design of cabin pressure control system," *Complexity*, vol. 2021, no. 1, p. 6635571, 2021.

[49] W. Gai, Y. Zhou, M. Zhong, C. Sheng, and J. Zhang, "Simple adaptive control with an adaptive anti-windup compensator for the unmanned aerial vehicle attitude control," *IEEE Access*, vol. 8, pp. 52323–52332, 2020.

[50] T. Sato, K. Fujita, N. Kawaguchi, T. Takagi, and I. Mizumoto, "Null-space-based steady-state tracking error compensation of simple adaptive control with parallel feedforward compensator and its application to rotation control," *Control Engineering Practice*, vol. 105, p. 104651, 2020.

[51] K. Akaike and I. Mizumoto, "ASPR-based adaptive feedback control with adaptive PFC and FF input based on RBF NN for unstable systems," *60th IEEE Conference on Decision and Control*, pp. 378–383, 2021.

[52] Z. Guan, I. Mizumoto, and T. Yamamoto, "Design of PCA-based data-driven adaptive output feedback control for nonlinear systems," *28th IEEE International Symposium on Industrial Electronics*, pp. 497–502, 2019.

[53] S. Harada and N. Uchiyama, "Robust simple adaptive control with augmented output signal and friction compensation for industrial feed drive systems," *22nd IEEE International Conference on Industrial Technology*, pp. 99–104, 2021.

[54] H. Sato and N. Uchiyama, "Simple adaptive control using augmented output signal with acceleration for industrial feed drive systems," *IEEE/SICE International Symposium on System Integration*, pp. 109–113, 2022.

[55] I. Barkana, "Simple adaptive control: the optimal model reference–short tutorial," *IFAC Proceedings Volumes*, vol. 46, no. 11, pp. 396–407, 2013.

[56] M. Khodarahmi and V. Maihami, "A review on Kalman filter models," *Archives of Computational Methods in Engineering*, vol. 30, no. 1, pp. 727–747, 2023.

[57] A. Dumanli and B. Sencer, "Optimal high-bandwidth control of ball-screw drives with acceleration and jerk feedback," *Precision Engineering*, vol. 54, pp. 254–268, 2018.

[58] K. Mokhtari, A. Elhadri, and M. Abdelaziz, "A passivity-based simple adaptive synergetic control for a class of nonlinear systems," *International Journal of Adaptive Control and Signal Processing*, vol. 33, no. 9, pp. 1359–1373, 2019.

[59] B. Sencer and A. Dumanli, "Optimal control of flexible drives with load side feedback," *CIRP Annals*, vol. 66, no. 1, pp. 357–360, 2017.

[60] A. K. Mohammad, N. Uchiyama, and S. Sano, "Reduction of electrical energy consumed by feed-drive systems using sliding-mode control with a nonlinear sliding surface," *IEEE Transactions on Industrial Electronics*, vol. 61, no. 6, pp. 2875–2882, 2013.

[61] N. Uchiyama, S. Sano, and T. Nakamura, "Contouring controller design for biaxial feed drive systems considering compliance of transmission mechanism," *The International Journal of Advanced Manufacturing Technology*, vol. 44, pp. 428–436, 2009.

[62] A. A. E. K. Mohammad, N. Uchiyama, and S. Sano, "Energy saving in feed drive systems using sliding-mode-based contouring control with a nonlinear sliding surface," *IEEE/ASME Transactions on Mechatronics*, vol. 20, no. 2, pp. 572–579, 2014.

[63] N. Chen, Y. Lou, and Z. Li, "Adaptive contouring control for high-accuracy tracking systems," *IEEE International Conference on Systems, Man and Cybernetics*, pp. 50–55, 2006.

[64] C. Hu, B. Yao, and Q. Wang, "Coordinated adaptive robust contouring controller design for an industrial biaxial precision gantry," *IEEE/ASME Transactions on Mechatronics*, vol. 15, no. 5, pp. 728–735, 2009.

[65] A. Farrage and N. Uchiyama, "Energy saving in biaxial feed drive systems using adaptive sliding mode contouring control with a nonlinear sliding surface," *Mechatronics*, vol. 54, pp. 26–35, 2018.

[66] H. Weiss and I. Rusnak, "Add-on simple adaptive control improves performance of classical control design," *AIP Conference Proceedings*, vol. 1637, no. 1, pp. 1177–1201, 2014.

[67] T. Takagi and I. Mizumoto, "The design method of simple adaptive control system with PFC for MIMO system via DE," *SICE Journal of Control, Measurement, and System Integration*, vol. 16, no. 1, pp. 75–83, 2023.

[68] H. J. Nyobuya, M. S. Halinga, and N. Uchiyama, "Simple adaptive control for industrial feed drive systems using a jerk-based augmented output signal," *The International Journal of Advanced Manufacturing Technology*, vol. 128, no. 7-8, pp. 3613–3626, 2023.

[69] H. J. Nyobuya, M. S. Halinga, and N. Uchiyama, "Enhanced motion accuracy in industrial feed drive systems using simple adaptive control with a jerk-based augmented signal," *IFAC-PapersOnLine*, vol. 56, no. 2, pp. 9203–9208, 2023.

[70] R. Zhou, C. Hu, Z. Wang, S. He, and Y. Zhu, "Nonlinearity compensation and high-frequency flexibility suppression based RIC method for precision motion control systems," *IEEE Transactions on Industrial Informatics*, vol. 19, no. 2, pp. 1332–1342, 2022.

[71] C.-C. Lo and C.-Y. Chung, "Tangential-contouring controller for biaxial motion control," *ASME J. Dynamics, Meas., Control*, vol. 121, no. 1, pp. 126–129, 1999.

[72] I. Bar-Kana and H. Kaufman, "Simple adaptive control of uncertain plants," *26th IEEE Conference on Decision and Control*, vol. 26, pp. 20–25, 1987.

[73] L. Tang and R. G. Landers, "Multiaxis contour control—the state of the art," *IEEE Transactions on Control Systems Technology*, vol. 21, no. 6, pp. 1997–2010, 2013.

[74] Y. M. Hendrawan, A. Farrage, and N. Uchiyama, "Iterative NC program modification and energy saving for a CNC machine tool feed drive system with linear motors," *The International Journal of Advanced Manufacturing Technology*, vol. 102, no. 9, pp. 3543–3562, 2019.

[75] X. Li, H. Zhao, X. Zhao, and H. Ding, "Contouring compensation control based on high accuracy contour error estimation for multi-axis motion systems," *The International Journal of Advanced Manufacturing Technology*, vol. 93, pp. 2263–2273, 2017.

[76] T. Huang, Y. Kang, S. Du, Q. Zhang, Z. Luo, Q. Tang, and K. Yang, "A survey of modeling and control in ball screw feed-drive system," *The International Journal of Advanced Manufacturing Technology*, vol. 121, no. 5, pp. 2923–2946, 2022.

[77] M. S. Halinga, H. J. Nyobuya, and N. Uchiyama, "Generation and experimental verification of time and energy optimal coverage motion for industrial machines using a modified s-curve trajectory," *The International Journal of Advanced Manufacturing Technology*, vol. 125, no. 7, pp. 3593–3605, 2023.

[78] Y. Wu, X. Yu, and Z. Man, "Terminal sliding mode control design for uncertain dynamic systems," *Systems & Control Letters*, vol. 34, no. 5, pp. 281–287, 1998.

[79] C.-S. Chiu, "Derivative and integral terminal sliding mode control for a class of MIMO nonlinear systems," *Automatica*, vol. 48, no. 2, pp. 316–326, 2012.

[80] K. Sobel, H. Kaufman, and L. Mabius, "Implicit adaptive control for a class of MIMO systems," *IEEE Transactions on Aerospace and Electronic Systems*, no. 5, pp. 576–590, 1982.

[81] I. Bar-Kana and H. Kaufman, "Global stability and performance of a simplified adaptive algorithm," *International Journal of Control*, vol. 42, no. 6, pp. 1491–1505, 1985.

[82] M. Yasser, A. Trisanto, J. Lu, H. Sekiya, and T. Yahagi, "Adaptive sliding mode control using simple adaptive control for SISO nonlinear systems," *IEEE International Symposium on Circuits and Systems*, pp. 2153–2156, 2006.

[83] H. J. Nyobuya, M. S. Halinga, and N. Uchiyama, "Simple adaptive contouring control for feed drive systems using jerk-based augmented output signal," *The International Journal of Advanced Manufacturing Technology*, vol. 130, no. 9, pp. 4985–5001, 2024.

[84] C. Edwards and S. Spurgeon, *Sliding mode control: theory and Applications*. Crc Press, 1998.

[85] Q. Zhang, H. Yu, and X. Wang, "Integral terminal sliding mode control for a class of nonaffine nonlinear systems with uncertainty," *Mathematical Problems in Engineering*, vol. 2013, no. 1, p. 636494, 2013.

[86] Y. Wang, B. Chen, and H. Wu, "Joint space tracking control of underwater vehicle-manipulator systems using continuous nonsingular fast terminal sliding mode," *Proceedings of the Institution of Mechanical Engineers, Part M: Journal of Engineering for the Maritime Environment*, vol. 232, no. 4, pp. 448–458, 2018.

[87] M.-Y. Cheng and C.-C. Lee, "Motion controller design for contour-following tasks based on real-time contour error estimation," *IEEE Transactions on Industrial Electronics*, vol. 54, no. 3, pp. 1686–1695, 2007.

Publication list

International journal papers

- H. J. Nyobuya, M.S. Halinga , and N. Uchiyama, "Simple adaptive control for industrial feed drive systems using a jerk-based augmented output signal," *The International Journal of Advanced Manufacturing Technology*, vol. 128, pp. 3613-3626, 2023. (Impact Factor 3.2)
- H. J. Nyobuya, M.S. Halinga , and N. Uchiyama, "Simple adaptive contouring control for industrial feed drive systems using a jerk-based augmented output signal," *The International Journal of Advanced Manufacturing Technology*, vol. 130, pp. 4985-5001, 2024. (Impact Factor 3.2)

International conference papers

- H. J. Nyobuya, M.S. Halinga, and N. Uchiyama, "Enhanced motion accuracy in industrial feed drive systems using simple adaptive control with a jerk-based augmented signal," *22nd World Congress of the International Federation of Automatic Control*, Yokohama, Japan, pp. 9452-9457, 2023.